The Influence of Interannual Carbon Variability on Long-Term Sequestration in Proximate Northern Forests and Wetlands

By

Nikaan Koupaei-Abyazani

A thesis submitted in partial fulfillment of

the requirements for the degree of

MASTER OF SCIENCE

(Atmospheric and Oceanic Sciences)

at the

UNIVERSITY OF WISCONSIN-MADISON

2022

Abstract

Carbon dioxide (CO_2) levels are rising dramatically as a result of increased anthropogenic activity. One way of countering excessive CO_2 emissions is by restoring natural ecosystems that have historically been found to be efficient carbon (C) sinks. To be economically viable, these efforts must consider biomes with long-term sustained C sequestration capacities. Low interannual variation in this sink capacity minimizes risk of sequestration reversal. The goal of this study was to compare the interannual variability (IAV) of C at eight proximate Ameriflux eddy covariance sites across northern Wisconsin, Michigan's Upper Peninsula, Saskatchewan, Alberta, and the Northwest Territories with up to two decades of observations per site. Two wetlands (Allequash Creek (US-ALQ) and Lost Creek (US-Los)) and an unmanaged and managed forest (Sylvania Wilderness Area (US-Syv) and Willow Creek (US-WCr), respectively) were considered in the temperate region while boreal sites consisted of a bog (CA-SCB), peatland (CA-WP1), evergreen needleleaf forest (CA-SCC), and deciduous broadleaf forest (CA-Oas). To consider the fuller C budget, stream discharge data from the United States Geological Survey was also incorporated for some sites. In most of the measured years, on average, net ecosystem carbon dioxide exchange (NEE) in all ecosystems was negative, indicating C uptake by the ecosystem. The standard deviation of the yearly NEE cumulative sums for US-Los was 63 g C m^{-2} yr^{-1} while for US-Syv and US-WCr it was 111 g C m^{-2} yr^{-1} and 154 g C m^{-2} yr^{-1} respectively, implying greater variability for the deciduous forests than the wetlands. A similar result was found for the boreal sites. Mutual information analysis was used to determine influences of carbon components (gross primary productivity (GPP) and ecosystem respiration (RECO)) and drivers (photosynthetic photon flux density, air temperature, latent heat, and streamflow) on NEE. A larger influence on boreal NEE was found relative to temperate NEE on seasonal and yearly scales. NEE was also more impacted by GPP on hourly and diel scales and somewhat equally influenced by both GPP and RECO on mulitday, seasonal, and yearly scales. Our results demonstrate that for these regions, wetlands are a more reliable biome for C storage on decadal scales than forests.

Table of Contents

Acknowledgements

I would like to thank my advisor Dr. Ankur Desai for always being there to provide feedback and answer my questions. I greatly appreciate all he has done for me despite his busy schedule. I would also like to thank my committee members Paul Stoy and Min Chen for looking over my long manuscript and providing revisions. The quality of this paper has increased substantially as a result of your efforts. Thank you to my fellow lab members for guiding me through the research process when I first started and always being willing to assist me when I hit a roadblock. To my fellow graduate students who have inspired me with your hard work and input, I will cherish the conversations we've had and the experiences we've shared together. And lastly, I would like to give a special thanks to my family for supporting and being patient with me throughout this whole process. I am forever indebted to you for everything you've done for me.

1. Introduction and Background

One of the most urgent problems facing humanity today is global climate change. Carbon dioxide (CO_2) levels are rising dramatically as a result of increased anthropogenic activity. In its Fifth Assessment Report, the Intergovernmental Panel on Climate Change showed that atmospheric CO_2 concentrations had risen from 280 ppm in 1950 to 400 ppm in 2000 (Were et al., 2019). Additionally, computer models from the U.S. Climate Change Science Project have projected that in order to stabilize atmospheric CO_2 at 550 ppm (around two times the industrial level), annual global emissions must be reduced by 75% in the next century (Sundquist et al., 2008). If not combated, climate change will remain a major threat not only to the survival of species and ecosystems, but also to civilization as we know it (Erwin, 2009). Flooding and drought-induced damages have been estimated to cost billions of US dollars annually, with the latter being responsible for the 2007 California wildfires which displaced nearly one million people (Trenberth, 2005).

One way of countering excessive CO_2 emissions is by restoring natural ecosystems that have historically been found to be efficient C sinks. In order to make informed decisions on restoration measures, an analysis of C flux interannual variability (IAV) must be conducted. This is a useful approach for determining the long-term C sequestration potential of biomes. In addition, water and energy fluxes must also be considered since these drivers govern the magnitude of variability over time. It is important to note, however, that these efforts, known as natural climate solutions (NCS), must be complemented by drastic mitigation efforts in industry and energy if we are to meet the Paris goal (Anderson et al., 2019).

1.1 The Global Carbon Cycle

C is a vital element that helps maintain life on Earth. It is responsible for creating organic molecules that are crucial for cellular reproduction and metabolism, provides a “heat blanket” in the atmosphere that regulates global temperatures, and is dominantly used as a source of energy via the burning of C-based fossil fuels. In the past few centuries, human-induced emissions due to rapid economic development have caused anthropogenic radiative forcing to increase by 11% from 1750 to 2017, resulting in unprecedented increases in global temperatures (Bruhwiler et al., 2018). The effects of these changes may be seen in the form of more severe floods and droughts (threatening global food production) and intense acidification of the world's oceans (threatening marine life and biodiversity) (Bruhwiler et al., 2018).

C is stored in many different reservoirs across the Earth system (**Table 1**) and is constantly being transferred mechanically, chemically, or biologically from one stock to another (**Figure 1**). One of the relatively rapid exchanges occurs between the terrestrial biosphere and atmosphere, where vegetation uptakes and emits CO_2 via photosynthesis and respiration respectively. Anthropogenic disturbances (degradation and deforestation), biological interruptions (insect outbreaks), and natural hazards (fires) may cause a rapid increase in respiration, therefore increasing C emission rates and exacerbating global warming.

The direction of exchange between the ocean surface and atmosphere depends on 1) the relative concentrations of C between each reservoir and 2) surface water temperature (Bruhwiler et al., 2018). Due to spontaneous gas flow from higher to lower concentrations, regional surface waters and atmospheres supersaturated with CO_2 will experience transfer towards the atmosphere and surface water respectively. Additionally, regions with upwelling warm water are known to experience C outgassing while those with sinking cold water are C absorbers (Bruhwiler et al., 2018).

Terrestrial C is a highly dependent variable, owing to natural or anthropogenic changes in water availability (section 1.2) and energy (section 1.3). As a result, a thorough evaluation of drivers will aid in better understanding C's spatial and temporal variability across biomes.

Reservoir	% of Earth System's Carbon
Ocean (Deep Water)	80%
Soil	5%
Permafrost	4%
Ocean Sediments	4%
Oil, Gas, Coal	3%
Ocean (Surface Water)	2%
Atmosphere	2%
Vegetation	1%

Table 1: *C reservoirs along with percentage of total C residing in each. Table was created with information provided by The Second State of the C Cycle Report (SOCCR2).*

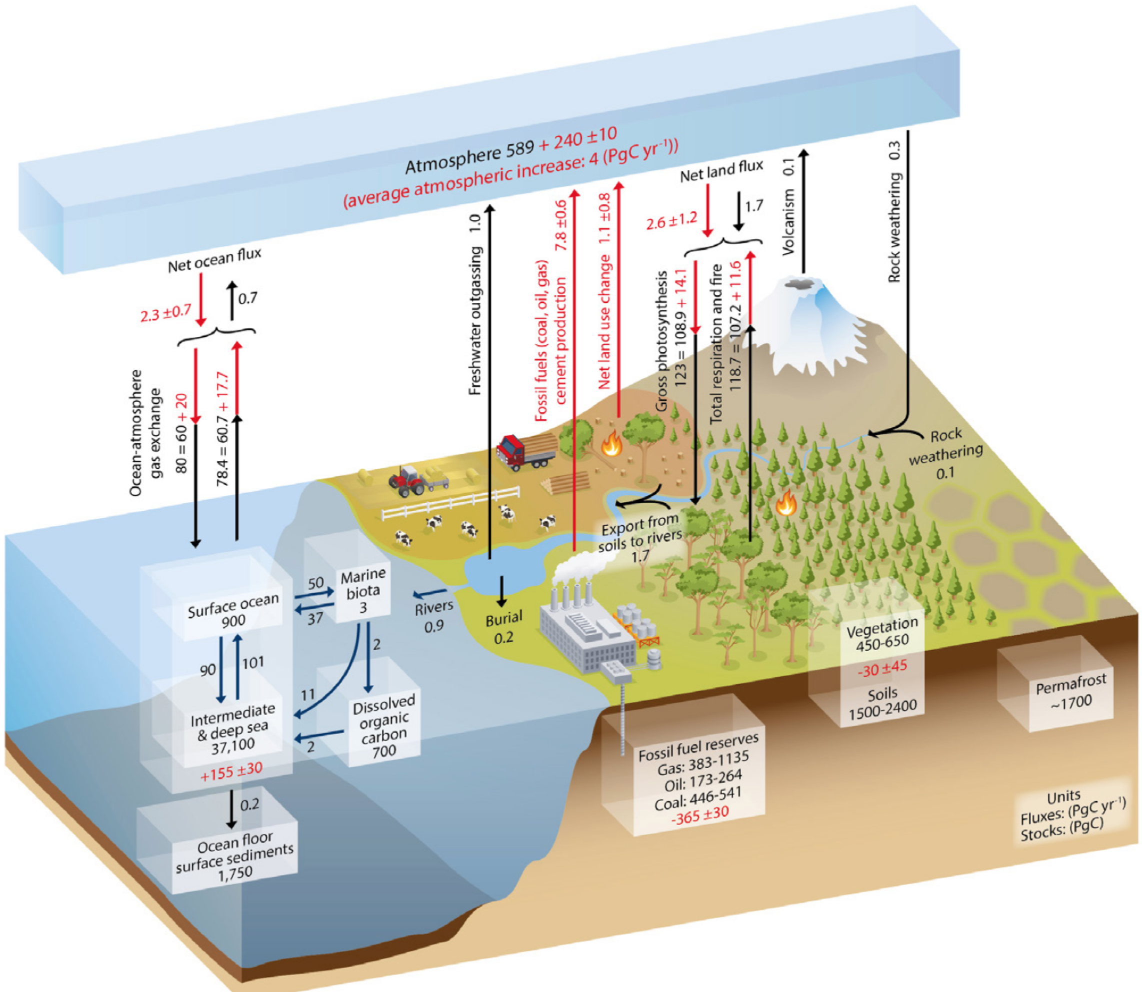

Figure 1: *The global C cycle. Boxed numbers and arrows showcase C reservoirs (Pg C) and fluxes (Pg C yr^{-1}) respectively. Black numbers and arrows represent pre-industrial stocks and flows while red numbers with arrows denote average yearly anthropogenic fluxes from 2000 to 2009. Red numbers inside boxes show cumulative changes in anthropogenic C for the industrial period (Figure taken from [Bruhwiler et al., 2018](#)).*

1.2 Carbon and Water

The water budget of a particular ecosystem depends on inflows via precipitation (P) and outflows via evapotranspiration (ET) and discharge. Water storage is usually ignored due to its negligible contribution on long temporal scales (Gedney et al., 2006).

Water has a significant influence on the local ecosystem C budget. An increase in atmospheric CO_2 concentrations, for instance, has been shown to close stomatal apertures which decreases transpiration rates and causes water outflow to be dominated by discharge (Gedney et al., 2006).

C can also be physically transported through runoff. In fact, a study has shown that lateral hydrologic C inflows and outflows through discharge have a significant impact on wetland C budgets (Chu et al., 2014).

C in streams and rivers can take the forms of organic and inorganic. Organic C includes methane (CH_4) or is synthesized from photosynthetically-assimilated CO_2. It can enter inland waters directly as plant detritus (particulate organic C (POC)) or leached material (dissolved organic C (DOC)). Inorganic C can take the form of dissolved CO_2, carbonic acid, bicarbonate, or carbonate and is the product of chemical and mechanical weathering or rock erosion. These processes release particulate inorganic C (PIC) as calcium carbonate, calcite minerals, and C alkalinity (Drake et al., 2017).

Due to the tightly bound relationships between C and water, it follows that water availability plays a crucial role in determining an ecosystem's C source/sink status. Wetlands such as small lakes, floodplains, and marshes, contain a large portion of the world's C despite their small global land cover (~2-6%). Wetland C has been described as originating from five main reservoirs: plant biomass, POC, DOC, microbial biomass, and gaseous CO_2 and CH_4. The latter four of which reside in the water or soil (Kayranli et al., 2009).

Another important link can be found between CH_4 and water table level. A study by Harriss et al. (1982) on the Great Dismal Swamp in Virginia has revealed low water table levels to correspond to a greater CH_4 sink. On the other hand, during high water table levels, the swamp was observed to become a significant CH_4 source. This was later confirmed via CH_4 monitoring at a German minerotrophic fen by Augustin et al.

Along with wetlands, another common ecosystem to consider is the deciduous forest. Water cycling at these biomes mainly depends on daily P patterns and soil-water storage capacity. Due to a variety of factors, the interplay between C and water can be very different than that of a wetland.

Temperate forests are known to hold ~20% of the global plant biomass and ~10% of the terrestrial C (Bonan, 2008). Due to deforestation, many of these forests have become C sources. There have been efforts, however, that aim to restore these ecosystems and bring them back to C sink status (Bonan, 2008). Temperate deciduous forests respond to high atmospheric CO_2 concentrations through reducing stomatal conductance, leading to a decrease in transpiration which ultimately augments discharge (Leuzinger and Körner, 2010).

1.3 Carbon and Energy

The interplay between C and energy can be described in terms of radiation absorption and chemical reactions. One example is the role of latent heat (LE) in causing turbulent energy exchange in the form of ET. As a result, larger LE contributes to a stronger linkage between heat fluxes and water transport.

Solar energy and vegetation also play a crucial role in ecosystem C production via photosynthesis. C uptake typically peaks during the warm season and when sunlight is available. The dependence of C accumulation on sunlight can be quantified in terms of net ecosystem exchange (NEE) and photosynthetic photon flux density (PPFD). One finding indicated that NEE increases and then levels off at a positive value as PPFD increases. The same study also found these trends to be similar for different ecosystems within the same category (rich and poor fens) (Frolking et al., 1998). Furthermore, daytime CO_2 uptake and PPFD were found to be positively correlated for a mixed conifer forest, mixed short-grass prairie, and sagebrush shrubland (Kelly et al., 2002).

1.4 Water and Energy

The interplay between water and energy has not been as well documented as those of C/water and C/energy. However, one notable relationship between these two components is encompassed in the LE term. In this context, by definition, LE represents the amount of heat added to a substance to change its phase while keeping its temperature constant. In ecosystem dynamics, LE is a mechanism that cools the surface through water evaporation. This form of energy is mainly responsible for the vertical transfer of water vapor from the surface to the atmosphere.

Due to the strict tie between LE and water, energy partitioning is also governed by water availability. For example, a study conducted on two ecosystems in Florida, scrub oak and pine flatwoods, found that the partitioning of net radiation into its sensible and latent heat flux components was mainly driven by fluctuations in soil moisture and leaf area. Specifically, a decrease in Bowen ratio was found with increasing soil moisture and leaf area (Bracho et al., 2008). The rate of ET has also been shown to vary with the development of leaf area index, generally increasing and decreasing as leaves develop and senesce respectively (Zhou and Zhou, 2009). Moreover, increases in canopy interception have been shown to increase ET. This reduces discharge and eventually leads to a decline in water availability (Liu et al., 2016).

1.5 Wetlands

Due to their high potential to sequester atmospheric CO_2, wetlands are regarded as one of the most important ecosystems when it comes to global warming mitigation (Were et al., 2019). Atmospheric CO_2 is transferred, accumulated, and trapped into wetland soils as soil organic matter. Other major inputs of C include organic matter from senesced vegetation and lateral transport of dissolved C via inflowing waters. C may also exit the wetland through outflowing water or, most commonly, be released directly as CO_2 and CH_4 through decomposition (Villa and Bernal, 2018).

Other factors such as water table depth (WTD), temperature, and oxygen availability also have an influence. WTD is the most significant driver of greenhouse gas fluxes in peatlands. Agricultural activity has caused peatlands to be drained for cultivation, converting the land from a net C sink to a net C source.

These ecosystems are also extremely sensitive to small changes in WTD (Evans et al., 2021). In addition, during dry and wet periods, the land has been found to become a net CH_4 sink and source, respectively (Kayranli et al., 2009).

Temperature is also an important controller of C sequestration due to its role in accelerating organic matter decomposition. Higher temperatures have been associated with higher CH_4 emissions but do not override the overall C sink capacity of most wetlands (Mitsch et al., 2012; Olsson et al., 2015;). Aerobic conditions only allow CO_2 formation during decomposition while both CO_2 and CH_4 are formed in anaerobic conditions (Kayranli et al., 2009).

Although these dynamics have been found to be generally true for the typical midlatitude wetland, it is important to acknowledge that these findings may not hold for other regions. Temperature and water table level in tropical wetlands and ultra-wet wetlands, for example, have a weaker influence on C sequestration (Christensen et al., 1998; Sjögersten et al., 2014; Villa and Bernal, 2018).

1.6 Terrestrial Forests

Terrestrial forests (hereon referred to as "forests") have also been known to play a key role in climate warming mitigation. Like wetlands, many variables play a role in determining their net C sink/source status. Over the past few decades, deforestation and forest degradation have been responsible for a fifth of global greenhouse gas emissions (Schrope, 2009), while intact forests are important global C sinks (Pan et al., 2011). Specifically, these ecosystems store 40% of the belowground C and 80% of the aboveground C while also carrying 90% of the C exchanges between the land and atmosphere (Wei et al., 2014).

A majority of the C storage in forests takes place in soil and vegetation. Boreal forests store a majority in soil while temperate forests sequester mostly in woody biomass. Furthermore, influences on plant and soil C sequestration potential are driven by forest management and soil moisture respectively (Ma et al., 2015).

The ability of a forest to efficiently sequester C is sensitive to factors such as temperature, precipitation, topology, human activity, and natural disturbances (Ma et al., 2015). Soil organic C, for instance, is known for its high sequestration capacity but is believed to have been reduced due to anthropogenic land cover change (Murty et al., 2002). Climatic changes over the past few decades are responsible for elongating the growing season and have a positive impact on forest productivity (Boisvenue and Running, 2006). In some cases, this has even resulted in higher growth rates (Cole et al., 2009).

1.7 Interannual Variability

Researchers have been studying the interactions between the land and atmosphere for multiple decades. Throughout this endeavor, new technologies have been implemented to facilitate the quantification of meteorological, hydrological, and gas flux variables. Eddy Covariance (EC) (see section 2.4), which debuted in the early 1990s, has proved to be the most ubiquitous method for obtaining flux measurements. The community's confidence in this approach eventually led to the integration of international/continental flux networks across the globe (Baldocchi et al., 2017). Since these stations have been sustained for decades, it is now possible to conduct analysis on C interannual variability (IAV) between sites on multi-decadal scales.

Due to the climatic impacts on carbon components, NEE may experience significant year-to-year fluctuations. For example, the spatial variability of ecosystem respiration (RECO) and gross primary productivity (GPP) has been shown to be strongly linked to temperature and precipitation while radiation availability only influences GPP (Yi et al., 2010).

Based on location and ecosystem type, C flux IAV can vary greatly. For datasets that cover temperate deciduous forests, the standard deviation of interannual NEE is approximately ± 100 g C m^{-2} yr^{-1} (Baldocchi et al., 2017). Furthermore, a mixed forest in southern Ontario, Canada was found to switch relatively quickly between being a C source or sink. Over the 17 years of the study, net ecosystem productivity increased by approximately 15.7 g C m^{-2} yr^{-1} due to decreases in RECO and increases in GPP. It was also found that PPFD and TA were the main drivers of C fluxes at the site (Froelich et al., 2015). On a seasonal scale, earlier start to leaf emergence caused by earlier spring TA has also been deemed responsible for these interannual variations (Saigusa et al., 2005).

Wetlands are also prone to NEE IAV. On average, these ecosystems mainly act as C sinks and their dynamics are driven mostly by plant phenology and WTL. Lower WTL reduces CO_2 uptake. Therefore, future drier conditions due to climate change may lead to NEE that is less negative during the growing season (McVeigh et al., 2014). In addition, warmer TAs during the winter have been associated with increases in CO_2 uptake (Helfter et al., 2015). It is important to note, however, that one wetland has been found to change its C sink/source status in a period of as little as two years, with its NEE variability being mostly attributed to the transition period between vegetation growth and senescence (Serrano‐Ortiz et al., 2020). Other drivers of IAV include vapor pressure deficit, annual maximum leaf area index, and growing season mean stomatal conductance.

A study by Zscheischler et al. has also found that IAV is caused by the most active (high percentile) fluxes at temperate forests on an hourly and daily scale. Therefore, it was concluded that IAV is governed by only a small handful of short-term fluxes (less than 20% of the total dataset).

Lastly, various models have been introduced to predict future trends in biome IAV. While these have been shown to reproduce IAV magnitudes, they fail to agree with the timing of observations made in mid-latitude forests across North America. GPP and RECO have been found to be drastically underestimated in deciduous and evergreen forests respectively, indicating model errors due to processes related to vegetation type (Keenan et al., 2012).

1.8 Natural Climate Solutions

NCS involve cost-effective restoration and conservation practices that increase C sequestration and consequently mitigate impacts of climate warming. Different biomes require different strategies. For example, forests may see increased fire management and reforestation while wetlands would need peat and coastal restoration.

NCS will play a major role in limiting increases in global temperatures to 2 °C due to its high C sequestration potential in relatively short amounts of time. When taking into account the constraints of food security, fiber security, and biodiversity conservation, it has been found that the maximum potential for NCS is ~23.8 Pg CO_2 equivalent (CO_2e) yr^{-1}. In addition, these practices are expected to deliver ~37% of CO_2e mitigation from now until 2030 and ~20% from now until 2050. These estimates are more likely if fossil fuel emissions are held constant for ten years, brought down to 7% of current levels by 2050, and completely abolished by 2095 (Griscom et al., 2017).

Forests are one of the most important biomes for C sequestration. In 2018, 11.6% of the total annual greenhouse gas emissions were offset by forests in the contiguous United States (EPA, 2020). The most effective mitigation practices have been found to be reforestation (307 Tg CO_2e yr^{-1}), tree management (267 Tg CO_2e yr^{-1}), and fire management (267 Tg CO_2e yr^{-1}) (Fargione et al., 2018).

When stands reach the climax of mean annual increment, they are usually logged for economic purposes. If the harvesting interval is increased (i.e. less harvests during the same period of time), it would allow for potential increases in forest C stocks (Kaarakka et al., 2021).

Wetlands are also known to have great sequestration potential and are therefore a prime candidate for NCS. Inland wetland restoration is known to have a net cooling effect on decadal and century time-scales and therefore would not prove to be effective for rapid mitigation. These biomes also require a major investment (~$4200-$49200 per ton C) rendering them economically inferior compared to other restoration efforts (Taillardat et al., 2020). On the other hand, conservation and restoration of coastal wetlands (such as mangroves) is more cost effective (~$1800 per ton C). The downside, however, is that these ecosystems cover a small percentage of the global land, making them appropriate for mitigation efforts on a national rather than global scale (Taillardat et al., 2020).

Despite evidence of their effectiveness as a mitigation strategy, NCS will undoubtedly face challenges in its implementation. Some potential roadblocks include complexities in social-ecological systems and doubt regarding the costs of ecosystem services. Furthermore, its ongoing uncertainty as a long-term C sink may lead to hesitation of action by policy makers (Seddon et al., 2019).

In Wisconsin, NCS has not been explored as much as in other regions despite the relatively high density of forests and wetlands in the area. Our work on the sites in northern Wisconsin and Michigan's Upper Peninsula (UP) will attempt to fill in these knowledge gaps and paint a clearer picture regarding C sequestration potential in the upper Midwest.

1.9 This Study

To better understand how local biomes can contribute to global warming mitigation, accurate descriptions of the C cycle must be made on the regional scale. Previous studies on C dynamics in wetlands have considered lateral transport (Gao et al., 2018; Bogard et al., 2020), storage (Kayranli et al., 2009), and climatic/meteorological controls (Evans et al., 2021). In the meantime, prior studies on forests have covered C flux responses to meteorological/phenological variability (Beamesderfer et al., 2020), sequestration distributions between plants and soil (Ma et al., 2015), and the effects of restoration efforts (Wei et al., 2014). Intercomparisons between different adjacent ecosystems, however, are limited.

Taking into account everything that is already known about the C sink capacity of forests and wetlands, this study will aim to conduct a direct comparison between four proximate forests and wetlands in northern Wisconsin and Michigan's UP. The water and energy budgets of each ecosystem will be analyzed with an attempt to determine their broader role in influencing long-term C sink capacity. Comparisons will be carried out on multiple time scales (hourly, diel, multi-day, seasonal) to determine C IAV and its drivers. These temperate sites will also be compared to boreal forest and wetland sites to determine the influences of location on carbon-driver dynamics. This study will aim to answer the following questions:

- How does the NEE IAV of the forest sites compare to that of the wetland sites? Is this more a function of GPP or RECO?
- Are there any significant differences in C drivers between or within biome types on multiple time scales?
- What do these findings imply for NCS?

Our hypotheses are the following:

- Stream C export will be more pronounced at the wetland sites, therefore leading to lower IAV than the forest sites
- Both biome types will have PPFD serve as the dominant driver on short time scales (hourly, diel) while water availability and temperature will be responsible for variability on longer time scales (multi-day, seasonal) for the wetlands and forests respectively.

2. Methods

2.2 Site Descriptions

2.2.1 Allequash Creek (US-ALQ)

This site is located in the Allequash Wetland near Allequash Creek (Latitude: 46.0308, Longitude: -89.6067) (**Figure 2**). The wetland is dominated by peat and covers ~32 hectares of the Trout Lake basin. It is one of the regions within the National Science Foundation's North Temperate Lakes Long-Term Ecological Research and is also included in the United States Geological Survey's (USGS) Trout Lake Water, Energy and Biogeochemical Budgets site (WEBB). The basin is monitored with a network of 60 observation wells and 4 stream gaging stations.

Since the soil consists of highly conductive outwash sand and gravel on top of crystalline bedrock, groundwater discharge to Allequash Creek is highly promoted (Anderson and Lowry, 2007). The creek flows downstream through the wetland and drains into Allequash Lake. The vegetation comprises a mix of broad-leaved evergreen/deciduous shrub/trees and narrow-leaved persistent emergent and wet meadow (Turner et al., 2019).

2.2.2 Lost Creek (US-Los)

This site is situated in a shrub wetland near Lost Creek (Latitude: 46.0827, Longitude: -89.9792; **Figure 2**) at an elevation of ~480 m and was established in September 2000. Since the creek and associated floodplain provide a consistent source of water, the wetland experiences a large amount of peat accumulation. Vegetation near the flux tower mostly consists of alder, willow, and sedges. Since it is located near a stream and has a long, narrow shape, this ecosystem shares many of the characteristics of typical minerotrophic wetlands in the Great Lakes region (Sulman and Desai et al., 2009). Its climate is characterized by warm, wet growing seasons and cold, dry winters. The growing season in the region starts at around June and ends in August (Pugh et al., 2017).

2.2.3 Sylvania Wilderness Area (US-Syv)

The Sylvania Wilderness Area site (hereafter referred to as Sylvania) (Latitude: 46.2420, Longitude: -89.3477; **Figure 2**) is an old-growth forest that was established in late 2001. Tree age ranges from 0 to 350 years old with the dominant vegetation consisting of sugar maple and eastern hemlock. Other types of vegetation include yellow birch, basswood, and ironwood. The climate can be considered northern continental (short growing seasons and cold winters) and the average elevation is ~540 m. Most of Sylvania's area is sheltered by hemlock-northern hardwood forest (66%), along with lakes and forested wetlands/marshes covering 21% and 13% of the area respectively (Desai et al., 2005).

2.2.4 Willow Creek (US-WCr)

Willow Creek is a deciduous broadleaf forest that is dominated by sugar maple, basswood, and green ash. Beneath the canopy consists of sugar maple and ironwood saplings, leatherwood maidenhair, bracken ferns, and blue cohosh. The elevation and flux footprint are approximately 515 m and 0.6 km respectively. Willow Creek is located in the Chequamegon-Nicolet National Forest in northern Wisconsin (Latitude: 45.8059, Longitude: -90.0799; **Figure 2**), experiences significant precipitation in all seasons, and is around 60-80 years old. Soils at the site have been subject to mixing and are saturated between 50 and 100 cm below the surface depending on the time of year (Cook et al., 2004). The site's leaf area index is 5.3 and the average canopy height is 24 m (Desai et al., 2005).

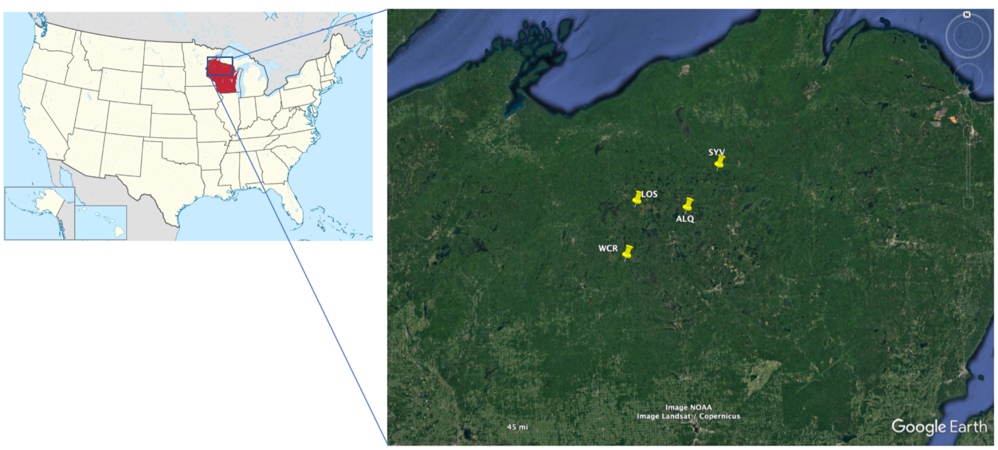

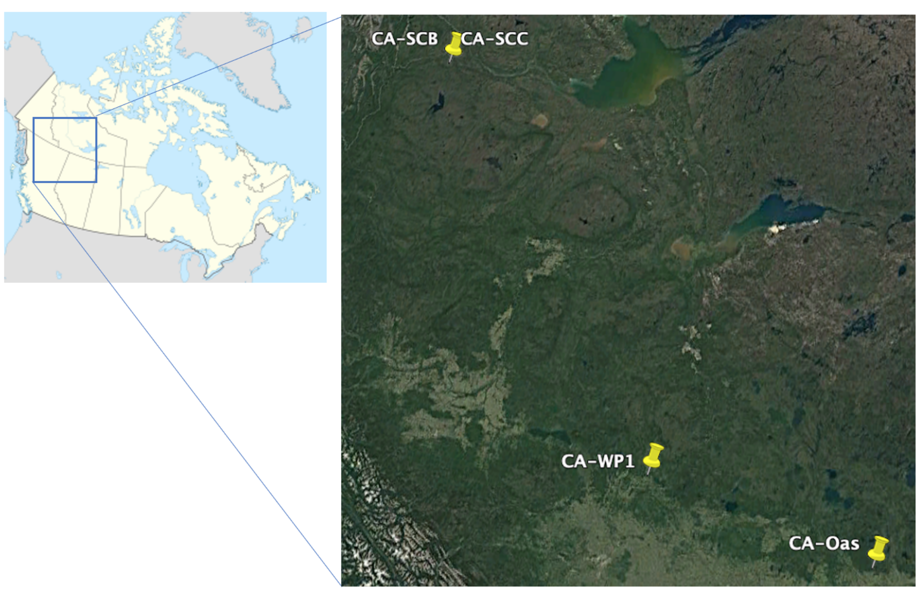

Figure 2: *Locations of sites. US-ALQ, US-Los, CA-SCB, and CA-WP1 are wetlands while US-Syv, US-WCr, CA-SCC, and CA-Oas are forests. Images are taken from Wikipedia and Google Earth Pro.*

2.2.5 Scotty Creek Watershed

CA-SCC and CA-SCB are characterized as a boreal forest and wetland respectively. These sites will be used to compare C dynamics and drivers with the four main temperate sites. Both are located in Scotty Creek (Latitude: 61.3, Longitude: -121.29; **Figure 2**) which is a 152 km^2 watershed near Fort Simpson, NT in the southern Taiga plains in northwestern Canada. The region experiences an average TA of -2.8 °C and mean total precipitation of 388 mm (149 mm of which is snow). The wetlands in this landscape are composed of bryophytes, ericaceous shrubs, and to a lesser extent black spruce and tamarack. The forests consist of a dense cover of black spruce along with ericaceous shrubs, bryophytes, and lichens dominating the understory (Helbig et al., 2017).

2.2.6 Alberta Western Peatland (CA-WP1)

CA-WP1 (lat: 54.9538; long:-112.4670; **Figure 2**) is one of many ecosystems located in the southern boreal forest of Canada. The regional climate has been characterized as having long, cold winters and short, cool summers with a mean annual temperature of 2.1 °C. Average yearly precipitation is composed of both rain (382 mm) and snow (122 mm). The terrain is relatively flat and is composed of nearly homogenous vegetation. Dominant tree and shrub species include *Picea mariana*, *Larix laricina, and Betula pumila* (Syed et al., 2006).

2.2.7 Saskatchewan - Western Boreal, Mature Aspen (CA-Oas)

CA-Oas is a mature deciduous forest site located on the southern end of Prince Albert National Park in Saskatchewan, Canada (lat: 53.6289, long: -106.1978; **Figure 2**). Average yearly precipitation and temperatures according to the nearby airport are reported to be 406 mm and 0.5 °C respectively. The warmest spring temperatures occurred in 1998 and 2001 while the coolest were in 1996 and 2003. A drought has also been recorded to have begun around 2001 and persisted through 2003 (Barr et al., 2004).

2.3 USGS Streamflow Gages

USGS streamflow gages near US-ALQ, US-Los, and US-Syv were used to obtain discharge data. The gage at Bear River, WI (Latitude: 46.04889, Longitude: -89.98444, Drainage

Area: 211 km^2) and Cisco Lake Outlet, MI (Latitude: 46.25331, Longitude: -89.45247, Drainage Area: 131 km^2) were paired with US-Los and US-Syv respectively. US-ALQ has three gages in proximity with one located in Sayner, WI (Latitude: 46.03084, Longitude: -89.59939, Drainage Area: 11 km^2) and two residing near Boulder Junction, WI (County Trunk Highway M → Latitude: 46.02389 , Longitude: -89.65278, Drainage Area: 22 km^2 | Site No. 3 → Latitude: 46.03278, Longitude: -89.60778, Drainage Area: 10 km^2). No data was available for US-WCr or the boreal sites since no gages were found within a reasonable distance to be considered as a proxy. The distance from the gage at Cisco Lake Outlet and US-Syv is 8 km and the distance from the Bear River gage to US-Los is 4 km. The Allequash Creek gages are relatively closer to US-ALQ being a distance of 3.7 km, 0.6 km, and 0.24 km away for County Trunk Highway M, Sayner, and Site No. 3 respectively (**Figure 3**).

Figure 3*: Maps showing the relative locations of the Ameriflux sites and the USGS streamgages. Images provided by* [*Google Earth Pro*]().

2.4 The Eddy Covariance Method

The Eddy Covariance (EC) method has been used widely by researchers due to its relatively few theoretical assumptions and its potential for measuring micro-meteorological variables. Gas, energy, and momentum fluxes may be directly measured, giving direct observations of land-atmosphere interactions within the flux tower footprint. EC has also benefited from technological advances in the past two decades, making it one of the most popular methods for data acquisition among the micro-meteorological community (Liang and Wang, 2020).

Measurements of ecosystem variables are determined through the covariance between vertical wind velocity and the quantity being measured. An anemometer is used to measure wind speed and direction, an infrared gas analyzer measures gas concentrations in the air, and radiation sensors measure solar radiation (section 2.5).

2.4.1 Theory

This overview will follow the discussion outlined in (Baldocchi, 2003). Vertical turbulent motions in the atmosphere are responsible for transporting CO_2 and other constituents between the atmosphere and biosphere. The EC technique involves keeping track of these turbulent motions in order to determine net inflows and outflows of these constituents with respect to the land and atmosphere. To achieve this, the Reynolds averaging method is applied on the following flux equation:

$$F_{inst} = w\rho_c \qquad (1)$$

where F_{inst} is the instantaneous mass flux density, w is the vertical wind velocity, and ρ_c is the CO_2 density. This will yield the following expression:

$$F = \overline{\rho_a}\,\overline{w'c'} \qquad (2)$$

where F represents the average flux density of the constituent over some specified period of time (i.e. hourly, monthly, yearly, etc.), ρ_a is the air density, and c is the ratio between ρ_c and ρ_a (ρ_c / ρ_a). The overbars represent the time averages and primes indicate deviations from the mean (i.e. $c = \bar{c} + c'$). Positive and negative values of covariance denote a loss and gain of constituents by the ecosystem respectively.

Interpretations of EC measurements can be done through assumptions and manipulation of the mass conservation equation:

$$\frac{d\bar{c}}{dt} = \underbrace{\frac{\partial \bar{c}}{\partial t}}_{\mathrm{I}} + \underbrace{\bar{u}\frac{\partial \bar{c}}{\partial x} + \bar{v}\frac{\partial \bar{c}}{\partial y} + \bar{w}\frac{\partial \bar{c}}{\partial z}}_{\mathrm{II}} = -(\underbrace{\nabla \bullet \mathbf{F}}_{\mathrm{III}} + \underbrace{S(x, y, z)}_{\mathrm{IV}}) \qquad (3)$$

where c is defined above, $\mathbf{F}$ is the three dimensional flux vector, S is the source/sink term, and u, v, and w are the wind velocities in the x, y, and z directions respectively. Term I represents the change in CO_2 mixing ratio with time, II is the advection of CO_2 by the zonal, meridional, and vertical winds, III is the flux divergence, and IV takes into account any biological sources or sinks and is dependent on location.

With two key assumptions, equation 3 can be simplified such that only one term remains on each side. The assumptions are the following: *the average CO_2 mixing ratio is constant with time* and *the terrain being measured is flat and horizontally homogeneous*. This implies that term I and the horizontal parts of terms II and III may be set equal to zero. As a result, only the vertically-dependent source/sink term and the vertical flux divergence terms survive, yielding the following:

$$\frac{\partial F_z}{\partial z} = -S(z) \qquad (4)$$

Multiplying by ∂z and then taking an integral from zero to an arbitrary height above the canopy h gives an expression for the mean vertical CO_2 flux density at that location:

$$F_z(h) = F_z(0) - \int_0^h S(z)\, dz \qquad (5)$$

where $F_z(0)$ is the mean vertical CO_2 flux density at the surface (i.e. fluxes from the soil or underlying vegetation). One of the main purposes for the EC method is to evaluate $F_z(h)$ in equation 5 for numerous ecosystems around the globe.

2.4.2 u^* Filtering

High quality data acquisition via the EC method requires high turbulence in the measurement area. During stable conditions, CO_2 flux measurements have been found to be underestimated using this technique (Goulden et al., 1996). Therefore, filtering methods must be applied to discard data taken during periods of low turbulence.

Goulden et al. proposed that friction velocity (u^*) may be used as a means of determining the validity of flux measurements. Once a threshold u^* (u^*_{th}) is determined, any fluxes below that threshold would be discarded. One shortcoming of this technique is that the same u^*_{th} cannot be used universally for all sites due to its dependence on local topography, surface roughness, and heterogeneity. Despite this, its effectiveness has made it the most-used flux-filtering method.

To obtain a lower threshold, one must know the point at which NEE becomes insensitive to changes in u^*. Therefore, nighttime NEE is plotted as a function of several different u^* classes. Afterwards, statistical comparisons are made to determine when the difference between the averaged nighttime NEE of a u^* class is not statistically significant with the NEE at higher values of u^*. The u^* value where this occurs is deemed to be the u^*_{th}. If it is found that u^* is co-varying with other drivers of respiration, the data is normalized to remove any covariation between respiration and the variable in question. Due to the likeliness of u^* covariance with temperature in temperate regions, an NEE-temperature function is typically used for normalization (Aubinet et al., 1999; Aubinet et al., 2012).

2.4.3 NEE Uncertainties

This section builds upon section 2.4.2 by discussing the role of u^* in determining NEE uncertainties. The FLUXNET 2015 dataset utilizes two main methods for calculating u^* thresholds, namely the change-point-detection (CP) (Barr et al., 2013) and moving-point-transition (MP) methods (Papale et al., 2006; Reichstein et al., 2005). These techniques involve dividing a year of data into four seasonal and seven temperature classes that have an identical number of observations. Each of these groups are then further divided into twenty u^* classes where the average NEE of each class is computed.

Next steps then depend on the method. For CP, two linear regressions are implemented between NEE and u^* (with one having zero slope). The point at which these lines cross is noted as the “change point” and is used as a guide for estimating appropriate u^* thresholds. On the other hand, the MP method compares the average NEE of the twenty u^* classes with the average NEE of the ten u^* classes with the greatest magnitude. A threshold is then determined if the u^* class contains a mean nighttime NEE greater than 99% of the mean NEE at the ten highest u^* classes. An improvement of this method has also been implemented that reduces the effects of noise. More details may be found in Pastorello et al., 2020.

To determine NEE uncertainties for this study, the REddyProc Software was used from the Max Planck Institute for Biogeochemistry. The software was utilized as a means to create reasonable bounds for NEE. The percent error between the exact (measured) and approximate (gap-filled) cumulative annual NEE was calculated to determine uncertainty. Most uncertainties were within 10% of the measured values for all sites and years except for CA-Oas. This discrepancy is believed to be due to the disparate flux processing methods used at the site.

2.4.4 Gap Filling

Due to the great temporal resolution of EC flux measurements, gaps in data are not uncommon. These may be due to various reasons (i.e. winter power failures, dusty solar panels, etc.). Since one of the many purposes of EC is to compile averages of C fluxes over long time scales, it is essential to have sophisticated techniques for filling in missing data. According to the discussion in Papale, 2012, there are multiple methods for gap filling, including mean diurnal variation (MDV), look-up tables (LUT), artificial neural networks (ANNs), and nonlinear regressions.

The MDV approach fills gaps by taking the average of valid values on adjacent days during the same period. It is recommended that the length of the averaging period doesn't exceed two weeks since after this time nonlinear dependencies may introduce significant uncertainties and errors. The position of the averaging periods may be fixed or may vary depending on the data. Preferably, the latter should be used since periods will be defined based on each gap, resulting in more accurate results.

LUT looks at meteorological conditions for missing fluxes and then gap-fills with the average of valid flux measurements during similar conditions. Several classes of meteorological drivers (e.g. radiation, air or soil temperature, soil water content, vapor pressure deficit, etc.) are considered depending on site characteristics. These are then tabulated and "looked-up" in order to gap-fill fluxes accordingly. Linear interpolation is used if no flux data is available for a specific combination of the drivers.

ANNs consist of empirical nonlinear regression models that predict missing fluxes through various algorithms. These operate in a set of nodes and are connected to weights that represent different regression parameters. To utilize an ANN, it must first be "trained". Training involves feeding sets of data to the ANN (usually meteorological drivers) and receiving the associated outputs. The dependency of the output on the meteorological drivers is mapped onto the weights which ANN then uses to gap-fill the data. This method is used as a standard technique for gap-filling fluxes in the FLUXNET global network (along with marginal distribution sampling which is an extension of LUT; see Reichstein et al.).

Similar to the LUT method, the nonlinear regressions approach bases its gap-filling on relationships between CO_2 fluxes and its associated drivers. Instead of tabulating data, however, parameterized nonlinear equations are used to estimate missing data. Daytime gap-filling typically takes PPFD to be the main driver and uses a rectangular hyperbola or exponential function for estimation (Falge et al., 2001). Due to lack of PPFD during the nighttime, equations where temperature is the main driver are used instead (Lloyd and Taylor, 1994; Falge et al., 2001; Moffat et al., 2007). To obtain estimations for gap-filling, the inputs for these equations must all be valid fluxes.

It's important to note that while there are a variety of gap-filling techniques, methodological comparison studies have shown most approaches to agree with synthetic data on several timescales (Moffat et al., 2007; Desai et al., 2008). However, other factors, such as ease of use, may lead researchers to employ one method over another.

2.4.5 Partitioning Fluxes

Due to technological limitations not allowing for direct measurements of GPP and RECO, these dependent variables must be inferred from measured NEE via equation 6:

$$NEE = RECO - GPP \quad (6)$$

To obtain an estimation of NEE, the following equation is used:

$$NEE = F_C^{EC} + F_C^{STO} \quad (7)$$

where F_C^{EC} is the estimated turbulent CO_2 flux via EC through the horizontal plane at an arbitrary height above the canopy and F_C^{STO} is the change in CO_2 storage below the horizontal plane (see sections 1.4.2 and 2.5 in *Eddy Covariance* (Foken et al., 2012; Munger et al., 2012)). Many methods have been proposed on how to partition NEE into its constituent fluxes. One of the most popular is the night-time data based method.

The night-time based approach exploits GPP's heavy dependence on radiation. After data has been quality filtered, all night-time data points for NEE are assumed to represent RECO (i.e. GPP is zero). A simple model of RECO's dependence on TA is then formulated. One of the most common methods is using the Q_{10} equation:

$$RECO = RECO_0 \bullet Q_{10}^{\frac{T-10°C}{10°C}} \quad (8)$$

where $RECO_0$ is the base respiration at 10°C, T is the TA, and Q_{10} is the temperature sensitivity parameter which represents the change in RECO for every 10 °C change in temperature. After calculating RECO, equation 6 is used to calculate GPP.

Unfortunately, RECO is driven by a multitude of other variables (e.g. nutrient levels and soil moisture) causing this method to introduce possible errors and biases. The lack of measurements of these variables at FLUXNET sites is one of the main reasons why nutrient level and soil moisture-dependent models are lacking (Reichstein et al., 2012).

Other models include using variants of the Arrhenius equation (Lloyd and Taylor, 1994) or using soil temperature-dependent models such as the Eyring function (Sulman and Desai et al., 2009). Although a myriad of flux partitioning methods are available, no single technique produces more desirable results (Desai et al., 2008).

2.5 Flux Instrumentation

The instrumentation at all flux tower sites was virtually the same. Each was equipped with a sonic anemometer (Campbell Scientific, Inc., Logan, UT, CSAT-3), open path infrared gas analyzer (LiCor, Inc., Lincoln, NE, LI-7500A), temperature and relative humidity sensor (Campbell Scientific, Inc., Logan, UT, CS215), radiation sensor (Kipp & Zonen North America, Sterling, USA, Kipp-Zonen CNR4), and quantum sensor (LiCor, Inc., Lincoln, NE, LI- 190). These measured three-dimensional wind speed and sonic virtual temperature, CO_2 and water vapor mixing ratios, solar radiation, and photon flux, respectively. At US-Syv, the closed path infrared gas analyzer model was LI-6262 instead. The height of the flux tower at Allequash Creek and Lost Creek was 2.4 m and 10.2 m respectively (Turner et al., 2019; Reed et al., 2018). For the Sylvania site, CO_2 flux measurements were taken at ~36 m above the ground whereas latent and sensible heat fluxes were taken at ~30 m above ground.

These instruments recorded data at high frequency (10 Hz) but were then averaged and reported as half-hourly after processing. More detailed descriptions for the instrumentation at US-ALQ and US-Los are outlined in Reed et al., 2018 and Turner et al., 2019. Further information on instrumentation at US-Syv can be found in Desai et al., 2005.

Willow Creek had differing instrumentation than that of the other sites. Four sensors were used to determine incoming and reflected solar and infrared radiation (net radiation was calculated by summing measurements from the four sensors). Like the other sites, a quantum sensor (Li-Cor, Lincoln, NE, model LI190SZ) was used to determine PPFD. Temperature probes (R.M. Young, Traverse City, MI, model 41342; Campbell Scientific, Inc., Logan, UT, model CS500) were placed throughout the height of the tower and directly above the soil surface to measure TA. More detailed descriptions of instrumentation can be found in Cook et al., 2004.

Instrumentation at Scotty Creek, CA-WP1, and CA-Oas may be found in Helbig et al., Syed et al., and Blanken et al. respectively.

2.6 USGS Gage Instrumentation/Methods

All streamflow measurements made by the USGS follow a similar protocol. Streamgages are unable to measure discharge directly. Instead, these instruments directly measure stream velocity, stream depth, and stream width and then mathematically compute streamflow using the following equation:

$$D = (d)(w)(v) \quad (9)$$

Where D is discharge and d, w, and v are stream depth, width, and velocity respectively. The units for discharge are typically given in $\frac{ft^3}{s}$. While depth and width can be calculated relatively easily across many sites, stream velocity measurements are less trivial. The most common methods used include *The Mechanical Current-Meter Method* and *The Acoustic Doppler Current Profiler Method (ADCP)*. The former involves partitioning depth and width measurements in a way that resembles the Riemann Sum approximation. The stream velocity is then measured by placing a wheel of metal cups in each segment. As water flows, the cups rotate around a vertically oriented axis which then prompts an electric signal transmission. This signal counts the number of revolutions per unit time which is then converted to linear water velocity. Each partitioned width and height is multiplied by its respective water flow quantity and are then summed together to determine the stream velocity.

The latter method improves measurement accuracy by taking advantage of the doppler effect. ADCPs are hydroacoustic instruments that send pulses into the water and then measure the amount of time it takes for signal retrieval. The relative change in frequency is then translated into water velocity.

2.7 Data Acquisition and Analysis

The Ameriflux data repository was used to acquire all C, water, energy, and micro-meteorological data for all sites. Therefore, all data measurement and processing methods adhere to standard Ameriflux protocols (https://ameriflux.lbl.gov/). All temperate sites are located within a 50 km radius. CA-SCB/CA-SCC and CA-WP1/CA-Oas are within a 0.1 km and 230 km radius respectively.

Each site has a different time period of available data. US-ALQ's data availability is from 2015-01-01 to 2021-04-25, US-Los from 2000-01-01 to 2020-12-31, US-Syv from 2001-01-01 to 2020-12-31, and US-WCr from 1998-01-01 to 2020-12-31. CA-SCB, CA-SCC, CA-WP1, and CA-Oas have data available from 2014-01-01 to 2019-09-21, 2013-01-01 to 2016-08-30, 2003-01-01 to 2009-12-31, and 1996-01-01 to 2010-12-31 respectively. Gap-filling was carried out using the nonlinear regression technique (see section 2.4.3) and a flux partitioning method was used similar to Reichstein et al. (see section 2.4.4). Even after gap-filling, missing data was still present.

For variables where three-index position qualifiers were used (i.e."VariableName_HorizontalPosition_VerticalPosition_Replicate"), the position qualifier "VariableName_1_1_1" was chosen. More information on positional qualifiers and their use in data labeling can be found on the Ameriflux Website (https://ameriflux.lbl.gov/) → Data → About Data → Data Variables.

The Streamflow data was obtained from proximate USGS gage locations at each site (excluding US-WCr and boreal sites; see section 2.3; https://www.usgs.gov/). Relatively minimal data gaps were present in the gage data.

Regression analysis between PPFD and NEE was plotted via numpy's polyfit command in Python. We then obtained numerical values for the Pearson correlation coefficient and p-value using the "pearsonr" function in the Scipy Python library. Due to the non-linear relationship between C components and TA (Fei et al., 2017), we utilized a quadratic fit for GPP and NEE and an exponential fit for RECO (see section 3.2.4). The numpy polyfit function was then used to implement fits across years. To determine the r^2 and p values for these fits, the "Real Statistics

Data Analysis Tool" external Microsoft Excel package was utilized along with the scatter plot function.

2.8 Wavelet-Based Time Scale Decomposition

The maximal overlap discrete wavelet transform (MODWT) was used to decompose the time scales of variability for NEE, GPP, RECO, and various C drivers. These half-hourly fluxes (hourly for discharge) were reconstructed for scales 1 (2^1 measurements equal to 1 hour) to 14 (2^{14} measurements equal to 341 days). Scales 1-2, 3-6, 7-10, and 11-14 represent hourly (small perturbations such as clouds passing overhead), diel (day-night cycles of radiation and temperature), multiday (variabilities in water table and synoptic weather), and seasonal (vegetation phenology, solar cycle, and hydrologic cycle) scales respectively (Sturtevant et al., 2016). The Wavelet Methods for Time Series Analysis (WMTSA) as part of the MATLAB wavelet toolkit was utilized to wavelet decompose data into these scales (Cornish et al., 2003). Due to this toolkit's incompatibility with data gaps, all gaps were dropped during analysis.

2.9 Mutual Information

In information theory (Shannon 1948), mutual information describes the mutual dependence between two random variables. Its purpose is to measure how much information may be received from one variable through observation of the other variable. In other words, it is defining the mean tendency for a single paired state of two variables to co-exist (Fraser & Swinney, 1986). Since this method calculates the statistical dependence of Y on X, it lends itself to be an appropriate approach for resolving C flux-driver relationships (Knox et al., 2021).

In this study, we input one of the variables to be NEE and the other to either be GPP (no half-hourly data for CA-Oas), RECO, PPFD (incoming shortwave radiation was used for CA-SCB), TA, LE, or discharge (streamgage data only available for US-ALQ, US-Los, and US-Syv; no yearly scale analysis was conducted due to limited resolution). A mutual information score (MIS) was then calculated between NEE and the other variable to determine the extent of dependence. High and low magnitudes of MIS indicate stronger and weaker links between NEE and the other chosen variable, respectively.

One weakness with utilizing this method is the MIS's high dependency on the number of sampled data points. To account for this, we used a histogram approach. A set number of bins were determined depending on each site's number of data points n via the equation

$$\sqrt{n/5} \qquad (10)$$

On average, equation 10 provides five points for each cell on the histogram for two uniformly distributed random variables. This technique mirrors the adaptive partitioning approach discussed in Cellucci et al. Since all MISs are now characterized based on n, direct comparisons between sites is now possible.

3. Results

3.1 Interannual Variation of NEE

Among the temperate sites, the deciduous broadleaf forests had the largest range of annual cumulative NEE relative to the wetland sites. US-ALQ (2 years of data) and US-Los (15 years of data) had ranges of 17 and 193 g C m^{-2} yr^{-1} respectively. For US-Syv (12 years of data) this was 362 g C m^{-2} yr^{-1} and for US-WCr (16 years of data) it was 551 g C m^{-2} yr^{-1}. Similar results were found for the boreal sites. CA-SCB (3 years of data), CA-WP1 (6 years of data), and CA-Oas (10 years of data) had ranges of 85, 265, and 382 g C m^{-2} yr^{-1} respectively. CA-SCC (2 years of data), however, saw a range of only 10 g C m^{-2} yr^{-1}. This site is composed of mostly evergreen needleleaf forest and therefore has different carbon dynamics than that of a deciduous broadleaf. An alternative and more likely explanation for this discrepancy is a lack of sufficient data.

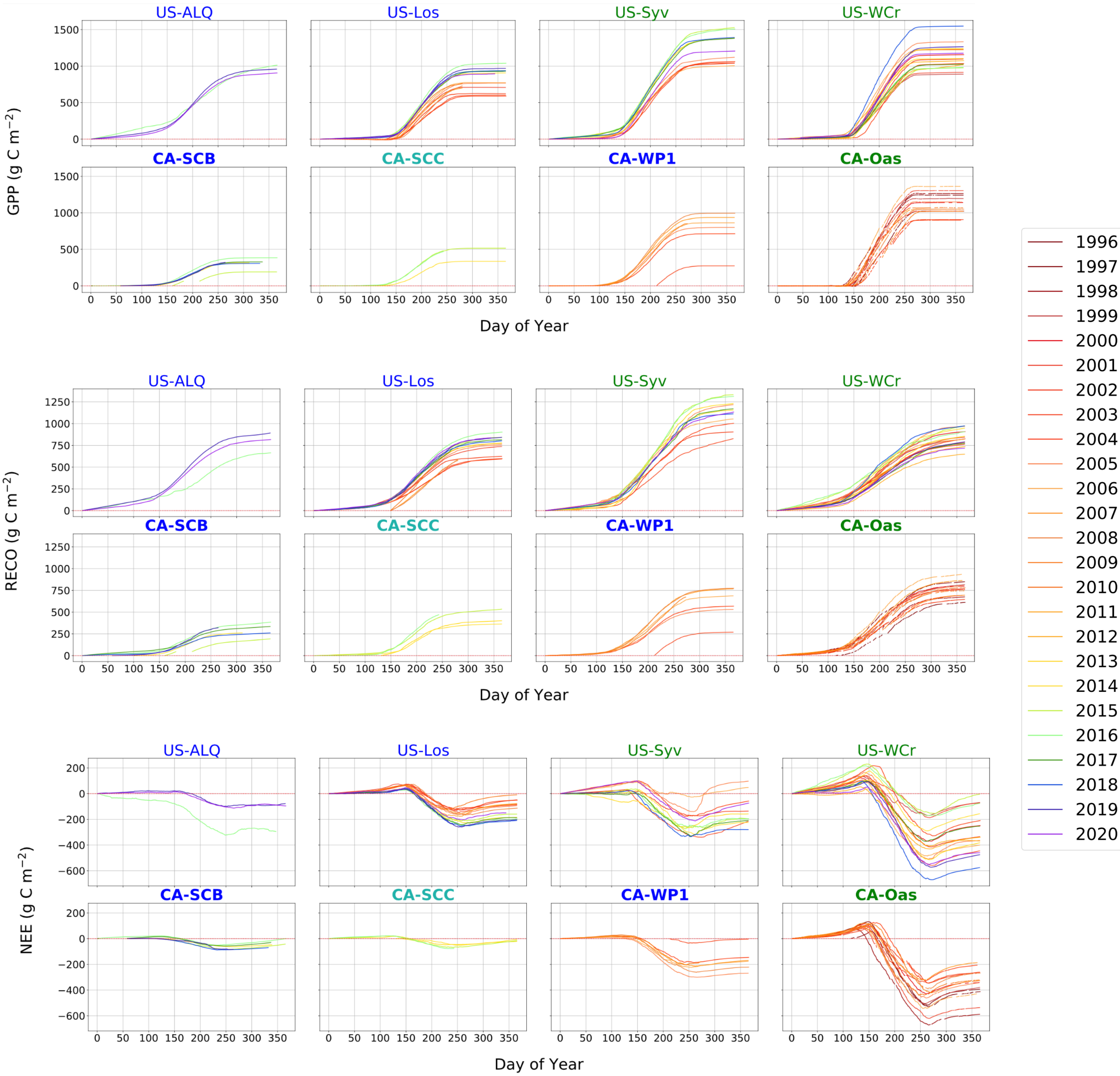

Figure 3: *GPP (top), RECO (middle), and NEE (bottom) over each measured year and across each site. Sites in green, blue, and turquoise represent deciduous broadleaf forest, permanent wetland, and evergreen needleleaf forest ecosystems respectively. Bolded names indicate boreal sites while non-bolded names show temperate sites.*

All sites transitioned from C source to sink in a similar window period (between DOY ~150-200). For the temperate region, yearly NEE variability was found to be substantially smaller at the wetland site (US-Los) than at the forest sites (US-Syv and US-WCr). On the last DOY, NEE at US-Los varied between -209 and -9 g C m^{-2} yr^{-1} across years, while at US-Syv and US-WCr, it was between -280 and 97 & -575 and -4 g C m^{-2} yr^{-1} respectively (**Figure 3**).

Annual sums of GPP at the temperate sites were greater at the deciduous broadleaf/mixed forest sites relative to the wetland sites. On the other hand, RECO was similar in magnitude across the sites with the exception of US-Syv. None of the sites were dominators in terms of NEE annual sums across all years. From 2002 to 2006, US-WCr was the greatest sink whereas US-Los and US-Syv had comparable NEE annual sums. From 2014 to 2020, NEE was still comparable between US-Los and US-Syv but US-WCr experienced dramatic fluctuations. From 2011-2013 and 2017-2020, US-WCr was a stronger sink than US-Los and US-Syv but from 2014-2016, US-WCr's NEE became more positive than that of the other sites.

Boreal sites were also found to be carbon sinks across all years and were comparable to their temperate counterparts (**Figure 4**). The deciduous broadleaf forest site (CA-Oas) was recorded to have a larger carbon sink potential relative to the wetland site (CA-WP1). CA-SCC and CA-SCB had limited data but the former saw higher rates of GPP and RECO relative to the latter for adjacent years (2014-2016). Due to the near equal partitioning of NEE, both biomes became either carbon neutral or modest carbon sinks during the measured years (**Figure 4**).

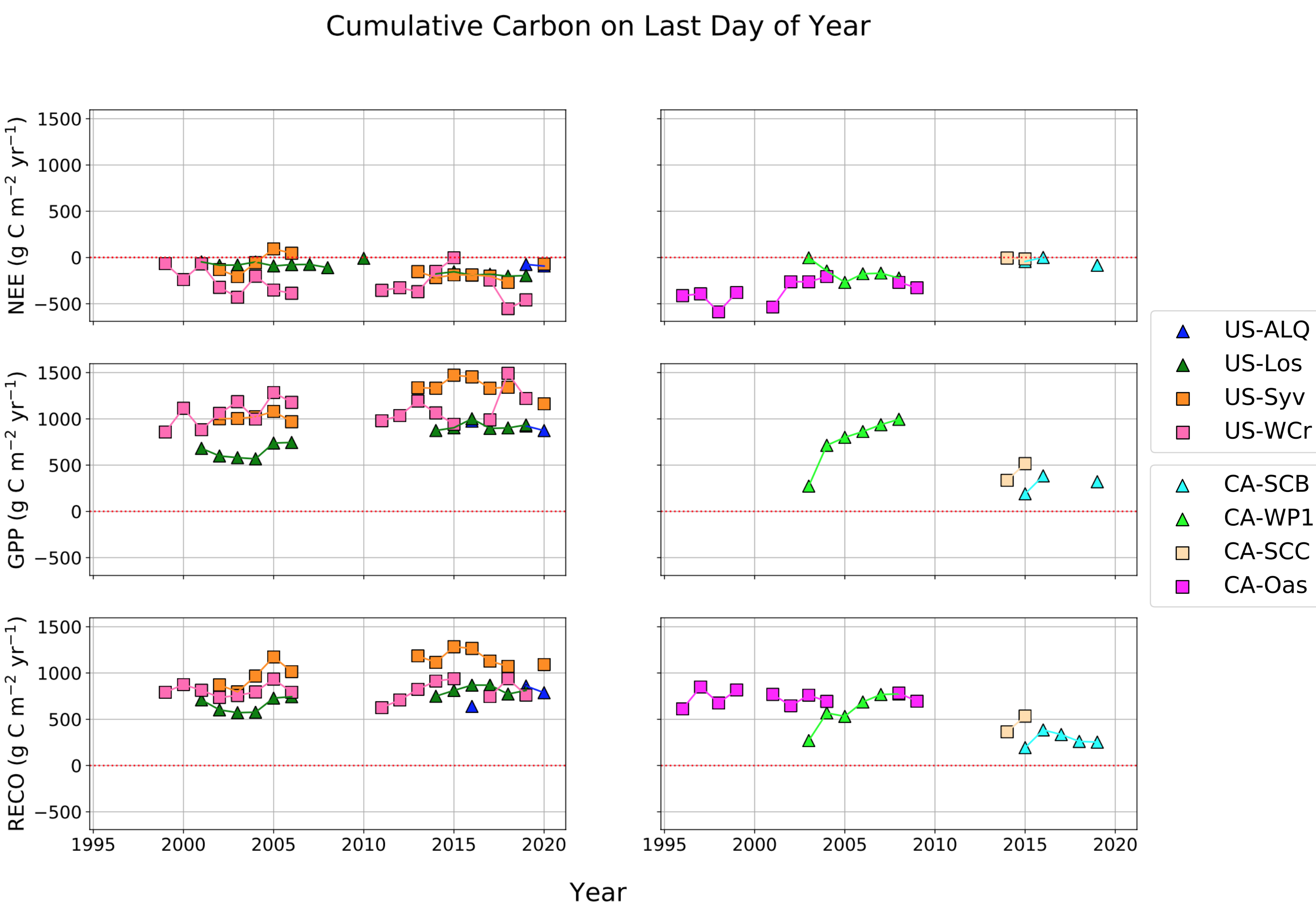

Figure 4: *Annual sums (i.e. cumulative sums on last DOY) of NEE, GPP, and RECO for US-ALQ (blue), US-Los (green), US-Syv (orange), US-WCr (pink), CA-SCB (cyan), CA-WP1 (lime), CA-SCC (navajo white), and CA-Oas (magenta). Triangle and square markers indicate wetland and forest ecosystems respectively. Dotted red line denotes zero NEE (i.e. when GPP equals RECO).*

3.2 NEE Zero-Crossing Day

Both types of temperate ecosystems had an NEE zero-crossing day (ZCD) within the range of the 150th (May 30th) and 210th (July 29th) day of the year (DOY). US-Los saw an earlier NEE sign change for each year from 2001-2020, while US-Syv and US-WCr were more variable (**Figure 5**). From 2002-2005, the minimum and maximum DOY when US-Syv became a net C sink was 138 (May 18th) and 189 (July 8th) respectively. The site then saw a steady earlier NEE sign change from 2014-2018 and became a C sink relatively later in 2020. US-WCr's DOY sign change was also very variable with no specific trend throughout the measured years (not shown).

For the boreal sites, CA-Oas experienced moderate variability with its average ZCD being around day 170 (June 19th). On the other hand, CA-WP1 became a net C sink during later parts of the year after 2005. We also found a steady earlier ZCD for CA-SCB and CA-SCC, but more data is needed to determine long-term trends (not shown).

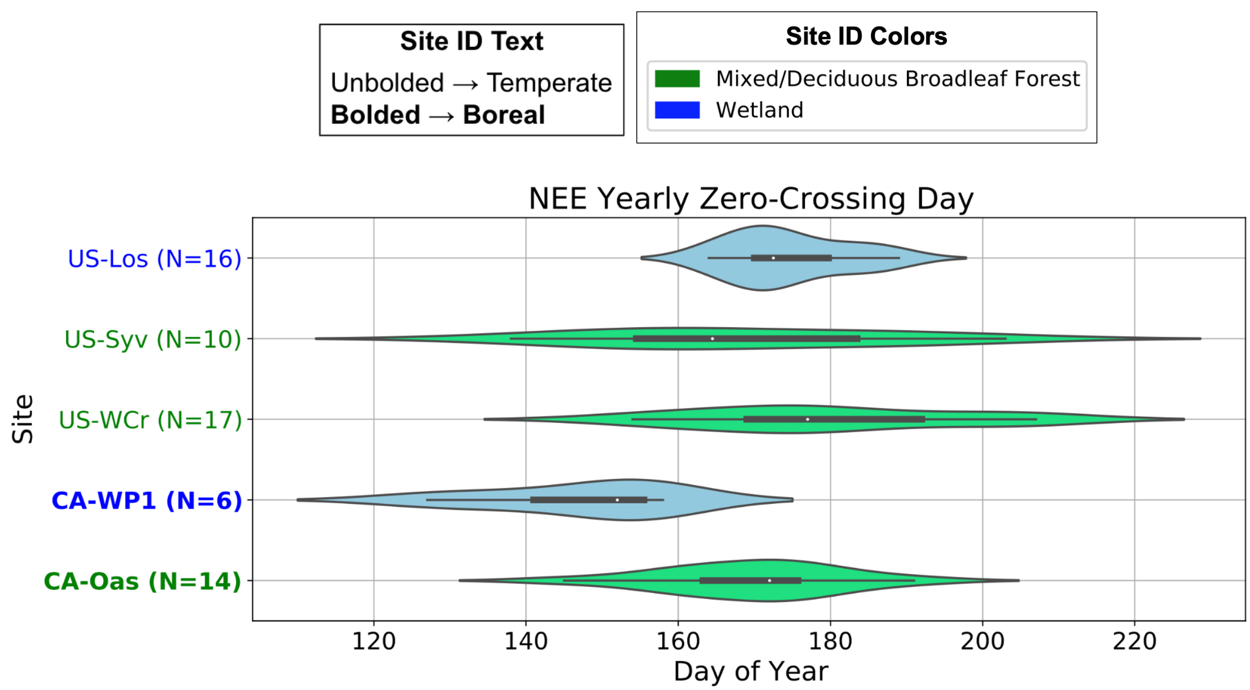

Figure 5: *Violin plot showcasing day of year when cumulative NEE flipped sign (from positive to negative) indicating when sites transitioned from being a net C source to a net C sink during the growing season (roughly defined from April 1st to October 31st).*

3.3 Component Fluxes

GPP annual sums were also found to be larger than most of the RECO annual sums at the sites. In general, US-WCr and CA-Oas experienced higher GPP values than US-ALQ, US-Los, and CA-WP1 (**Figure 6**). US-Syv had approximately the same yearly sum of GPP and RECO over the studied years. Cumulative GPP showed a similar trend across all sites and all studied years. Each site initiated GPP at ~150th DOY. There was year to year variability, however, for GPP annual sums, with US-Syv showing more IAV on average than US-WCr and US-Los. In comparison, average year-to-year variability for RECO annual sums were almost identical across all sites. RECO began earlier at US-WCr for most years (between DOY 50 and 100) and had a smoother curve. US-Los and US-Syv, on the other hand, initiated RECO at around DOY 150 and saw steeper slopes as they entered summer months (**Figure 4**).

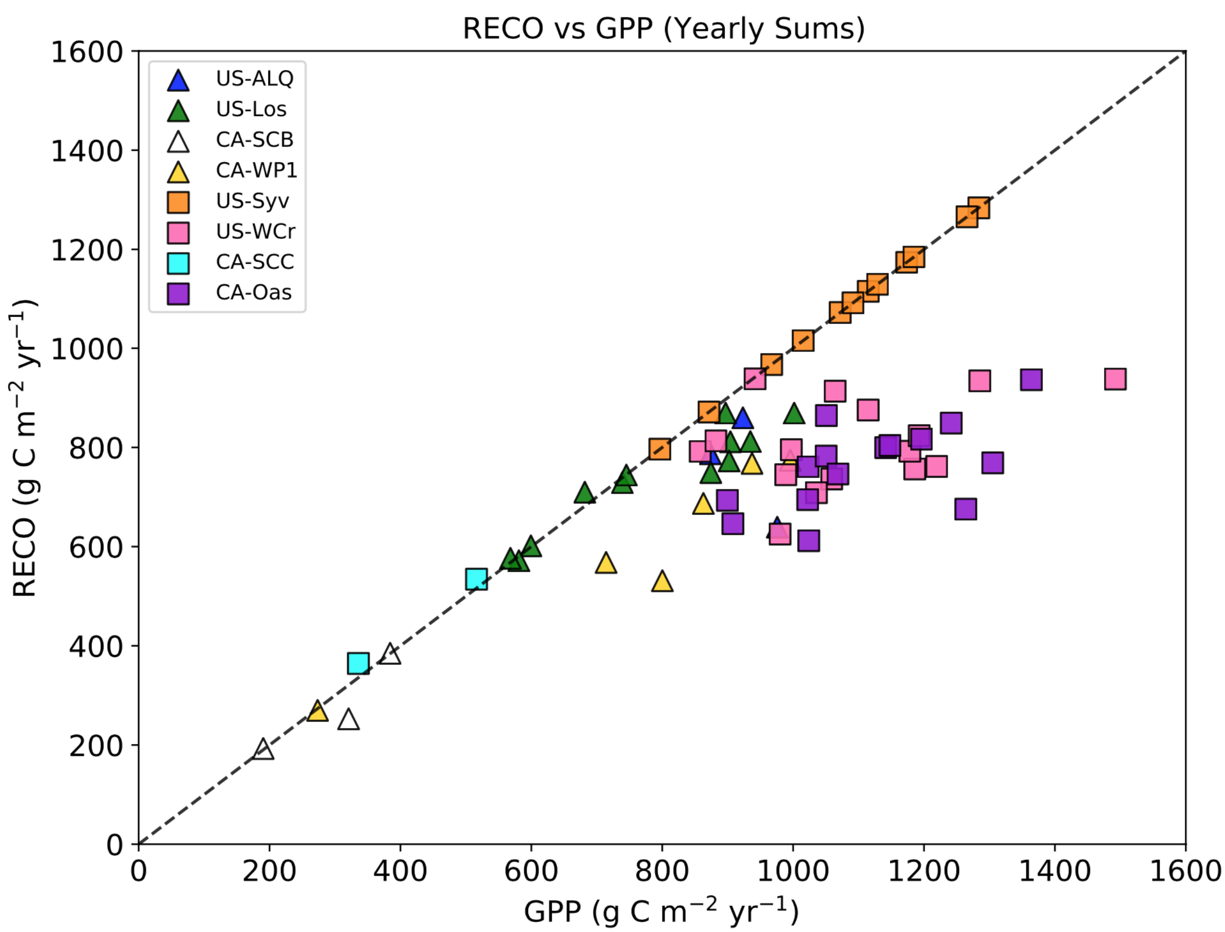

Figure 6*: Yearly sums of RECO plotted as a function of yearly sums of GPP for all sites. Squares represent forest sites and triangles represent wetland sites. The dotted line indicates a one-to-one relationship between the two variables.*

3.4 Drivers of IAV

3.4.1 Radiation

One of the main drivers of C accumulation across all sites was PPFD. As PPFD increased, NEE decreased most significantly during the months of June through September for the measured years. GPP's sensitivity to solar radiation caused a dramatic increase in production during these months, causing the second term on the right side of equation 6 to dominate. This is also reflected in (**Figure A.3)** and (**Table A.3)**, with the relationship between the two variables exhibiting a steeper positive slope (increased r-value) in the summer months for both wetlands and forests. Ultimately, this led to a general decrease in NEE during the summer months across all sites and years (**Figure A.2**; **Table A.2**).

Even though PPFD was found to be a driver for C accumulation on a multi-year scale, the correlation coefficient experienced substantial interannual variation. For the forest sites, the correlation between NEE and PPFD was somewhat constant over the years, with the strongest dependency occurring in August (not shown). The wetland site experienced the most variability across years, with a general increase in PPFD reliance for C accumulation over the two decade period. On average, Pearson correlation coefficients for NEE vs PPFD and GPP vs PPFD were -0.799 and 0.804 respectively from 2001-2010.

Of the three summer months, US-Syv and US-WCr had consistent periods of higher correlation during July and August throughout the two decades. US-Los, however, was more variable in this regard, showing increases and decreases in radiation dependence across all months and years (not shown).

3.4.2 Precipitation

Average cumulative precipitation across all years was greatest at US-WCr (mean ± standard error: 685 ± 38 mm) followed by US-Los (677 ± 69 mm) and US-Syv (378 ± 83 mm). The wettest recorded years for US-Los were 2002, 2007, and 2008, for US-Syv 2002, 2005, and 2016, and for US-WCr 2002, 2016, and 2017.

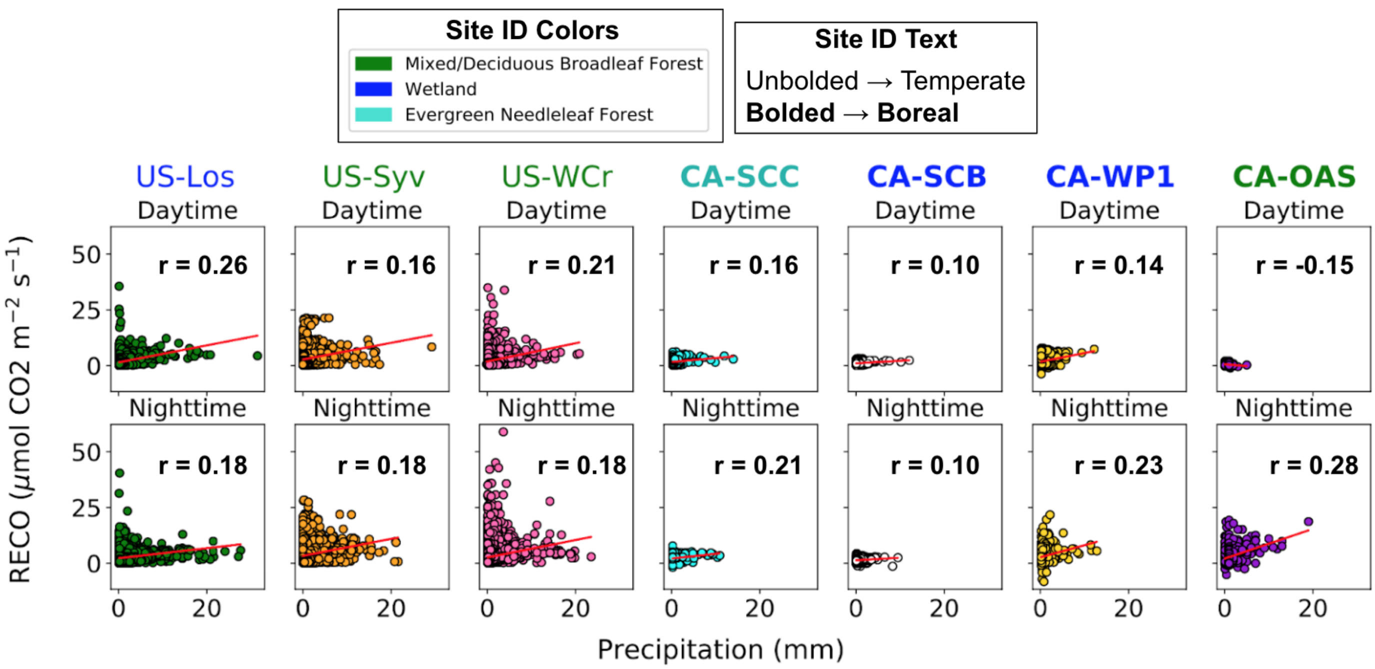

Figure 7: *RECO as a function of precipitation at half-hourly scale across sites during daytime (9:00:00 - 17:00:00) and nighttime (17:30:00 - 24:00:00; 00:30:00 - 8:30:00). All r-values had p-values less than 0.05. US-ALQ did not have precipitation data at the time of the study. Statistically insignificant and weaker correlations were found for GPP and NEE (not shown).*

P and carbon component data were divided into daytime and nighttime segments to determine relationships with and without solar radiation. Daytime and nighttime were defined as hours from 9:00:00 to 17:00:00 and from 17:30:00 to 24:00:00/00:30:00 to 8:30:00 respectively. CA-SCC, CA-SCB, and CA-WP1 utilized rainfall data instead of precipitation data. All P at 0 mm was dropped. GPP did not have any significant relationship with P during the daytime or nighttime across sites (not shown). RECO was generally positively correlated with increases in P. Daytime correlation with RECO was higher among the boreal sites while during the nighttime, RECO showed higher correlation among the temperate sites. The RECO-P relationship was not significantly affected by the type of ecosystem (**Figure 7**).

3.4.3 Air Temperature

Monthly averaged TA was found to be nearly identical across all sites, with temperatures generally residing between -16 and 22 °C. Yearly averaged TA, however, was more variable between sites. US-WCr was the warmest amongst the sites from 2001 through 2008. From 2015 through 2020, US-WCr starts out warmer but is then surpassed by US-Los beginning in 2017. US-ALQ had an abnormally warm year during 2015, but this is likely due to relatively high gaps in TA data during that year **(Table A.5)**. Excluding 2015, US-ALQ was cooler relative to US-Los and US-WCr during 2016, 2019, and 2020. Due to high amounts of data gaps during 2017 and 2018 for US-ALQ, TA was not considered during those periods (**Table A.5**).

To quantify the responses of GPP, RECO, and NEE to TA, quadratic (equation 10) and exponential (equation 11) regression models were used based on Fei et al., 2017:

$$f(x) = ax^2 + bx + c \quad (10)$$

$$RECO = d * e^{f\ (TA)} \quad (11)$$

where a, b, c, d, and f are fitted parameters, $RECO$ is ecosystem respiration, and TA is air temperature. The quadratic model was applied for GPP/NEE versus TA and the exponential model was utilized to evaluate the relationship between RECO and TA.

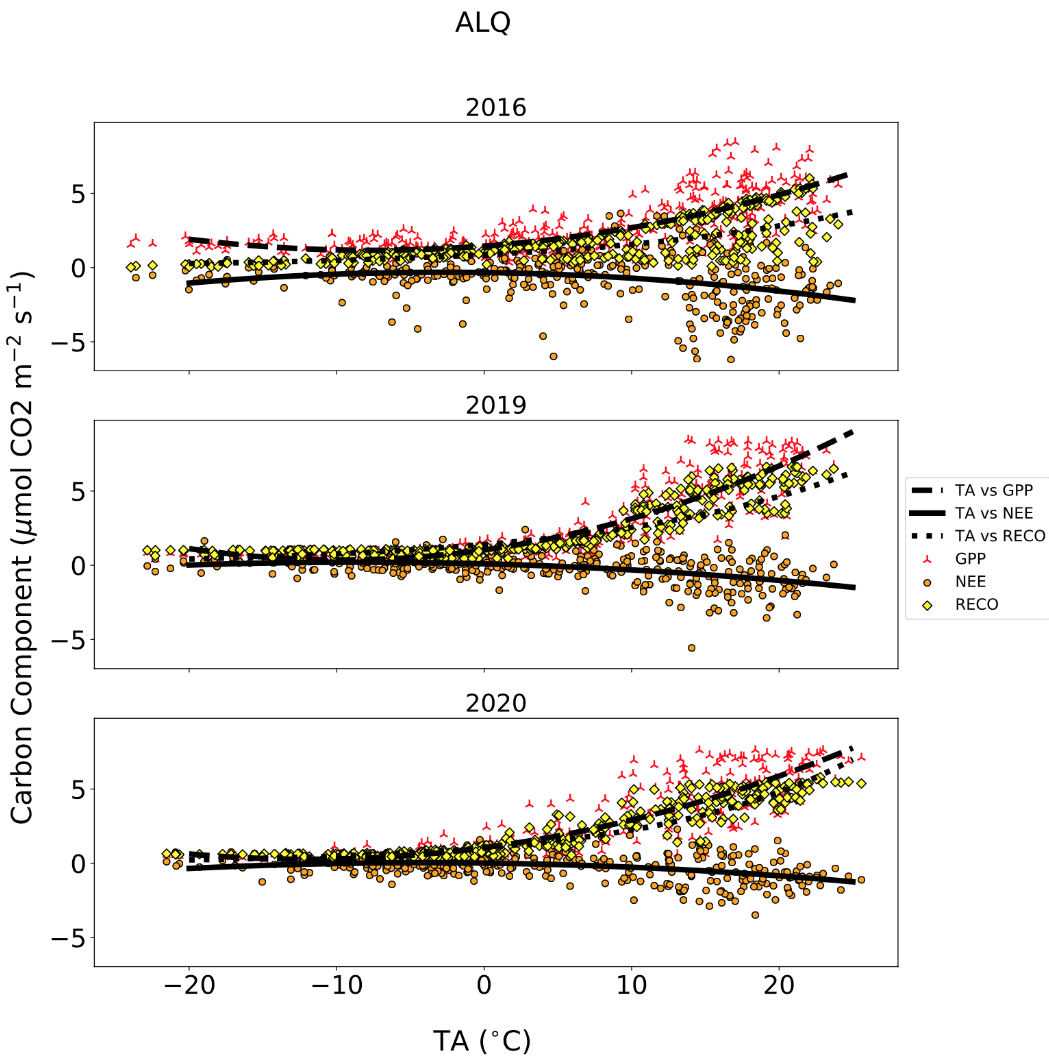

ALQ
2016
2019
2020
Carbon Component (μmol CO2 m−2 s−1)
TA (°C)
TA vs GPP
TA vs NEE
TA vs RECO
GPP
NEE
RECO

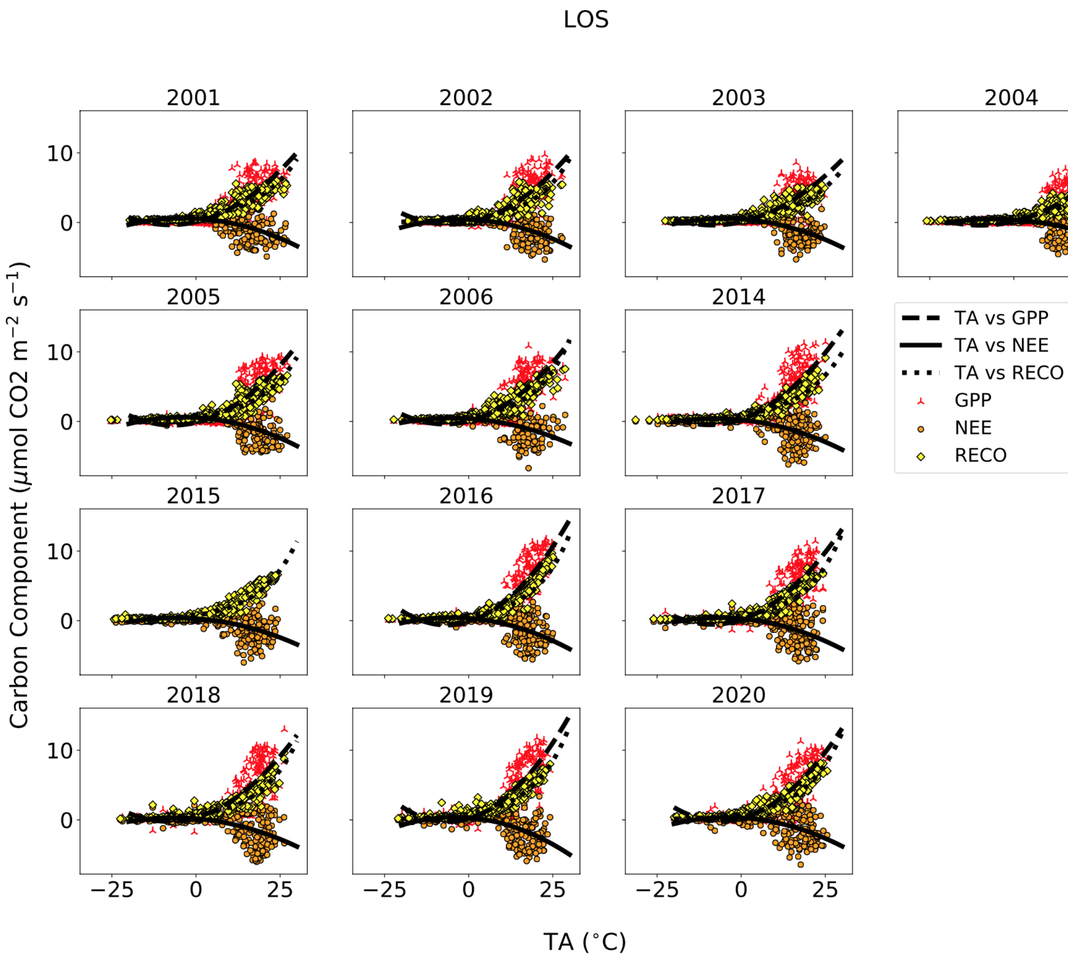
LOS
2001
2002
2003
2004
2005
2006
2014
2015
2016
2017
2018
2019
2020
Carbon Component (μmol CO2 m−2 s−1)
TA (°C)
TA vs GPP
TA vs NEE
TA vs RECO
GPP
NEE
RECO

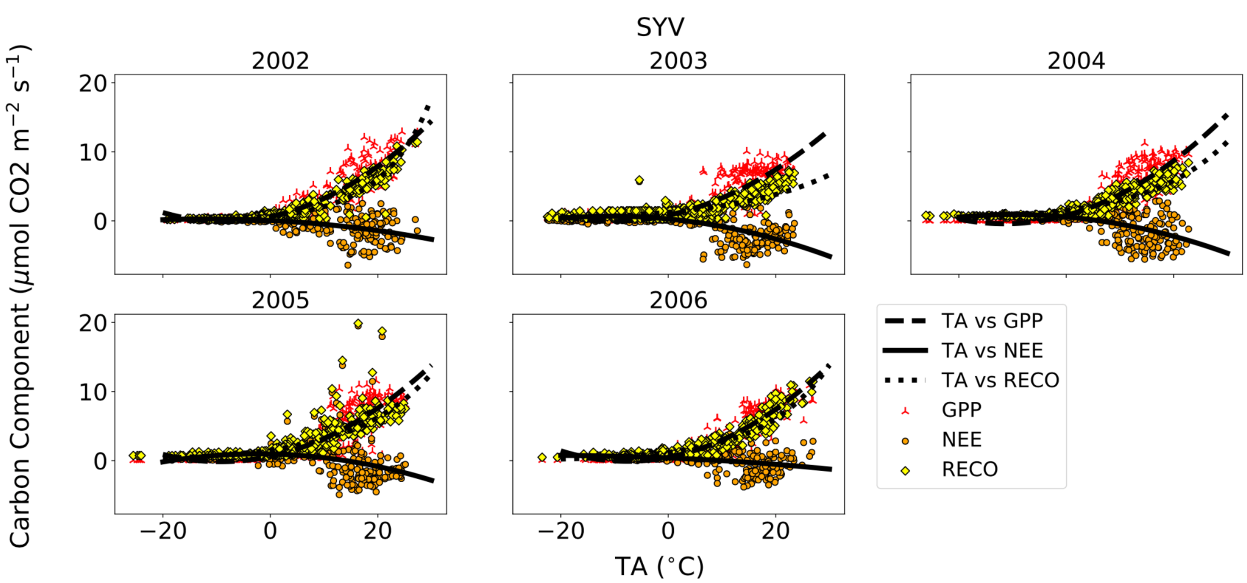
SYV
2002
2003
2004
2005
2006
Carbon Component (μmol CO2 m−2 s−1)
TA (°C)
TA vs GPP
TA vs NEE
TA vs RECO
GPP
NEE
RECO

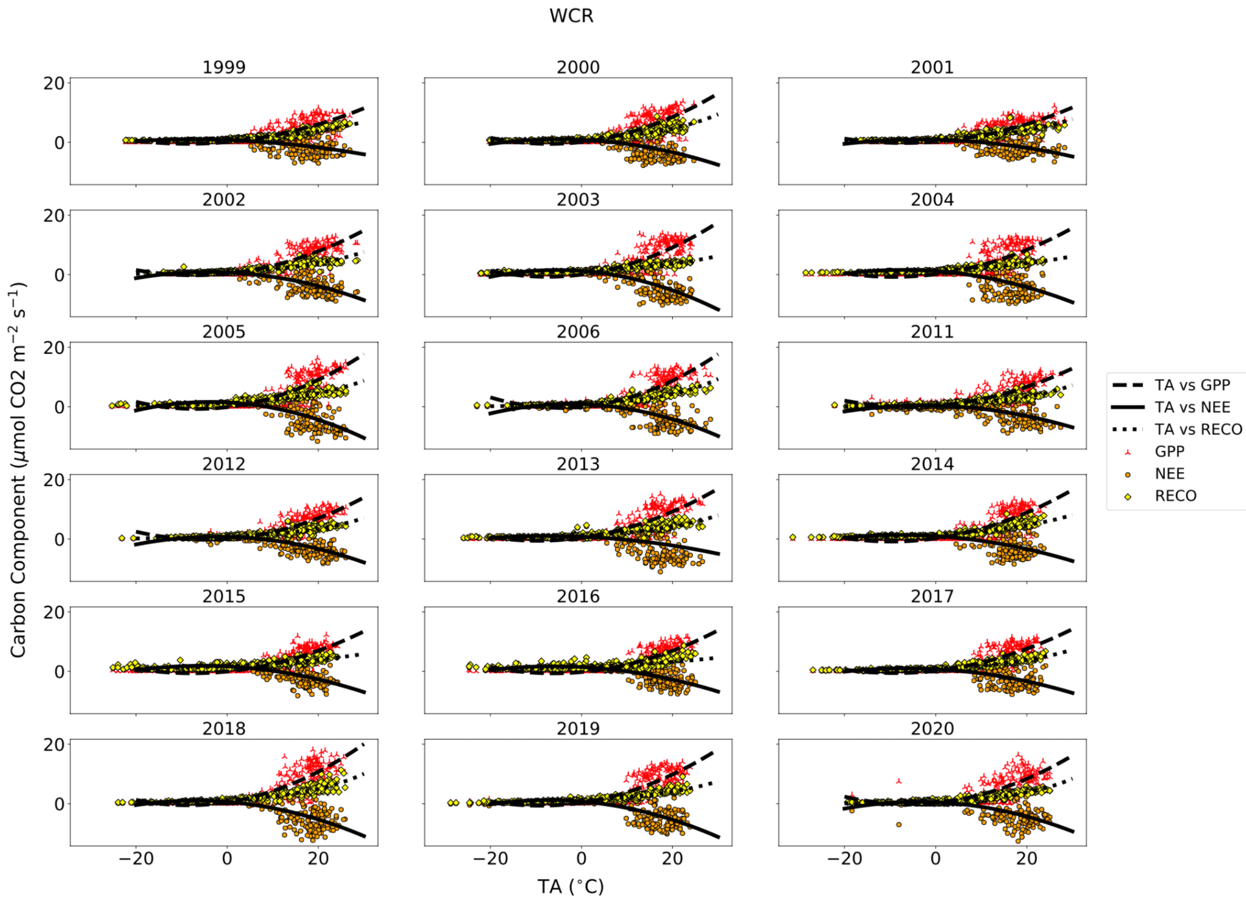

Figure 8: *Each C component plotted as a function of TA across all sites and years. GPP, NEE, and RECO are illustrated as red, orange, and yellow icons respectively. Black lines show regression fit, where dashed represents TA vs GPP, solid indicates TA vs NEE, and dotted shows TA vs RECO. Fits are based on equations utilized by [Fei et al., 2017](). Some years were not included due to gaps in both TA and C flux data.*

Overall, the regression models between the C components and TA agreed well across all sites and years (**Figure 8**). RECO was observed to increase exponentially with TA, while a quadratic relationship was found between NEE/GPP and TA. The regression equations were also variable from year to year. For equations representing RECO vs TA, the y-intercept term showed small variation (0.55 - 1.75 across all sites and years).

Due to its limited impact on the steepness of the regression curve, only the exponential growth constant was considered when determining TA's influence on RECO. When considering sites that had the least amount of data gaps (US-Los and US-WCr with n=13 and n=18 respectively), we observed the greatest impact of TA on RECO at US-Los relative to US-WCr (mean value for exponential growth constant was .09 and .06 for US-Los and US-WCr respectively). Furthermore, the variability of impact across years proved to be higher at US-WCr (SD = .012) than at US-Los (SD = .006).

To determine the extent of TA's impact on NEE/GPP, the year to year variabilities in the quadratic coefficient (QC) were considered. The average QC for GPP was .006, .008, .009, and .01 for US-ALQ, US-Los, US-Syv, and US-WCr respectively. The variability in QC (standard deviation) was similar across all sites. For NEE, all QC was found to be negative. The average QC was largest at US-WCr (-.006), followed by US-Los (-.003), US-Syv (-.0026), and US-ALQ (-.0018). The greatest variabilities in QC occurred at the forest sites (US-Syv: 0.001; US-WCr: 0.004) relative to the wetland sites (US-ALQ and US-Los: .0005).

3.4.4 Evapotranspiration

GPP was more impacted by increases in LE than RECO across all sites and years. RECO experienced a positive correlation with LE, with US-WCr having the lowest correlation relative to other sites (**Figure A.5**). In particular, increases in LE promoted GPP. Most Pearson correlation coefficients were calculated to be greater than 0.65 across all years and sites (**Table A.6**). Consequently, this resulted in an anti-correlation between NEE and LE across sites and years with most coefficients being less than -0.6. Some years experienced changes in RECO when LE was at 0 W m^{-2}, suggesting a more complex relationship between water balance and RECO at the sites.

3.5 Determining Dependency via Mutual Information

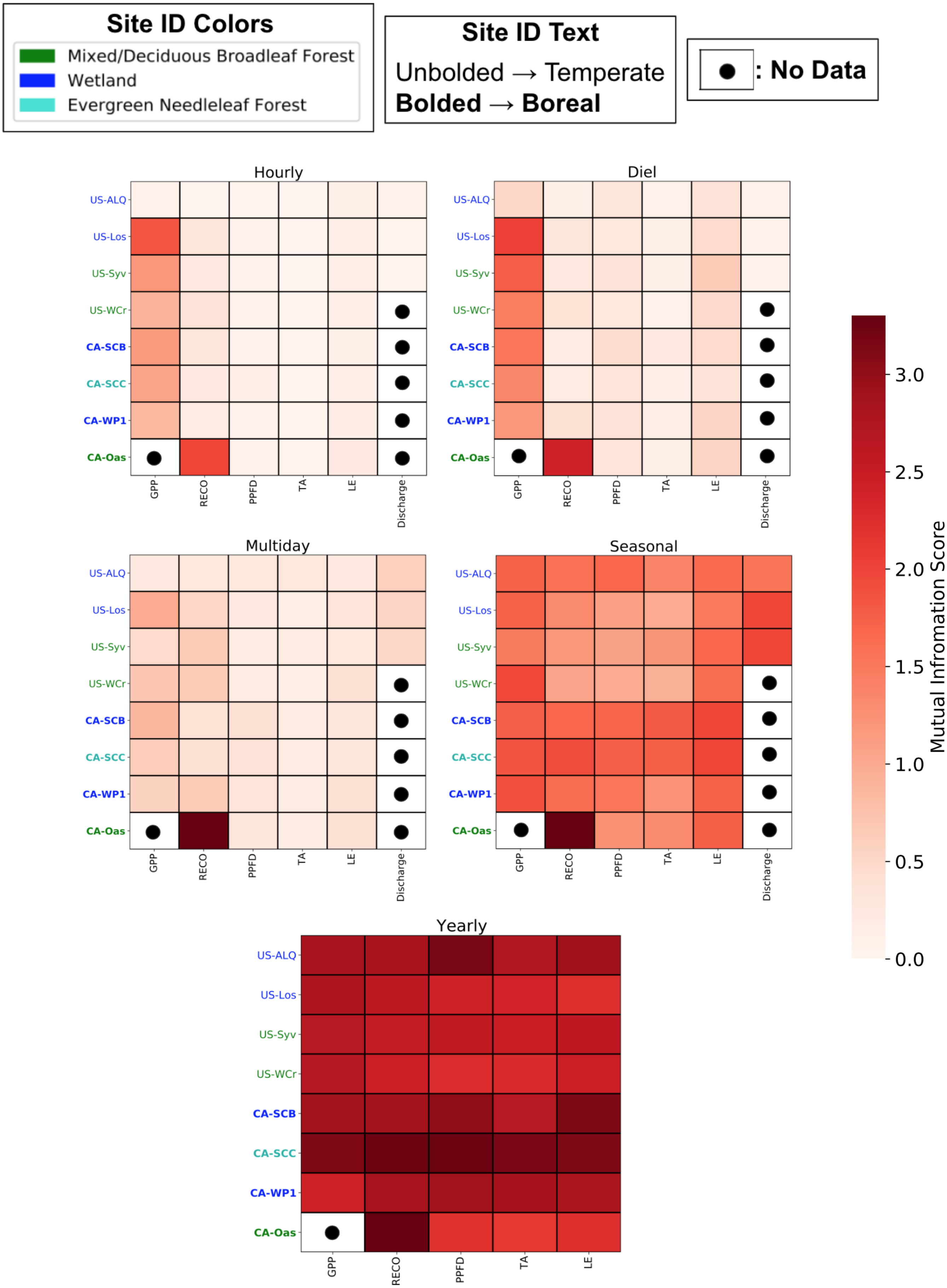
Site ID Colors
Mixed/Deciduous Broadleaf Forest
Wetland
Evergreen Needleleaf Forest
Site ID Text
Unbolded → Temperate
Bolded → Boreal
: No Data
Hourly
Diel
Multiday
Seasonal
Yearly
US-ALQ
US-Los
US-Syv
US-WCr
CA-SCB
CA-SCC
CA-WP1
CA-Oas
GPP
RECO
PPFD
TA
LE
Discharge
Mutual Infromation Score
3.0
2.5
2.0
1.5
1.0
0.5
0.0

Figure 9*:* *Barcode plots showing mutual information scores between NEE and environmental variables on multiple timescales. Black dots indicate no data availability. Blue, turquoise, and green text indicate wetland, evergreen forest, and deciduous forest respectively. Text in bold represent boreal sites while standard text are temperate sites.*

On hourly (1-2 hours) and diel (4 hours to 1.3 days) scales, GPP was the dominant predictor of NEE regardless of region or ecosystem type. On multiday (2.7-21.3 days), seasonal (42.7-341 days), and yearly scales, however, each variable showed indistinguishable magnitudes of predictability for NEE. The boreal sites saw more NEE predictability by biophysical variables relative to the temperate sites on long timescales (seasonal and yearly). Discharge did not have a drastically different NEE impact between sites and timescales (**Figure 9**).

4. Discussion

4.1 Interannual Variability and Ecosystem Type

One of the objectives of this study was to determine differences in C flux IAV between biome types in temperate and boreal regions. When partitioning NEE fluxes into its components, GPP was greater than RECO for both ecosystem types, resulting in negative NEE (**Figure 6**). GPP was more of an NEE predictor than RECO on short timescales (hourly and diel) for both the temperate and boreal wetland and forest sites (**Figure 9**).

Overall, the forest sites were found to have higher GPP. This is likely due to larger photosynthetic capacity and greater leaf area index, promoting high photosynthetic uptake relative to the wetland sites. These results agree with a comprehensive study that found deciduous forests to be one of the largest C sinks across the conterminous United States (Xiao et al., 2011).

In addition to higher uptake, the deciduous broadleaf forest sites experienced larger GPP variability with respect to the wetland sites. Due to productivity's high reliance on meteorological variables, year-to-year fluctuations in local weather patterns play a vital role in GPP IAV. This finding suggests an ecosystem type dependence as opposed to a regional dependence for year-to-year carbon uptake potential.

Ecosystem respiration was also found to have high IAV across sites, with similar variabilities at US-ALQ, US-Los, and US-WCr and the highest occurring at US-Syv (**Figure 3**). The boreal sites experienced similar RECO IAV with respect to one another.

A study observing a temperate mixed forest in northeastern China concluded that only leaf respiration increased among other modes of respiration (i.e. stem and soil) when TA increased (Guan et al., 2006). Even though RECO is not dominant when partitioning NEE fluxes, leaf respiration's high temperature sensitivity has the potential to influence IAV and must be taken into account. Research on 15 European forests from 1996 to 1998 has shown variabilities in RECO to be the main determiner of NEE, indicating its important role in influencing IAV magnitudes (Valentini et al., 2000).

The C sink/source status of an ecosystem depends on the relative magnitudes of GPP and RECO, with the biome becoming a source or sink if RECO or GPP dominates respectively. In general, cumulative annual NEE was more variable from year-to-year at the forest sites than at the wetland sites regardless of region. GPP and RECO were also subject to variabilities (to a lesser extent) based on ecosystem characteristics. This result agrees with the finding that NEE IAV is larger than that of GPP and RECO (Xie et al., 2014).

Due to higher GPP potential at the forest sites relative to the wetland sites, US-Syv and US-WCr were found to have more years where the magnitude of negative NEE was greater at the end of the year than that of US-Los. The cumulative NEE at the forest sites also did not follow a specific temporal trend on decadal scales. At US-Los, however, C uptake generally increased as years passed, with the greatest C uptake occurring during 2018 and 2019 and the least during 2000 and 2005 (**Figure 3**). Similar results were found for the boreal sites.

An increase in cumulative yearly NEE at the wetland site may be indicative of the fertilization effect as a result of increased atmospheric CO_2 concentrations. More years of C fluxes need to be measured, however, to be certain.

In addition to uptake on yearly scales, the forest sites generally had greater C uptake on seasonal scales. During the growing season, US-Syv and US-WCr had negative NEE that was ~1.5 and ~1.7 times more than US-Los on average. Year-to-year variabilities in growing season NEE were also larger at the forests versus the wetlands.

While NEE magnitude is helpful in determining the extent of C uptake, temporal variations in C fluxes must also be accounted for. One such measure is determining when NEE shifts from source to sink, indicating the first time when production rates surpass respiration rates. Due to significant increases in global temperatures in the past century, some ecosystems have been shown to respond with earlier leaf-out times and later senescence, therefore extending the growing season (Helfter et al., 2015). Only US-Los saw an overall earlier date of NEE sign change as years progressed. US-Syv and US-WCr were more variable in this regard. This was consistent with the boreal wetland and deciduous forest sites as well. CA-SCC (boreal evergreen needleleaf site), however, experienced similar yearly variabilities to that of the boreal wetland sites (CA-WP1 and CA-SCB).

Lengthier growing seasons have implications for higher rates of productivity. Therefore, consistently experiencing longer growing seasons as years progress may cause the wetland sites to reach GPP levels that are comparable to that of the deciduous forests. On the other hand, high IAV in NEE zero crossing day may prove inefficient for sustained C uptake on long timescales.

4.2 Drivers of Interannual Variability and Implications

Ecosystems owe their year-to-year C variability to external factors such as PPFD, TA, and water availability. Our results agree well with the notion that increases in PPFD and TA promote higher ecosystem productivity in both wetlands and forests (Froelich et al., 2015; Helfter et al., 2015). Therefore, longer periods of warmer temperatures and larger areas of foliage are amongst the most ideal conditions for enhanced GPP. It is important to note that linear regression has obvious shortcomings as an analysis tool, in that it is blind to non-linear relationships. Therefore, a lack of linear correlation with water parameters (i.e. precipitation and discharge) indicates a more sophisticated relationship between water availability and NEE (i.e. through changes in soil moisture (Xu et al., 2004)).

Precipitation's influence on C fluxes at US-Los, US-Syv, and US-WCr were observed to be modest when compared to those of other variables. When partitioned into daytime and nighttime sections, precipitation had more explanatory power for changes in NEE across all temperate sites, while GPP was not affected (**Figure 7**). RECO at US-Los was found to have a higher reliance on precipitation relative to US-Syv and US-WCr during the daytime, while nighttime influence on respiration was similar across all sites. This suggests that daytime C accumulated via photosynthesis (GPP) is being offset by enhanced RECO in the presence of precipitation. Alternatively, nighttime precipitation was observed to lead to more positive NEE values whereas no correlation was found during the daytime. Out of the temperate sites, NEE at US-Los was influenced most by this variable.

One study concluded that variability in net C balance depends more on PPFD than precipitation (Xie et al., 2014), indicating how different biomes respond differently to these drivers. As a result, for the sites considered, increased precipitation can be regarded as a way of advancing these biomes towards becoming a net source of C.

Due to precipitation's small influence on GPP, this leads NEE to be strongly characterized through precipitation (affecting RECO) and monthly PPFD (affecting GPP). Therefore, we would expect wet periods to lead to higher RECO and gradually lead these sites to becoming net sources of C. On the other hand, more sunlight exposure would promote higher rates of GPP and lead to a higher likelihood of the sites becoming a net C sink. These results were found at sites where zero precipitation was recorded 80%, 50%, and 94% out of all recorded days at US-Los, US-Syv, and US-WCr respectively at half-hourly scale. Hence, more studies need to be conducted at sites where precipitation rates are higher to determine the significance of this relationship across biomes. The boreal sites also saw increases in respiration rates during higher precipitation events (except for CA-Oas during the daytime). This may indicate that the RECO-P relationship is not regionally dependent, therefore pointing to a similarity between the temperate and boreal biomes considered in this study.

It is important to note that linear regressions have limitations when determining these relationships. A study has found that nonlinear fits may better capture year-to-year variabilities, although this was with regards to precipitation and aboveground net primary production (Knapp et al., 2016).

LE also had a significant impact on C fluxes. Increasing GPP with LE suggests higher rates of photosynthetic production with higher evapotranspiration magnitudes. Relating to what was found with precipitation, this creates a "tug-of-war" between drivers. Precipitation enhances RECO while LE promotes GPP. GPP was found to be less correlated with LE at US-ALQ whereas most other sites experienced correlation coefficients within 0.6 and 0.9. A relatively low correlation of LE with RECO across all temperate sites and years led NEE to decrease dramatically with increases in LE, with NEE at US-ALQ having the smallest correlation coefficient. This suggests a high dependence of C IAV on the water balance of each ecosystem. When the ecosystems lose water to the atmosphere, they are more prone to become net C sinks. Precipitation, however, promotes these biomes to become a net C source. No significant differences were found in evapotranspiration as a driver for C IAV when comparing temperate forests and wetlands. A similar relationship was found for the boreal sites regardless of ecosystem type. Furthermore, a study in China comparing C and water fluxes also found similar results, indicating that the C and water cycles are tightly coupled (Xiao et al., 2013).

In general, TA acted as a way of driving up rates of ecosystem production and respiration. Therefore, magnitudes of NEE remained largely unchanged with increasing temperature. RECO's exponential increase and GPP's quadratic correlation with increasing TA was found not to have significant IAV (**Figure 8**). This indicates that to maximize productivity, these biomes must be exposed to large amounts of solar radiation and also reside in warm climates. On the other hand, a warm climate also promotes respiration, and is maximized when combined with high amounts of precipitation. A study on multiple ecosystem types in China also found an exponential increase in respiration with increases in TA (Yu et al., 2012). Furthermore, a study found GPP at multiple deciduous forests to be negatively correlated with annual water balance (Law et al., 2002). Lastly, a synthesis report including 49 sites concluded NEE to be correlated linearly with mean annual temperature and had a logarithmic correlation with precipitation. It also determined PPFD and temperature to be the most significant predictors of annual NEE which is in agreement with our results (Kato and Tang, 2008).

Precipitation data was sporadic during the course of the study period and therefore we would expect each biome, on average, to be dominant in GPP versus RECO due to the greater abundance of sunlight relative to precipitation on yearly scales. During most of the years, on average, NEE was indeed found to be negative for all sites, giving each biome a net C sink status. Our findings agree with a study measuring terrestrial ecosystem respiration sensitivity to TA across 60 diverse FLUXNET sites, where no difference was found among biomes (Mahecha et al., 2010).

4.3 Study Limitations

As mentioned previously, most sites did not have stream gages located directly at the tower locations. Therefore, remote discharge data was used as a proxy for on-site discharge, which may introduce uncertainties when compared to NEE responses. The largest uncertainties may come from the Bear River (US-Los), Cisco Lake Outlet (US-Syv), and County Trunk Highway M (US-ALQ) stream gages since all were positioned 3 km or more from their respective Ameriflux towers.

Data inavailability was also a limitation in this study. For precipitation, US-Syv had the highest data gaps (2008-2013; 2019-2020) (**Table A.5**). Furthermore, most sites lacked continuous PPFD data (US-ALQ: 2015-2018; US-Los: 2009-2013; US-Syv: 2009-2012 and 2019) (**Table A.5**) while US-Syv was most affected by gaps in TA (2009-2020) (**Table A.5**). C flux data gaps (i.e. NEE, GPP, and RECO) were very sporadic across sites and years (**Table A.5**). As a result, when comparing C flux and micro-meteorological variables, this data gap problem was exacerbated. In some cases, this has inevitably caused an inability to conduct analysis on a continuous set of data on a yearly scale, resulting in some years not being considered entirely. This was also the case at the boreal sites. We believe this to be one of the main sources of uncertainty in this study.

4.4 Implications for Natural Climate Solutions

As mentioned in section 1.8, NCS is one of the most cost effective ways to increase C sequestration to limit global temperature increases due to greenhouse gas emissions. To fully take advantage of NCS's mitigation potential, ecosystem conservation and restoration practices must be implemented such that C uptake is maximized on decadal scales. To achieve this, each practice must be tailored with both ecosystem type and its corresponding C drivers in mind.

Increasing C storage requires increases in GPP while also reducing RECO. According to this study, the most effective way to promote increases in GPP across ecosystem types is through an increase of PPFD. Therefore, NCS efforts must implement afforestation and reforestation to increase leaf radiation interception such that PPFD-use is maximized. However, it is important to note that photosynthetic uptake has temporal limitations, peaking only during the summer months. On the other hand, reports of a lengthening growing season due to warmer temperatures may allow for significant C uptake as soon as early spring that lasts as late as mid-fall (Helfter et al., 2015).

To maximize C uptake and reduce risks of sequestration reversal, restoration efforts must also limit ecosystem RECO. This study shows RECO to be somewhat modulated by precipitation. NEE also became more positive with increased precipitation, indicating these biomes to likely become net C sources during high precipitation events. The dependency of the hydrologic cycle on RECO agrees well with a previous study on these sites (Sulman et al., 2009).

This correlation also goes beyond forests and wetlands. For instance, a mixed grass prairie in Wyoming was found to experience lower and higher respiration rates during decreases and increases in summer precipitation respectively (Chimner and Welker, 2005). This renders precipitation to potentially be a universal driver of RECO regardless of ecosystem type. However, other studies have shown that the magnitude of precipitation is also relevant, even causing net C uptake at a shortgrass steppe when total precipitation is above a certain threshold (Parton et al., 2012). This opens the possibility of the wetlands and forests to experience net uptake during periods of high rainfall (>10 mm day^{-1}), but this cannot be determined with certainty due to limited precipitation data at the study sites.

To effectively implement restoration strategies to minimize RECO, one must understand the underlying mechanisms behind the RECO-precipitation relationship. High amounts of soil water has been found to promote microbial decomposition of organic matter and consequently, the release of CO_2. Furthermore, high soil water content may also facilitate plant root/shoot growth which is associated with higher respiration rates (Chimner and Welker, 2005). It has also been documented that heterotrophic respiration is enhanced during small precipitation events (<10 mm day^{-1}) (Parton et al., 2012).

Therefore, restoration and conservation efforts as part of NCS must prioritize controlled drainage after minor precipitation events to reduce RECO. This reduction will cause higher GPP, resulting in more negative NEE. Methods such as tile drainage may be used to reduce soil water content. We believe these efforts will create optimal conditions for C sequestration at these sites.

5. Conclusion

Here we have observed that two wetland and forest ecosystems spread across northern Wisconsin and Michigan's UP differ drastically in terms of C IAV. Results show higher C IAV magnitude in the forests relative to the wetlands which has implications for ecosystem restoration and conservation prioritization for NCS. A mix of boreal wetland and forest sites showed similar results, revealing small dependency of these processes on latitudinal location.

GPP and RECO were found to have a quadratic and positive exponential relationship with increases in TA, respectively across all sites. In addition, PPFD was found to be highly correlated with productivity (mostly during the summer months) with little to no correlation with RECO. On the other hand, respiration rates increased during relatively high precipitation events with little to no correlation with GPP. This indicates both PPFD and precipitation to be major contributors to C IAV. Year-to-year variability in GPP was also found to contribute more to NEE IAV than yearly variabilities in RECO.

Mutual information analysis revealed NEE at the boreal sites to have more dependency on biophysical variables relative to the temperate sites on seasonal and yearly scales. This suggests that the extent of influence on C fluxes may be more regionally-dependent on long time scales. Moreover, NEE was more dependent on GPP on short timescales (hourly and diel) and dependent on GPP and RECO somewhat equally on multiday, seasonal, and yearly scales.

Due to large NEE IAV at the forest sites, we believe wetlands to be the most reliant biome for long-term C sequestration. Although the potential for large uptake is higher at the forest sites, the high variability is a cause for high uncertainty. On the other hand, while the wetlands were characterized by lower C uptake, their tendency for more constrained C flux magnitudes from year to year leads to a more reliable C sink in the long-term.

Due to the spatially limited nature of this study, more work needs to be conducted at other biomes, especially those in the tropics, to determine whether similar results hold in other regions.

6. Appendix

	Percentage of Gap-filled Data (NEE)							
	Temperate				Boreal			
Year	US-ALQ	US-Los	US-Syv	US-WCr	CA-SCB	CA-SCC	CA-WP1	CA-Oas
1996	-	-	-	-	-	-	-	44.35
1997	-	-	-	-	-	-	-	70.27
1998	-	-	-	0	-	-	-	67.35
1999	-	-	-	100	-	-	-	77.5
2000	-	30.05	-	100	-	-	-	70.18
2001	-	100	32.88	100	-	-	-	72
2002	-	100	100	100	-	-	-	72.72
2003	-	100	100	100	-	-	41.92	75.59
2004	-	100	100	100	-	-	100	73.72
2005	-	100	100	100	-	-	100	75.21
2006	-	100	100	100	-	-	100	70
2007	-	6	11.23	0	-	-	100	72.6
2008	-	100	0	0	-	-	100	69.41
2009	-	0	0	0	-	-	74.11	71.34
2010	-	100	0	44.11	-	-	-	64.59
2011	-	0	0	100	-	-	-	-
2012	-	0	66.67	100	-	-	-	-
2013	-	0	100	100	-	64.19	-	-
2014	-	100	100	100	65.1	100	-	-
2015	28.45	100	100	100	63.8	100	-	-
2016	94.14	100	100	99.73	100	100	-	-
2017	18.48	100	100	100	76.17	-	-	-
2018	30.68	100	100	100	73.84	-	-	-
2019	100	100	45.48	100	74.64	-	-	-
2020	100	93.72	100	99.73	-	-	-	-

Table A.1: *Percentage of available half-hourly NEE data across years and sites. A dash indicates a lack of data for that year.*

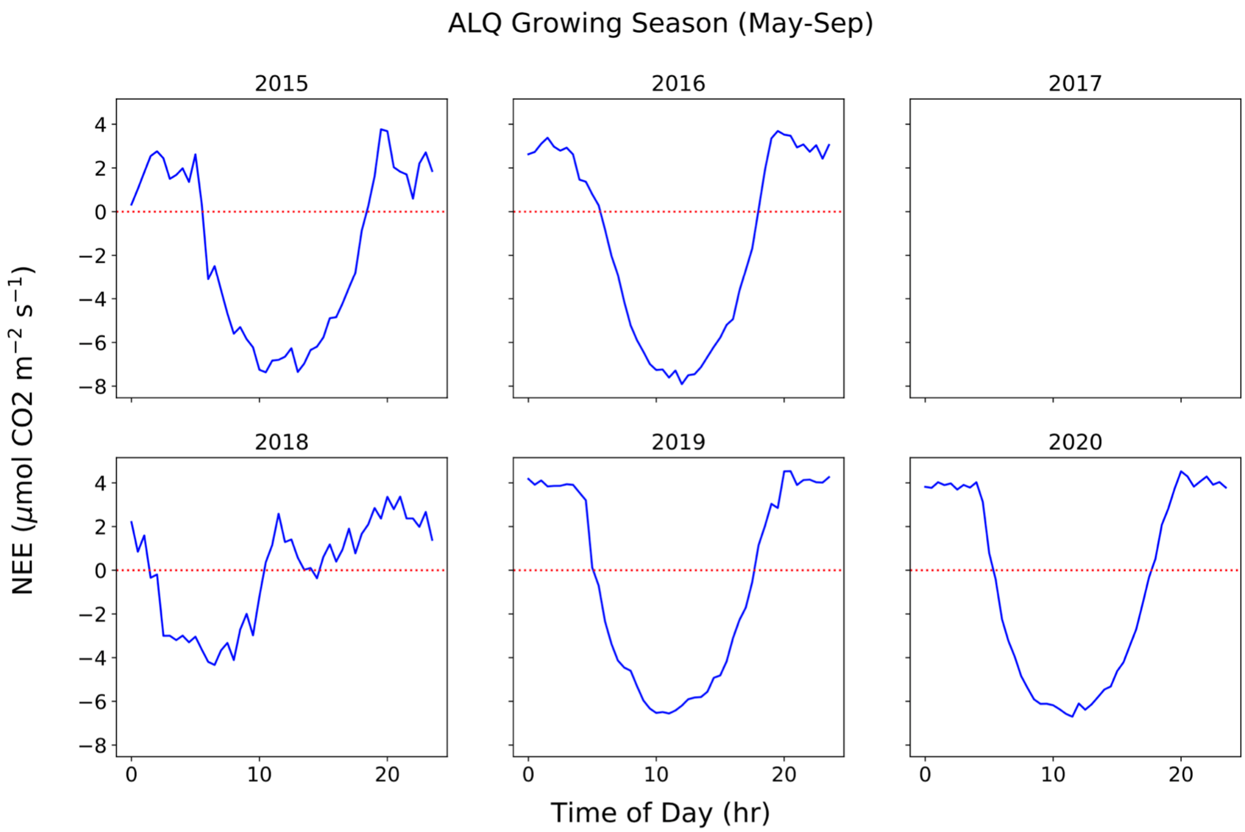
ALQ Growing Season (May-Sep)
2015
2016
2017
2018
2019
2020
NEE (μmol CO2 m−2 s−1)
Time of Day (hr)

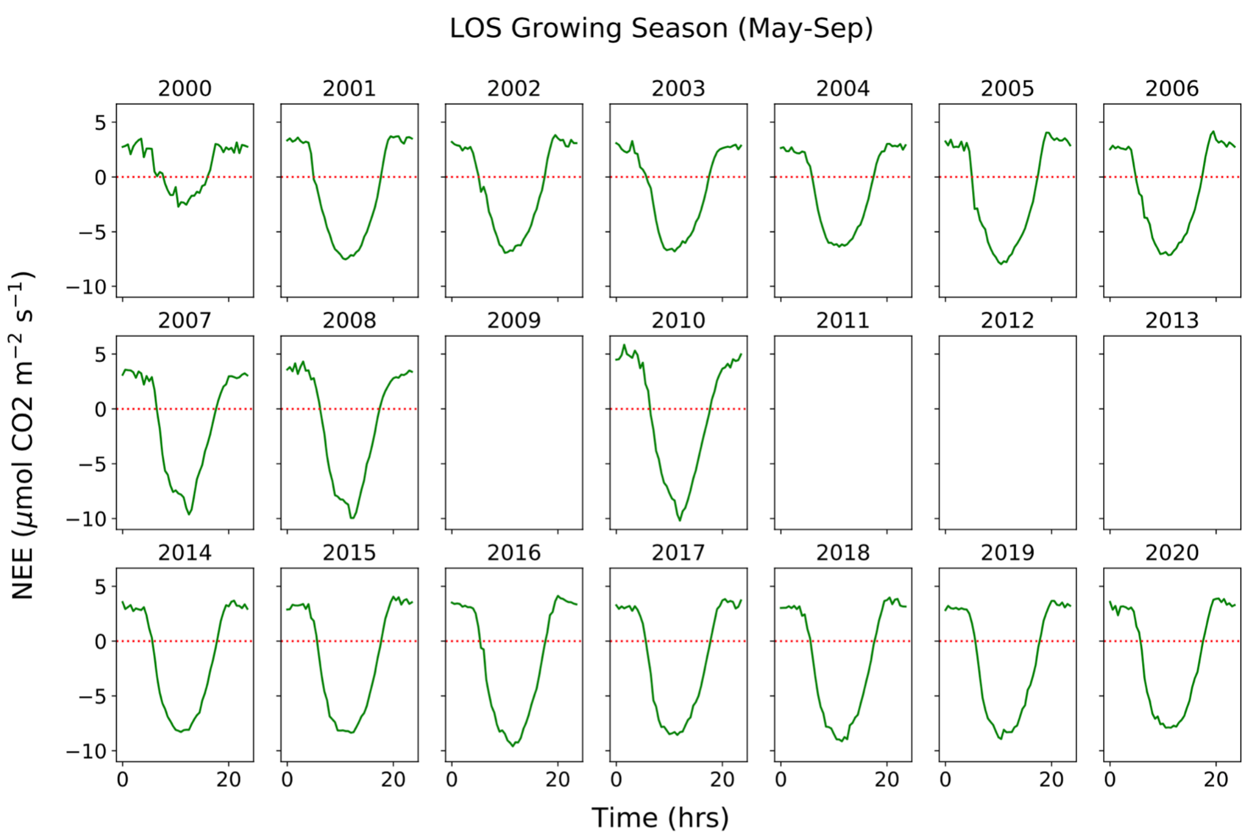
LOS Growing Season (May-Sep)
2000
2001
2002
2003
2004
2005
2006
2007
2008
2009
2010
2011
2012
2013
2014
2015
2016
2017
2018
2019
2020
NEE (μmol CO2 m−2 s−1)
Time (hrs)

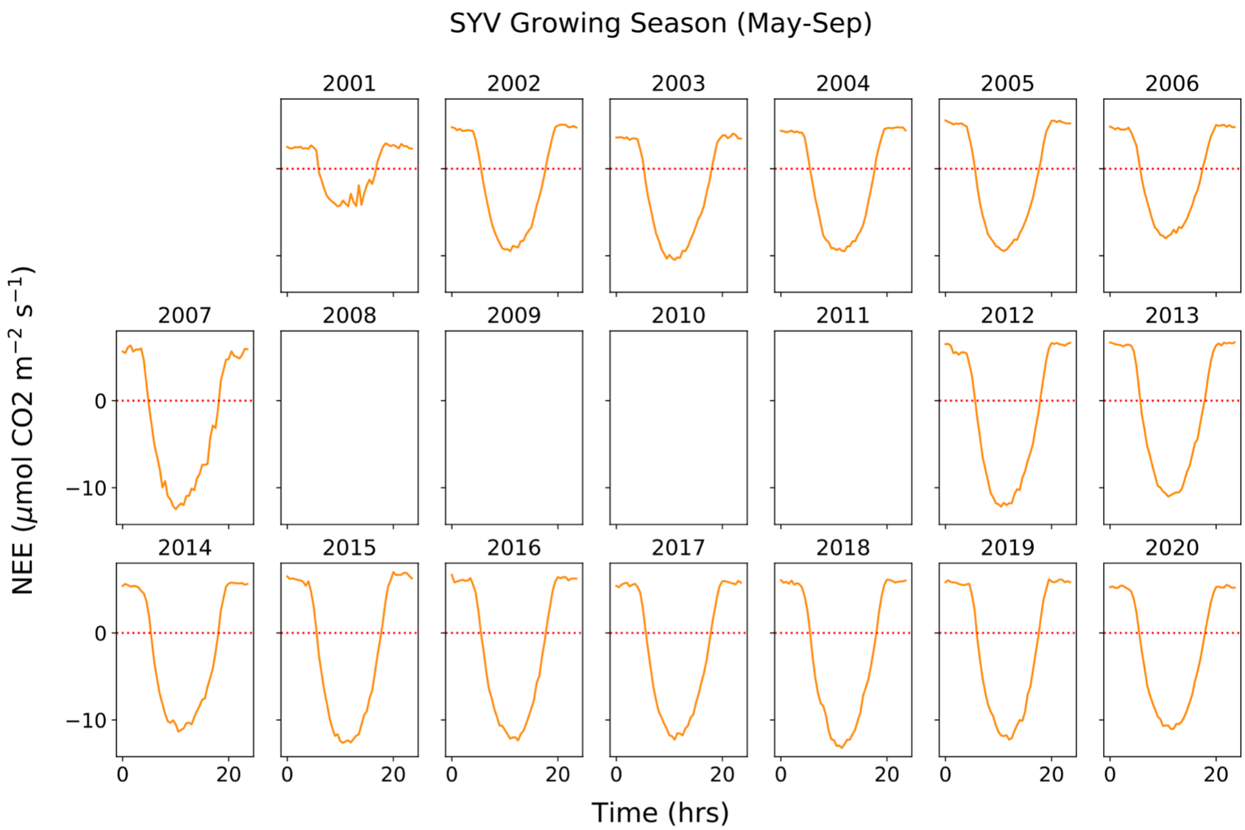
SYV Growing Season (May-Sep)
2001
2002
2003
2004
2005
2006
2007
2008
2009
2010
2011
2012
2013
2014
2015
2016
2017
2018
2019
2020
NEE (μmol CO2 m^{-2} s^{-1})
0
−10
0
20
Time (hrs)

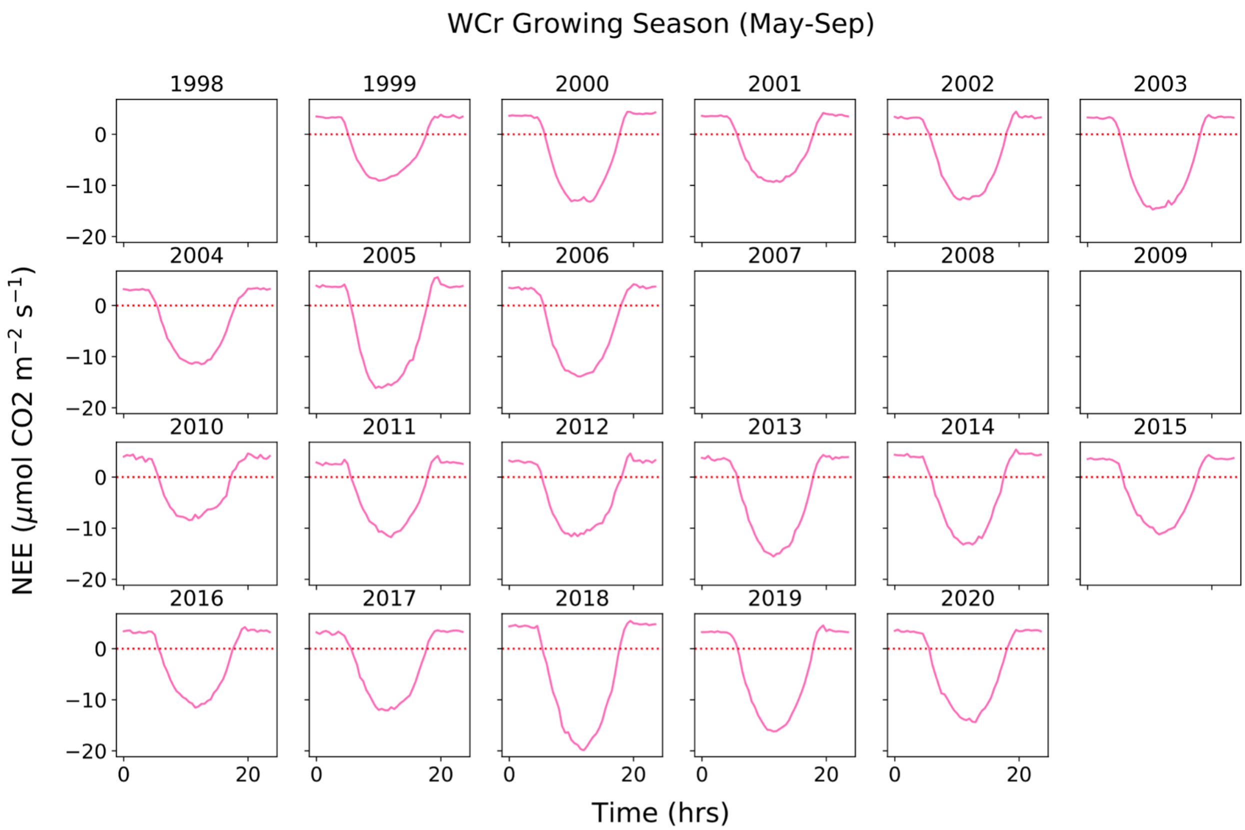
WCr Growing Season (May-Sep)
1998
1999
2000
2001
2002
2003
2004
2005
2006
2007
2008
2009
2010
2011
2012
2013
2014
2015
2016
2017
2018
2019
2020
NEE (μmol CO2 m^{-2} s^{-1})
0
−10
−20
0
20
Time (hrs)

Figure A.1: *Daily NEE cycles for each measured year at each site. This showcases half hourly NEE that was averaged over the growing season. Years with blank plots indicate no data for that time period. The red dotted line represents an NEE of zero throughout the day. Abnormal daily cycles of NEE are the result of missing data (see* ***[Table 2](#)****). Figures 8, 9, 10, 11 from top to bottom display US-ALQ, US-Los, US-Syv, and US-WCr respectively.*

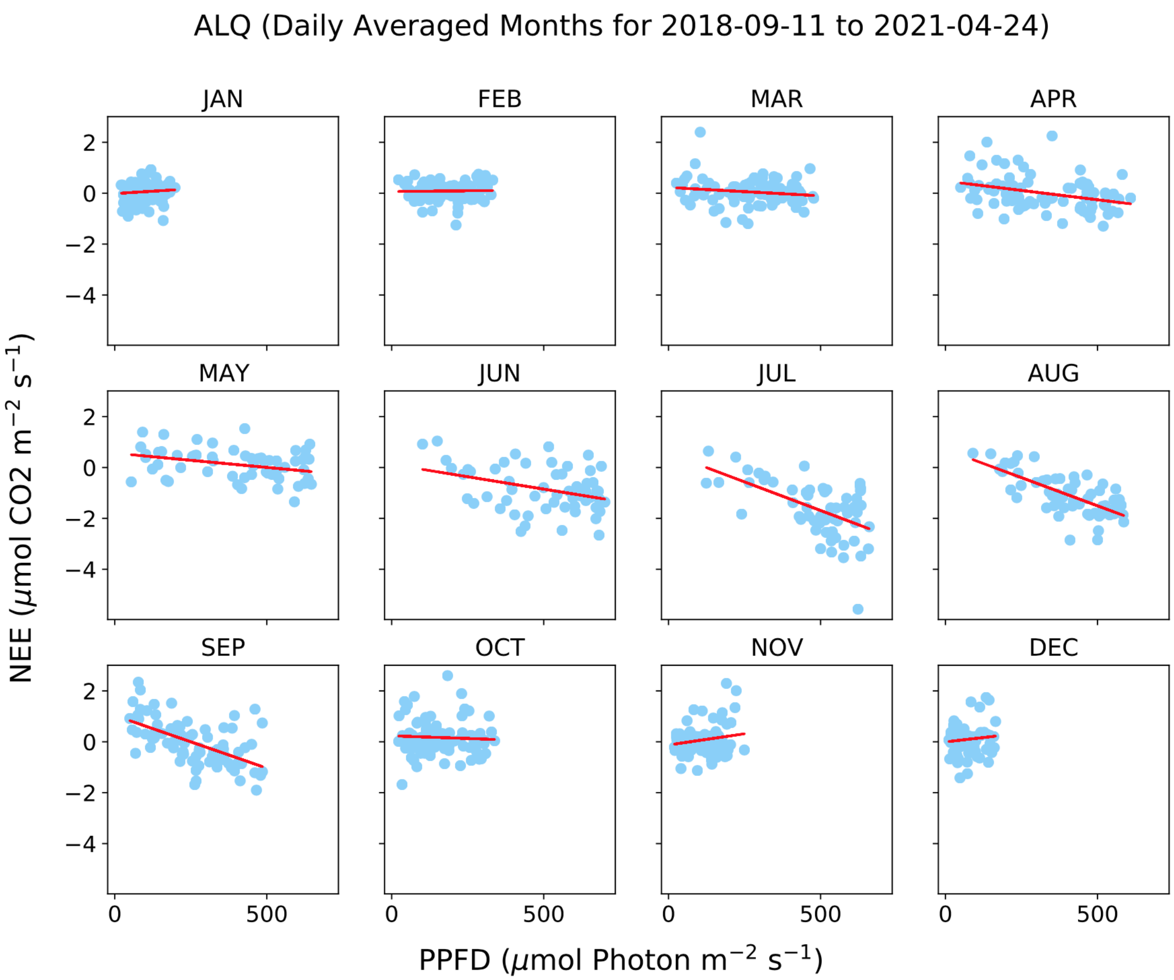

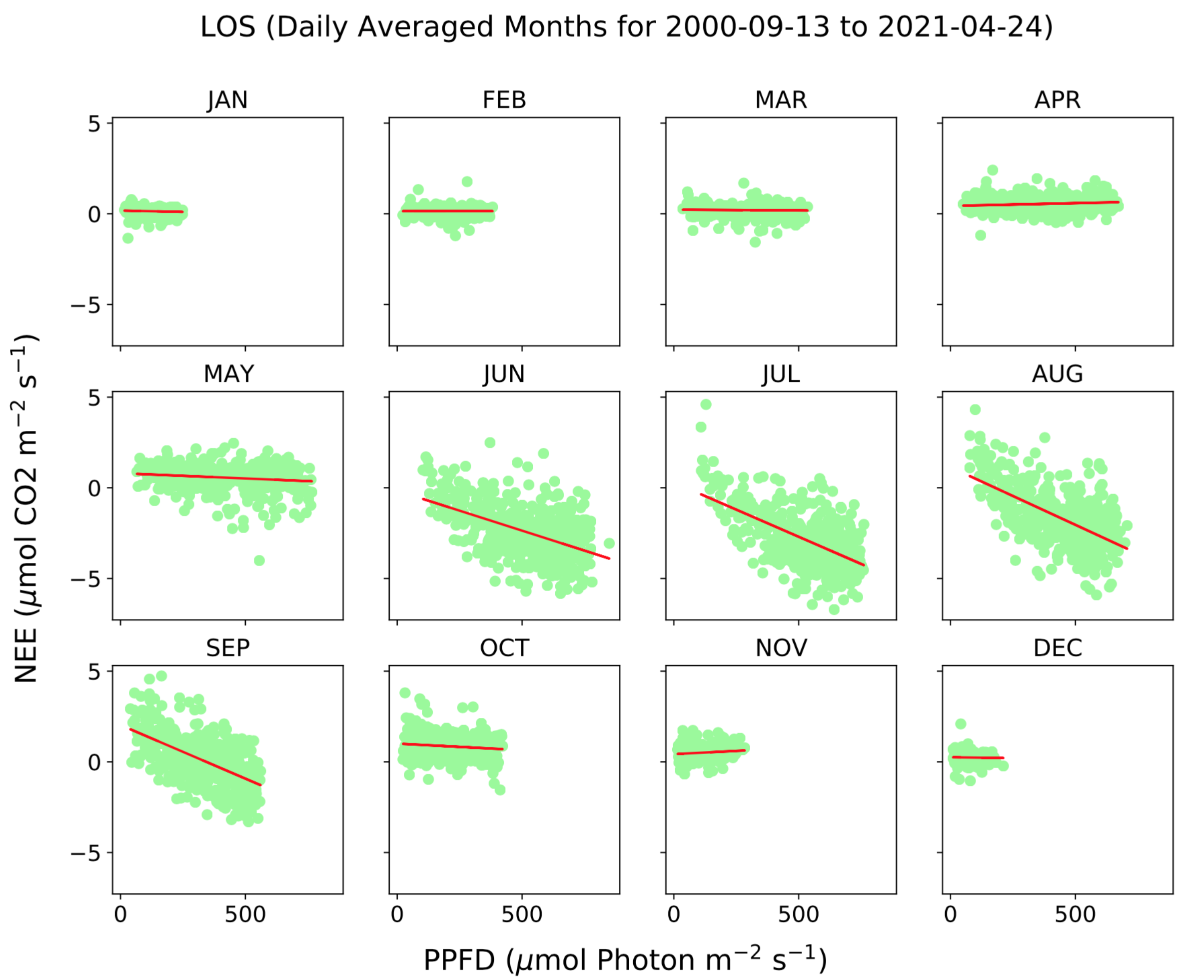
LOS (Daily Averaged Months for 2000-09-13 to 2021-04-24)
JAN
FEB
MAR
APR
MAY
JUN
JUL
AUG
SEP
OCT
NOV
DEC
NEE (μmol CO2 m^{-2} s^{-1})
PPFD (μmol Photon m^{-2} s^{-1})
5
0
−5
0
500

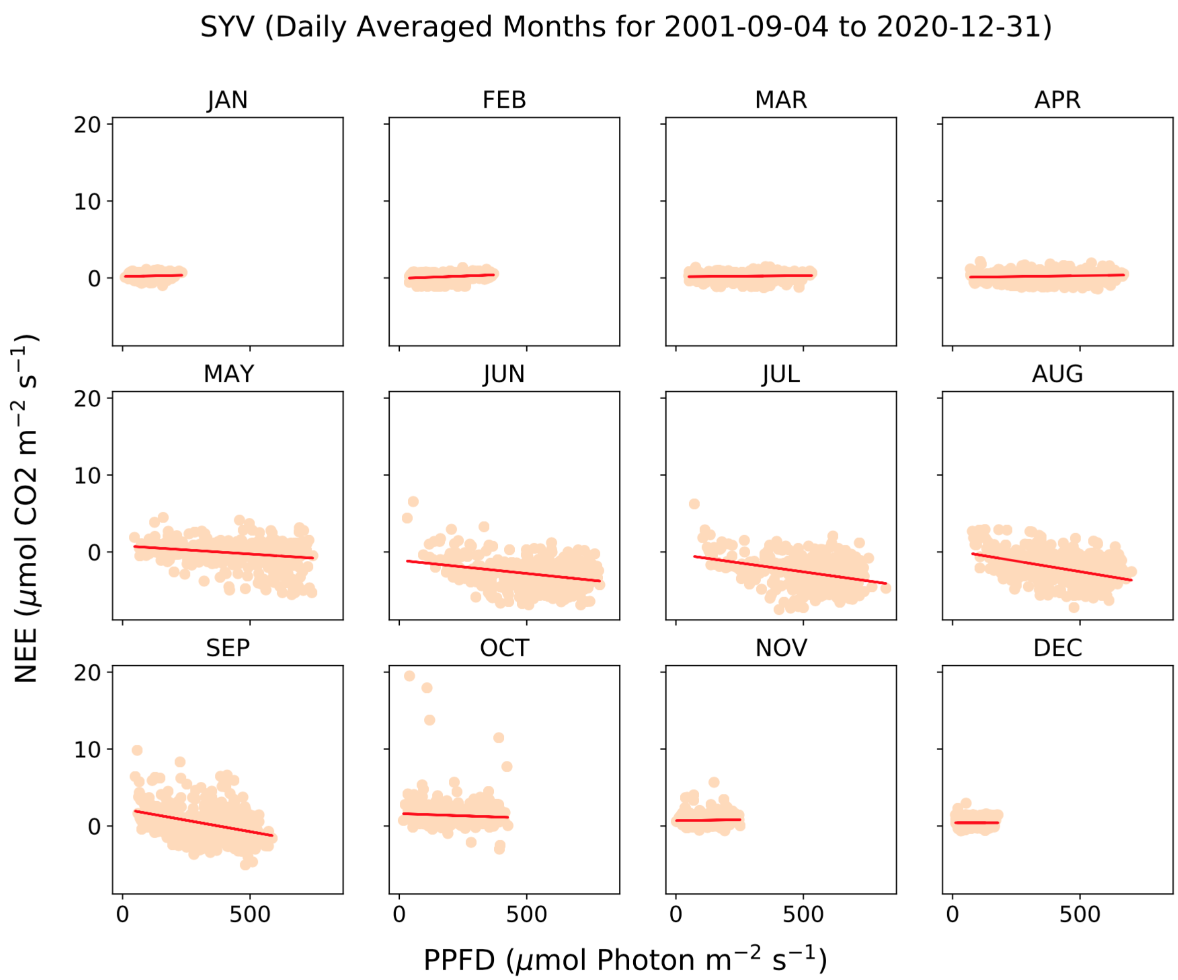

SYV (Daily Averaged Months for 2001-09-04 to 2020-12-31)
JAN
FEB
MAR
APR
MAY
JUN
JUL
AUG
SEP
OCT
NOV
DEC
20
10
0
0
500
NEE (μmol CO2 m^{-2} s^{-1})
PPFD (μmol Photon m^{-2} s^{-1})

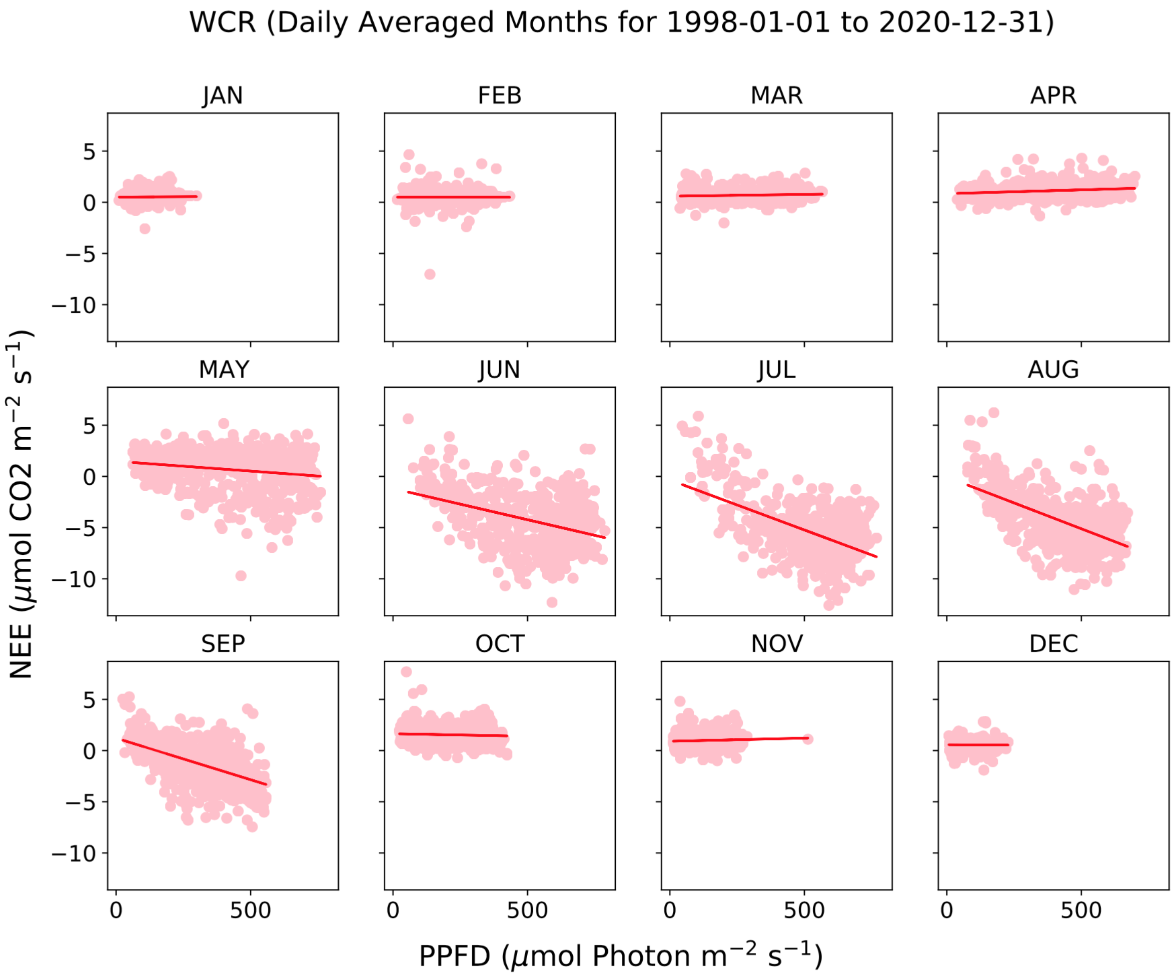

Figure A.2: *NEE plotted as a function of PPFD for each month across all of the sites. Note that all sites have a different time period of measurement (listed in the title of each figure). The red lines represent the line of best fit for each month. Specific values of the Pearson Correlation Coefficient can be found in* ***[Table 3](#)****.*

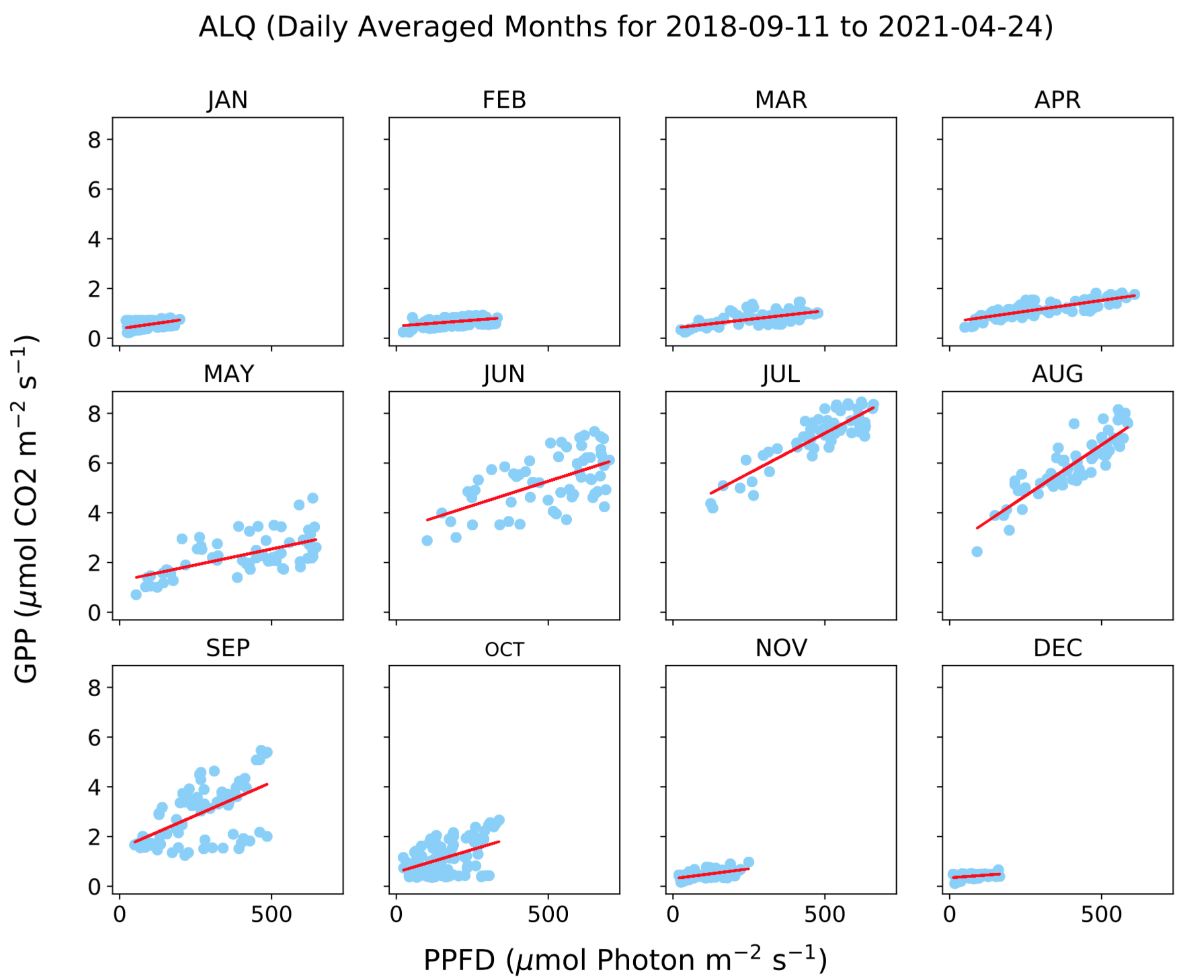
ALQ (Daily Averaged Months for 2018-09-11 to 2021-04-24)
JAN
FEB
MAR
APR
MAY
JUN
JUL
AUG
SEP
OCT
NOV
DEC
GPP (μmol CO2 m^{-2} s^{-1})
PPFD (μmol Photon m^{-2} s^{-1})
0
500
0
2
4
6
8

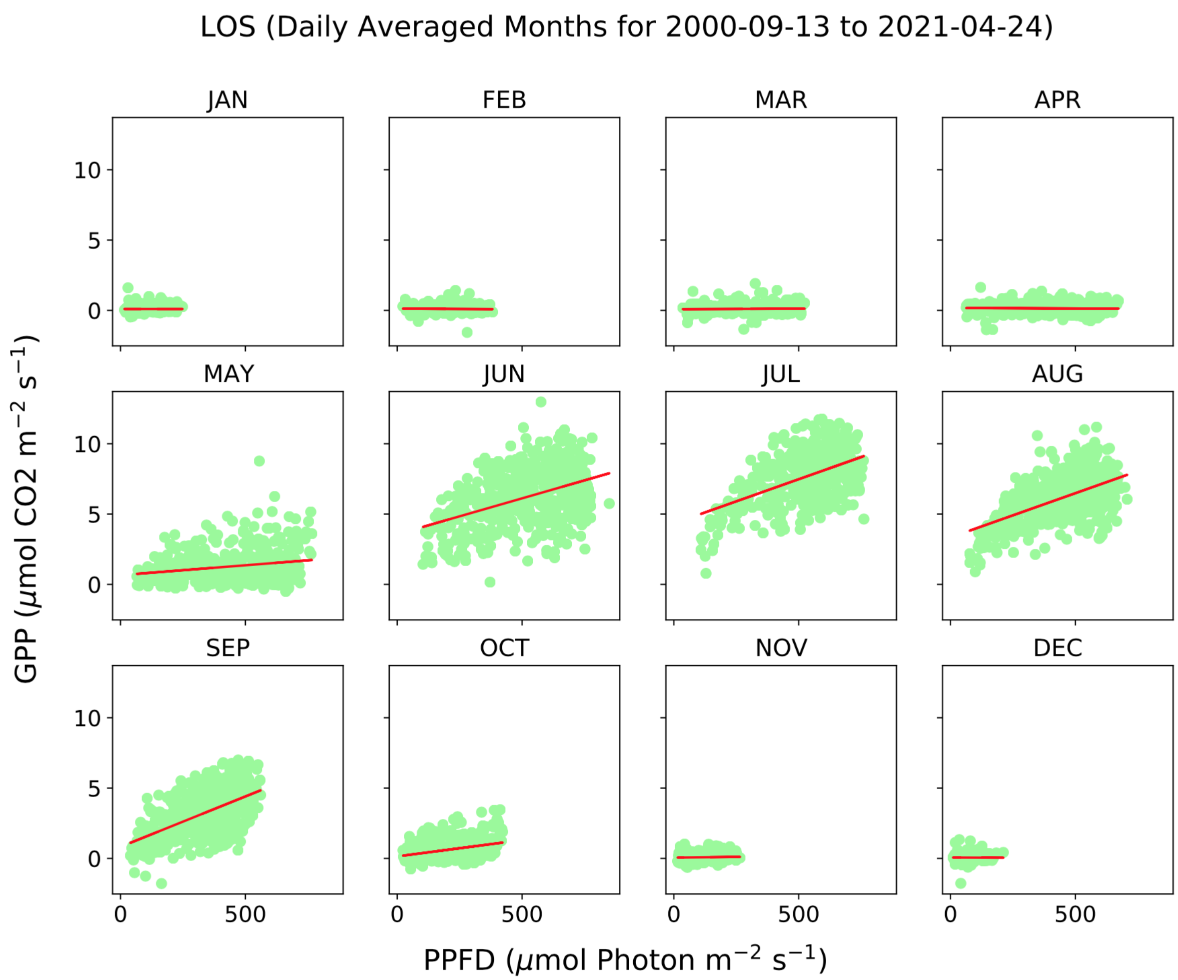
LOS (Daily Averaged Months for 2000-09-13 to 2021-04-24)
JAN
FEB
MAR
APR
MAY
JUN
JUL
AUG
SEP
OCT
NOV
DEC
GPP (μmol CO2 m^{-2} s^{-1})
PPFD (μmol Photon m^{-2} s^{-1})
0
5
10
0
500

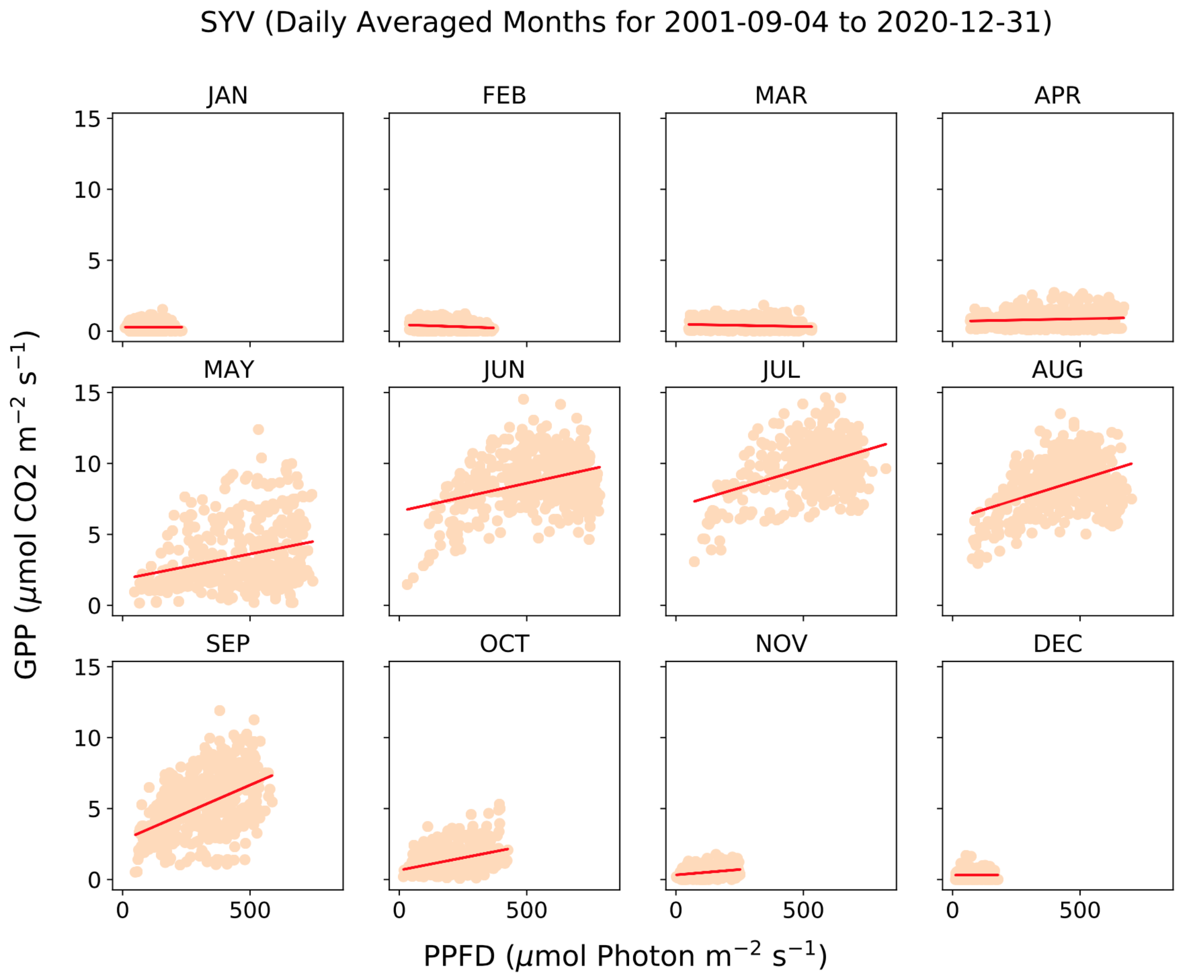
SYV (Daily Averaged Months for 2001-09-04 to 2020-12-31)
JAN
FEB
MAR
APR
MAY
JUN
JUL
AUG
SEP
OCT
NOV
DEC
0
5
10
15
0
500
GPP (μmol CO2 m^{-2} s^{-1})
PPFD (μmol Photon m^{-2} s^{-1})

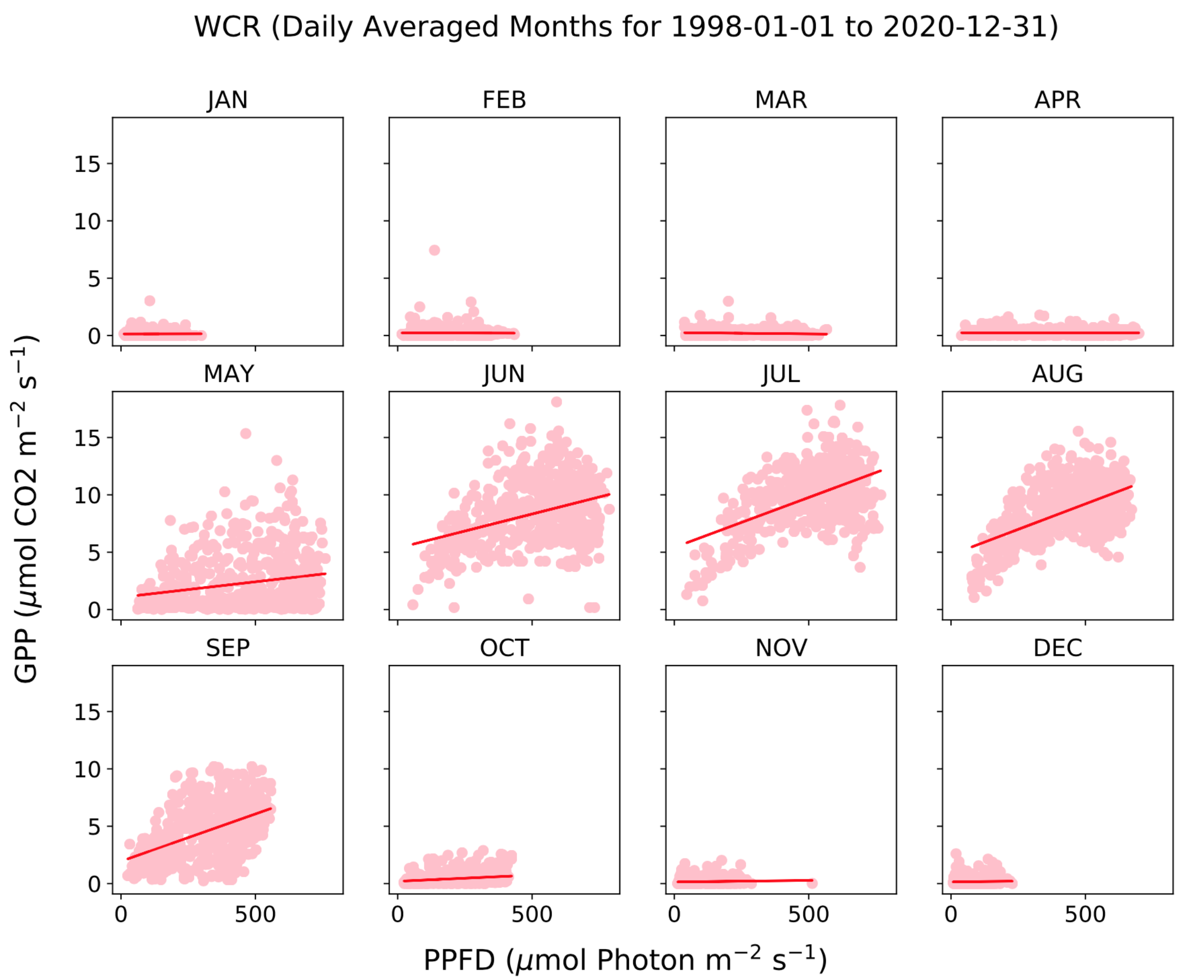

Figure A.3: *Similar to* [***Figures 14-17***]() *but with GPP plotted as a function of PPFD.*

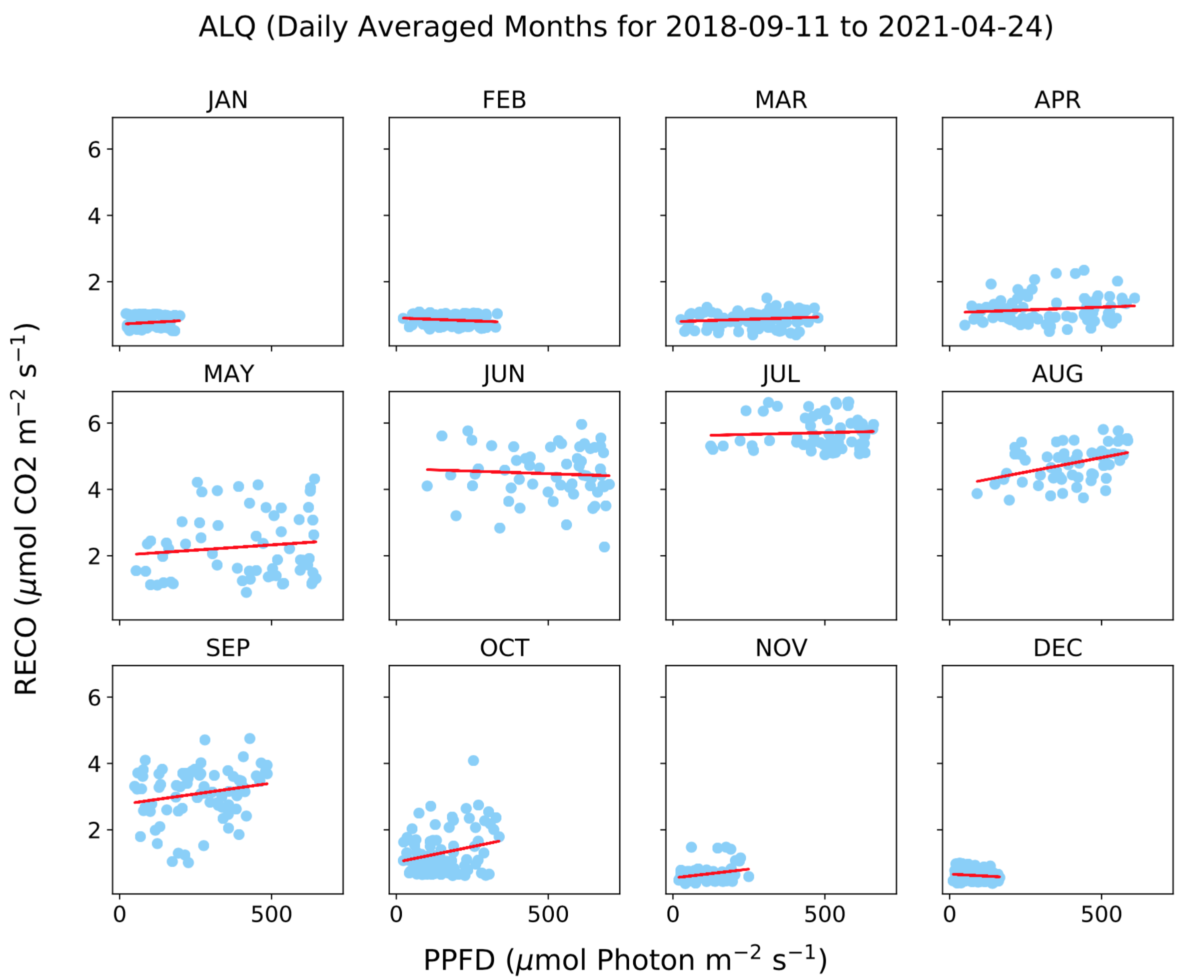
ALQ (Daily Averaged Months for 2018-09-11 to 2021-04-24)
JAN
FEB
MAR
APR
MAY
JUN
JUL
AUG
SEP
OCT
NOV
DEC
RECO (μmol CO2 m^{-2} s^{-1})
PPFD (μmol Photon m^{-2} s^{-1})
0
500
2
4
6

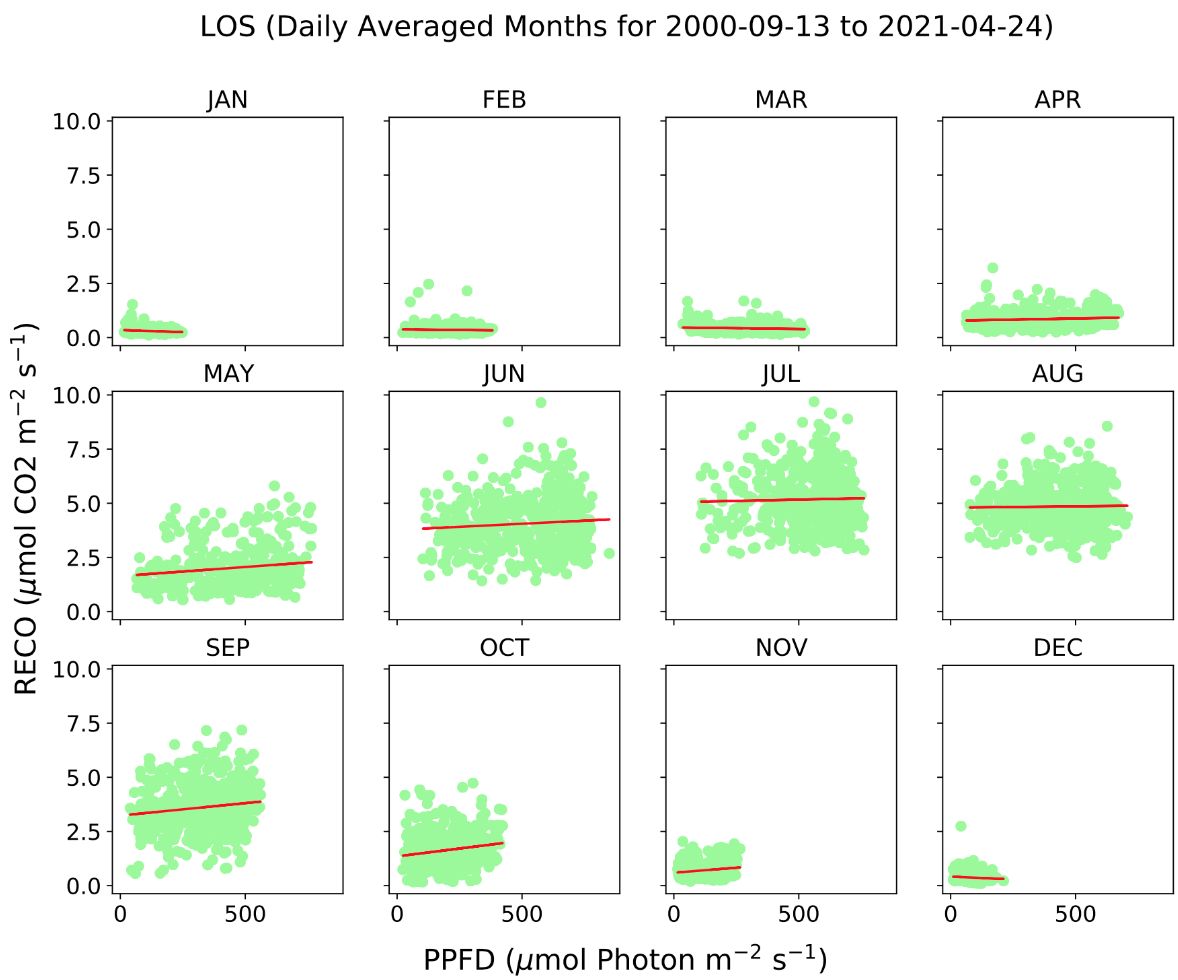
LOS (Daily Averaged Months for 2000-09-13 to 2021-04-24)
JAN
FEB
MAR
APR
MAY
JUN
JUL
AUG
SEP
OCT
NOV
DEC
RECO (μmol CO2 m^{-2} s^{-1})
PPFD (μmol Photon m^{-2} s^{-1})
0.0
2.5
5.0
7.5
10.0
0
500

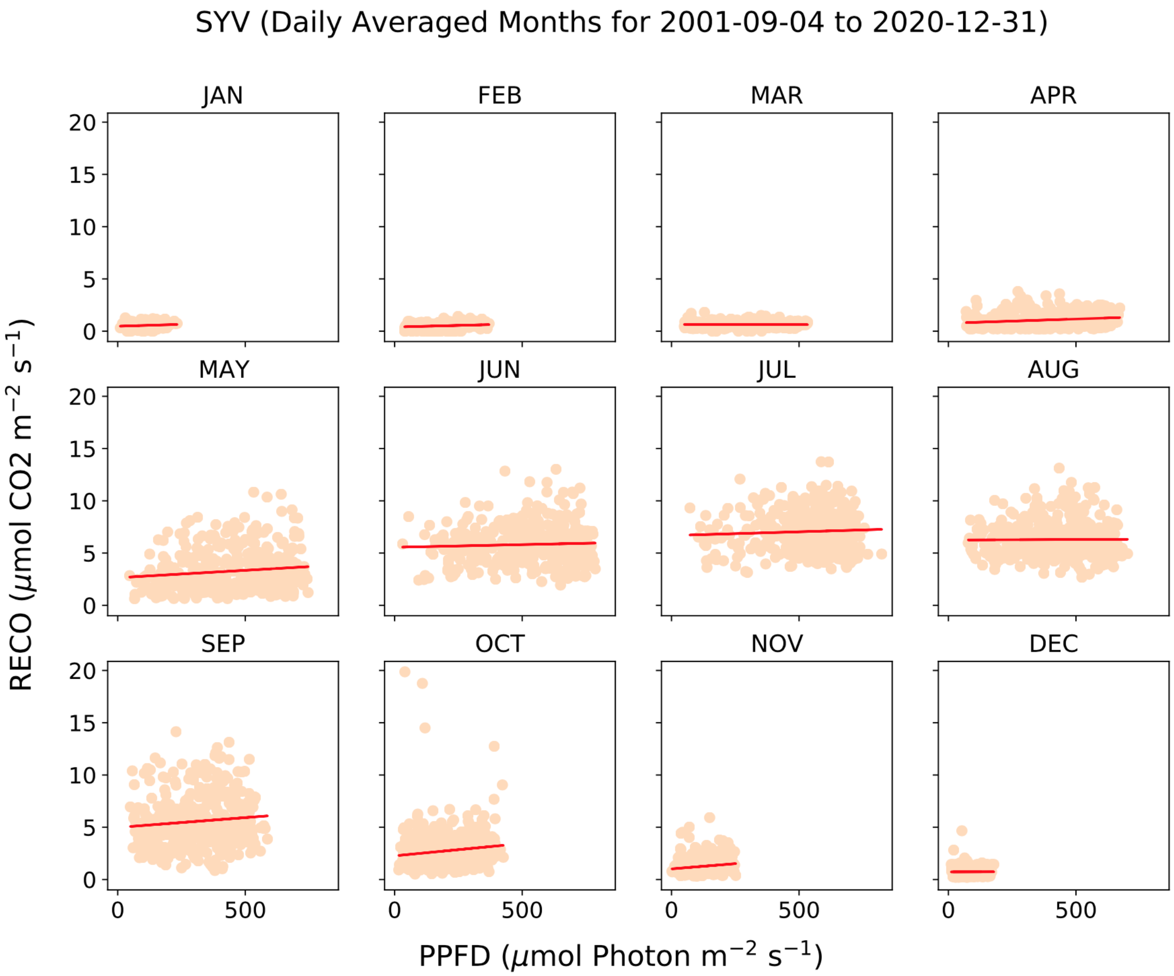
SYV (Daily Averaged Months for 2001-09-04 to 2020-12-31)
JAN
FEB
MAR
APR
MAY
JUN
JUL
AUG
SEP
OCT
NOV
DEC
RECO (μmol CO2 m^{-2} s^{-1})
PPFD (μmol Photon m^{-2} s^{-1})
0
5
10
15
20
0
500

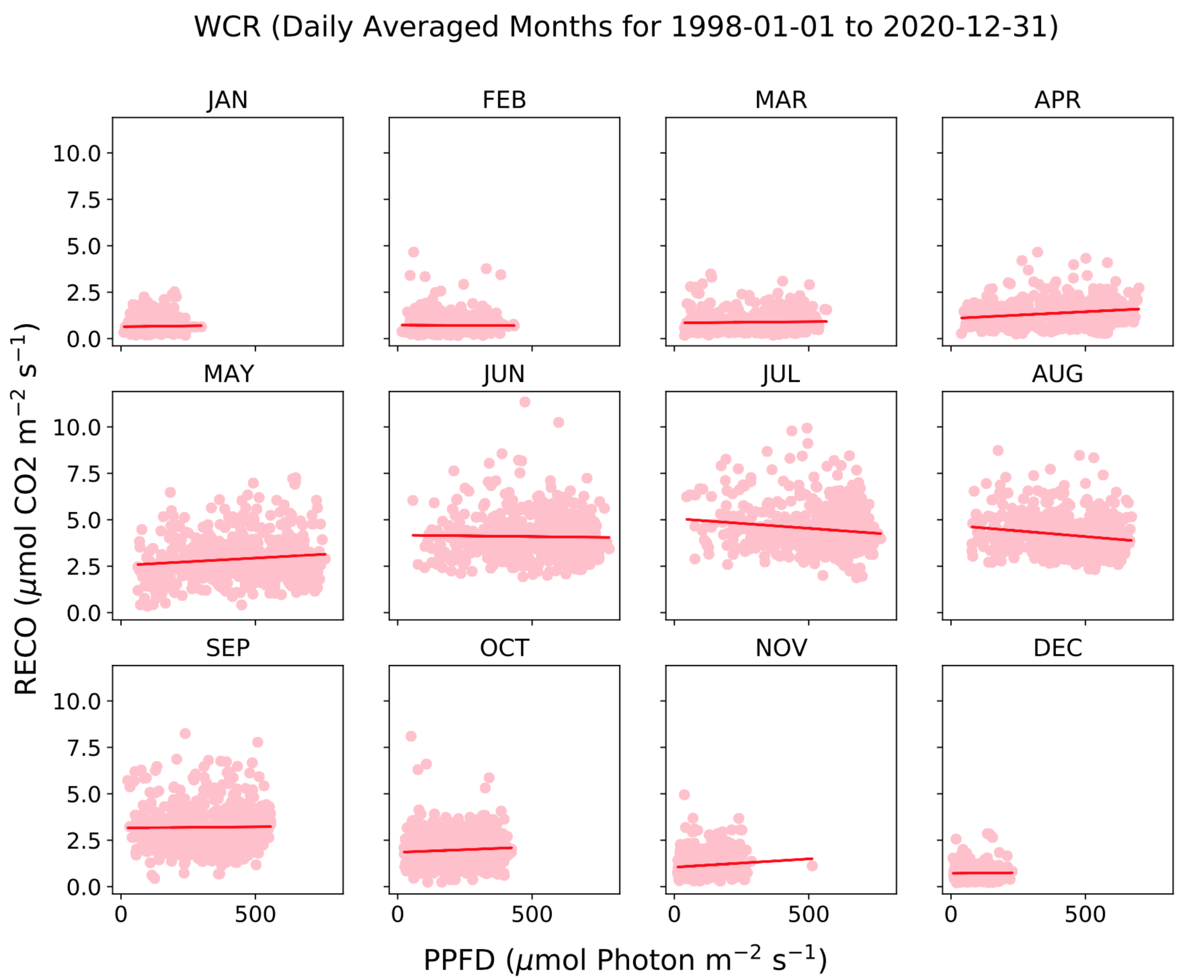

Figure A.4: *Similar to [Figures 14-17](#) but with RECO plotted as a function of PPFD.*

ALQ		
MONTH	**r-value**	**p-value**
JAN	o	o
FEB	o	o
MAR	o	o
APR	-0.3461	0.00126
MAY	-0.3446	0.00653
JUNE	-0.3662	0.004
JULY	-0.557	2.58E-06
AUG	-0.7068	1.37E-10
SEP	-0.5834	1.35E-08
OCT	o	o
NOV	o	o
DEC	o	o

LOS		
MONTH	**r-value**	**p-value**
JAN	-0.0902	0.04806
FEB	o	o
MAR	o	o
APR	0.1357	0.00314
MAY	-0.145	0.0018
JUNE	-0.5133	1.75E-33
JULY	-0.5848	1.79E-45
AUG	-0.6049	2.52E-49
SEP	-0.5832	1.60E-46
OCT	-0.1315	0.00289
NOV	0.1468	0.00091
DEC	o	o

SYV		
MONTH	**r-value**	**p-value**
JAN	o	o
FEB	0.2172	5.96E-05
MAR	o	o
APR	0.1199	0.02323
MAY	-0.2348	1.89E-06
JUNE	-0.3249	1.31E-11
JULY	-0.3698	1.65E-14
AUG	-0.4407	1.97E-21
SEP	-0.3677	1.07E-15
OCT	o	o
NOV	o	o
DEC	o	o

WCR		
MONTH	**r-value**	**p-value**
JAN	o	o
FEB	o	o
MAR	0.0883	0.03713
APR	0.1867	1.27E-05
MAY	-0.176	2.91E-05
JUNE	-0.3941	1.65E-21
JULY	-0.5539	8.13E-47
AUG	-0.573	1.07E-52
SEP	-0.5201	8.18E-41
OCT	o	o
NOV	o	o
DEC	o	o

Table A.2: *Pearson Correlation Coefficients (r-values) and p-values for all sites based on the results in **Figures 14-17** (NEE vs PPFD). Cells containing "o" indicate a p-value > 0.05 (not statistically significant).*

ALQ			LOS			SYV			WCR		
MONTH	r-value	p-value	MONTH	r-value	p-value	MONTH	r-value	p-value	MONTH	r-value	p-value
JAN	0.46571	3.29E-06	JAN	o	o	JAN	o	o	JAN	o	o
FEB	0.42692	5.13E-05	FEB	o	o	FEB	-0.162	0.00289	FEB	o	o
MAR	0.66185	5.08E-13	MAR	o	o	MAR	-0.1172	0.02618	MAR	-0.1259	0.00289
APR	0.81489	4.05E-21	APR	o	o	APR	o	o	APR	o	o
MAY	0.59956	3.30E-07	MAY	0.2009	6.03E-05	MAY	0.2765	1.67E-08	MAY	0.1998	1.96E-06
JUNE	0.57113	1.89E-06	JUNE	0.4205	6.70E-22	JUNE	0.345	5.49E-13	JUNE	0.3608	4.80E-18
JULY	0.86994	4.45E-20	JULY	0.5115	2.00E-33	JULY	0.4268	2.83E-19	JULY	0.5244	2.66E-41
AUG	0.88148	3.26E-21	AUG	0.5418	4.86E-38	AUG	0.4352	7.02E-21	AUG	0.5529	1.88E-48
SEP	0.57094	3.20E-08	SEP	0.5815	3.28E-46	SEP	0.4642	3.64E-25	SEP	0.4804	2.97E-34
OCT	0.47051	1.94E-06	OCT	0.3698	9.72E-16	OCT	0.4286	1.42E-21	OCT	0.2432	2.24E-09
NOV	0.62894	3.18E-11	NOV	o	o	NOV	0.2634	1.51E-08	NOV	o	o
DEC	0.39221	0.00011	DEC	o	o	DEC	o	o	DEC	o	o

Table A.3: *Pearson Correlation Coefficients (r-values) and p-values for all sites based on the results in **Figures 18-21** (GPP vs PPFD). Cells containing "o" indicate a p-value > 0.05 (not statistically significant).*

ALQ			LOS			SYV			WCR		
MONTH	r-value	p-value	MONTH	r-value	p-value	MONTH	r-value	p-value	MONTH	r-value	p-value
JAN	o	o	JAN	-0.16629	0.000613	JAN	0.15151	0.003909	JAN	o	o
FEB	o	o	FEB	o	o	FEB	0.19418	0.000343	FEB	o	o
MAR	o	o	MAR	o	o	MAR	o	o	MAR	o	o
APR	o	o	APR	o	o	APR	0.19439	0.000215	APR	0.1978	3.63E-06
MAY	o	o	MAY	0.15111	0.00267	MAY	0.13015	0.008905	MAY	0.1229	0.00364
JUNE	o	o	JUNE	o	o	JUNE	o	o	JUNE	o	o
JULY	o	o	JULY	o	o	JULY	o	o	JULY	-0.1426	0.00067
AUG	0.41499	0.000797	AUG	o	o	AUG	o	o	AUG	-0.1842	6.84E-06
SEP	o	o	SEP	0.13373	0.002844	SEP	0.10322	0.029468	SEP	o	o
OCT	0.24195	0.019461	OCT	0.19805	2.81E-05	OCT	0.13162	0.005117	OCT	o	o
NOV	0.28713	0.006071	NOV	0.17108	0.000443	NOV	0.17567	0.000186	NOV	0.1164	0.0054
DEC	o	o	DEC	-0.11826	0.017694	DEC	o	o	DEC	o	o

Table A.4: *Pearson Correlation Coefficients (r-values) and p-values for all sites based on the results in **Figures 22-25** (RECO vs PPFD). Cells containing "o" indicate a p-value > 0.05 (not statistically significant).*

Percentage of Available Data (TA)				
SITE → | YEAR ↓	ALQ	LOS	SYV	WCR
1998	-	-	-	100
1999	-	-	-	100
2000	-	100	-	100
2001	-	100	100	100
2002	-	100	100	100
2003	-	100	100	100
2004	-	100	100	100
2005	-	100	100	100
2006	-	100	100	100
2007	-	100	100	100
2008	-	100	100	100
2009	-	100	0	100
2010	-	100	0	100
2011	-	0	0	100
2012	-	0	0	100
2013	-	0	0	100
2014	-	100	0	100
2015	72.3288	99.726	0	100
2016	100	100	0	99.9203
2017	31.2272	100	0	100
2018	30.411	100	0	100
2019	100	100	0	100
2020	100	93.7158	0	100

Percentage of Available Data (Precipitation)				
SITE → | YEAR ↓	ALQ	LOS	SYV	WCR
1998	-		-	100
1999	-		-	100
2000	-	100	-	100
2001	-	100	34.08	100
2002	-	100	100	100
2003	-	100	99.93	100
2004	-	100	99.95	100
2005	-	100	100	100
2006	-	100	99.93	100
2007	-	100	95.98	100
2008	-	99.91	0	99.91
2009	-	99.99	0	99.97
2010	-	99.73	0	99.73
2011	-	0	0	99.99
2012	-	0	0	100
2013	-	0	0	100
2014	-	100	50.57	100
2015	-	99.95	93.15	99.5
2016	-	99.93	99.19	99.6
2017	-	99.99	97.95	99.99
2018	-	99.09	91.27	98.42
2019	-	99.93	0	97.47
2020	-	93.92	0	99.9

Percentage of Available Data (PPFD)				
SITE → | YEAR ↓	ALQ	LOS	SYV	WCR
1998	-	-	-	100
1999	-	-	-	100
2000	-	100	-	100
2001	-	100	100	100
2002	-	100	100	100
2003	-	100	100	100
2004	-	100	100	100
2005	-	100	100	100
2006	-	100	100	100
2007	-	100	100	100
2008	-	100	100	100
2009	-	0	0	100
2010	-	62.04	0	100
2011	-	0	0	100
2012	-	0	66.4	100
2013	-	0	100	100
2014	-	99.93	100	100
2015	0	99.73	100	100
2016	0	99.93	100	100
2017	0	99.93	100	100
2018	30.41	99.93	100	100
2019	99.93	99.93	45.48	100
2020	99.93	93.72	100	100

Percentage of Available Data (GPP)				
SITE → | YEAR ↓	ALQ	LOS	SYV	WCR
1998	-	-	-	0
1999	-	-	-	100
2000	-	30.0546	-	100
2001	-	100	32.6027	100
2002	-	100	100	100
2003	-	100	100	100
2004	-	100	100	100
2005	-	100	100	100
2006	-	100	100	100
2007	-	35.8904	11.2329	0
2008	-	35.7923	0	0
2009	-	0	0	0
2010	-	35.8904	0	44.1096
2011	-	0	0	100
2012	-	0	66.6667	100
2013	-	0	100	100
2014	-	100	100	100
2015	72.6027	100	100	100
2016	100	100	100	99.7268
2017	31.2272	100	100	100
2018	30.6849	100	100	100
2019	100	100	45.4795	100
2020	100	93.9891	100	99.7268

Percentage of Available Data (RECO)				
SITE → | YEAR ↓	ALQ	LOS	SYV	WCR
1998	-	-	-	0
1999	-	-	-	100
2000	-	30.0546	-	100
2001	-	100	32.6027	100
2002	-	100	100	100
2003	-	100	100	100
2004	-	100	100	100
2005	-	100	100	100
2006	-	100	100	100
2007	-	35.8904	11.2329	0
2008	-	35.7923	0	0
2009	-	0	0	0
2010	-	35.8904	0	44.1096
2011	-	0	0	100
2012	-	0	66.6667	100
2013	-	0	100	100
2014	-	100	100	100
2015	0.72603	100	100	100
2016	100	100	100	99.7268
2017	0.31227	100	100	100
2018	0.30685	100	100	100
2019	100	100	45.4795	100
2020	100	93.9891	100	99.7268

Tables A.5: *Percentage of available half-hourly precipitation, PPFD, GPP, and RECO data across years and sites. A dash indicates a lack of data for that year.*

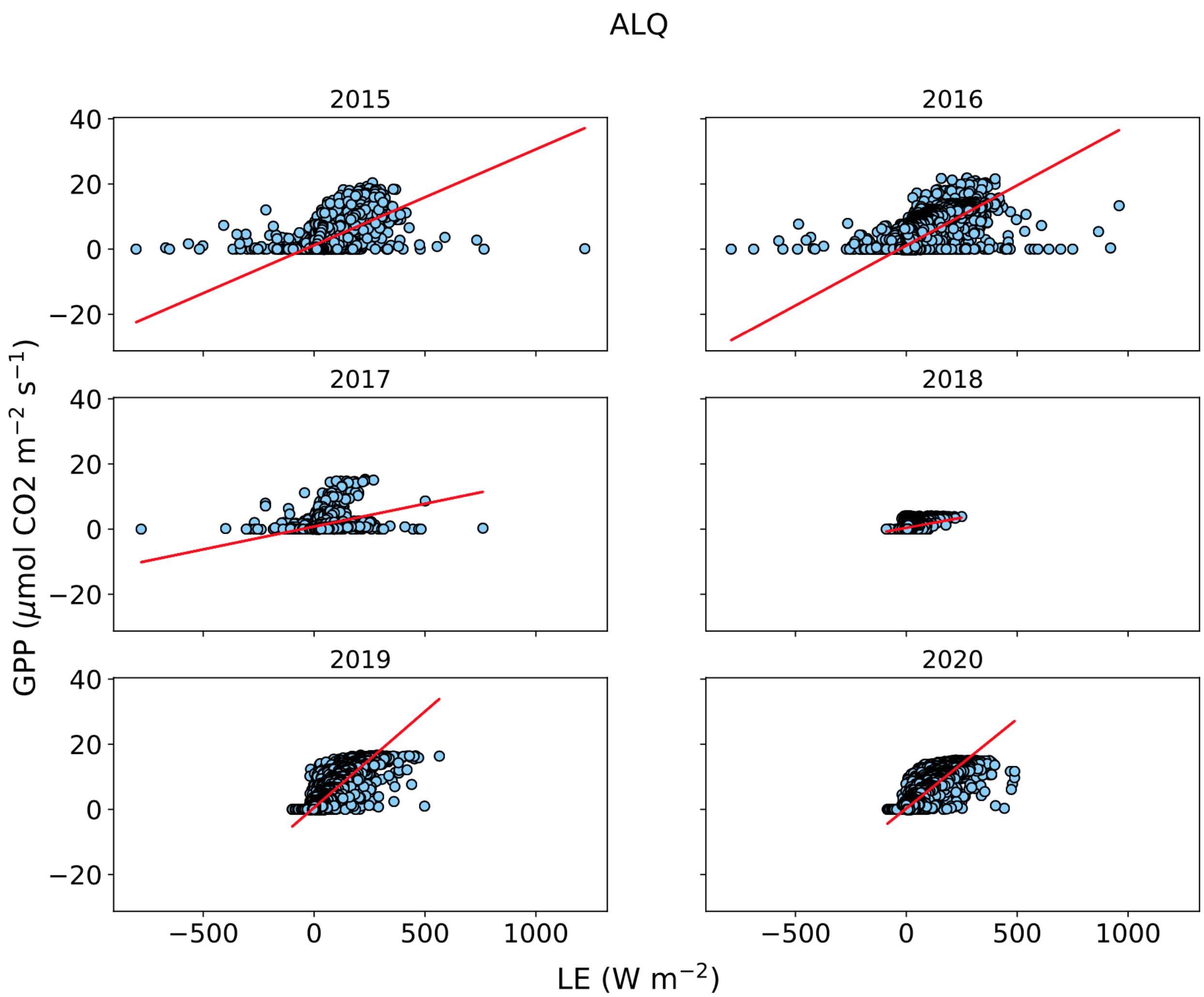

ALQ
2015
2016
2017
2018
2019
2020
40
20
0
−20
−500
0
500
1000
GPP (μmol CO2 m−2 s−1)
LE (W m−2)

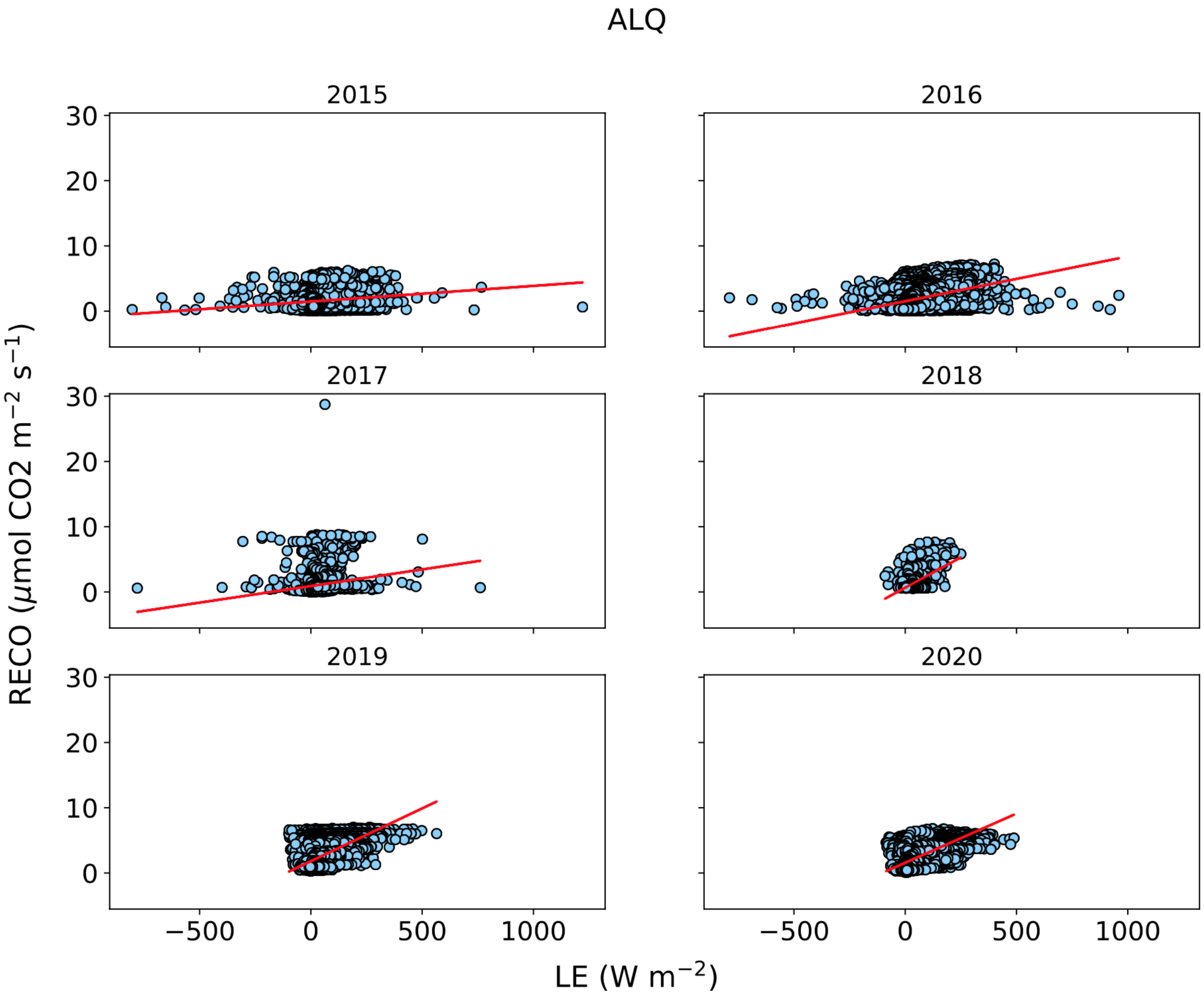
ALQ
2015
2016
2017
2018
2019
2020
RECO (μmol CO2 m−2 s−1)
LE (W m−2)
30
20
10
0
−500
0
500
1000

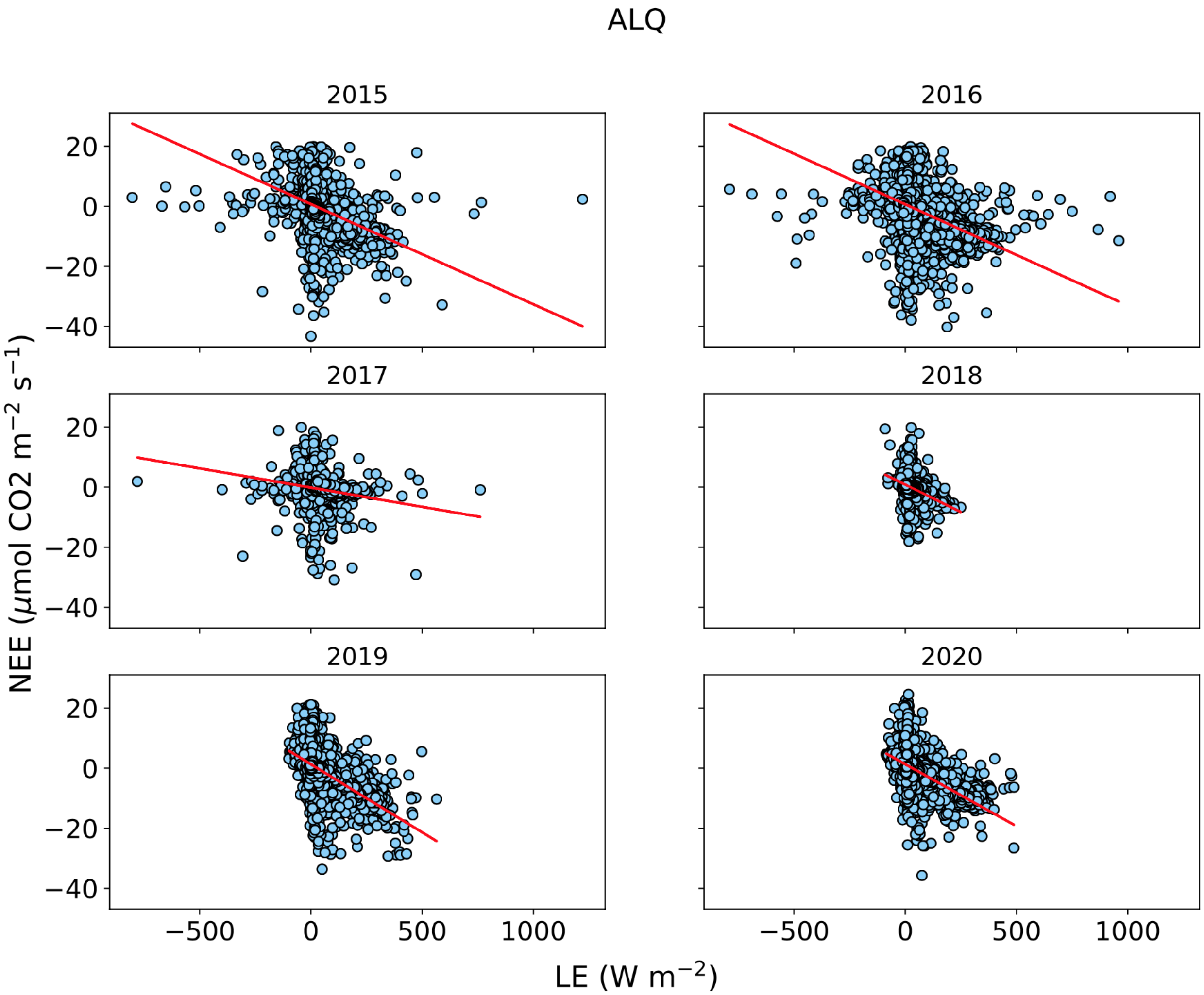
ALQ
2015
2016
2017
2018
2019
2020
NEE (μmol CO2 m⁻² s⁻¹)
LE (W m⁻²)
20
0
−20
−40
−500
0
500
1000

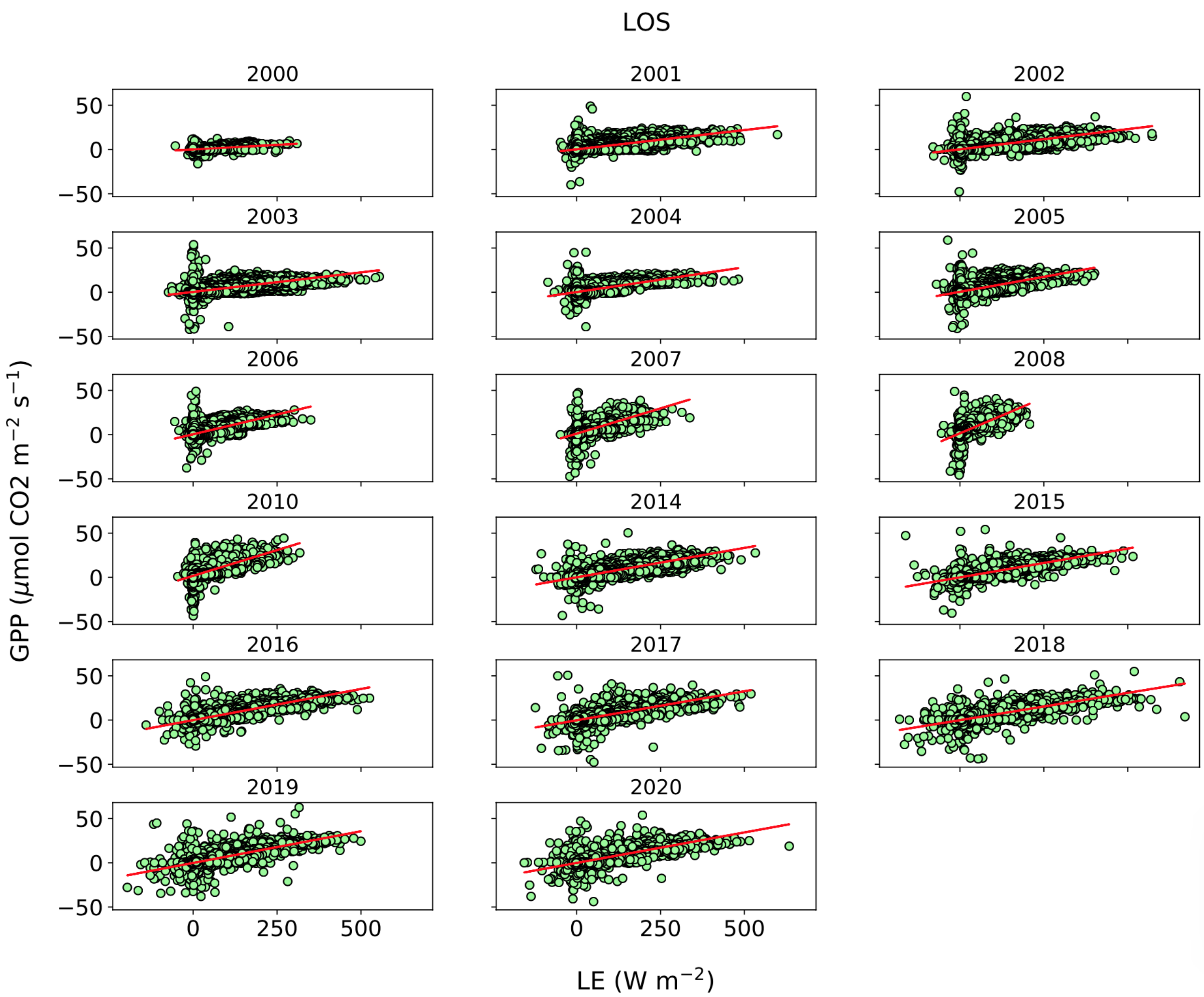
LOS
2000
2001
2002
2003
2004
2005
2006
2007
2008
2010
2014
2015
2016
2017
2018
2019
2020
GPP (μmol CO2 m^{-2} s^{-1})
LE (W m^{-2})
50
0
−50
0
250
500

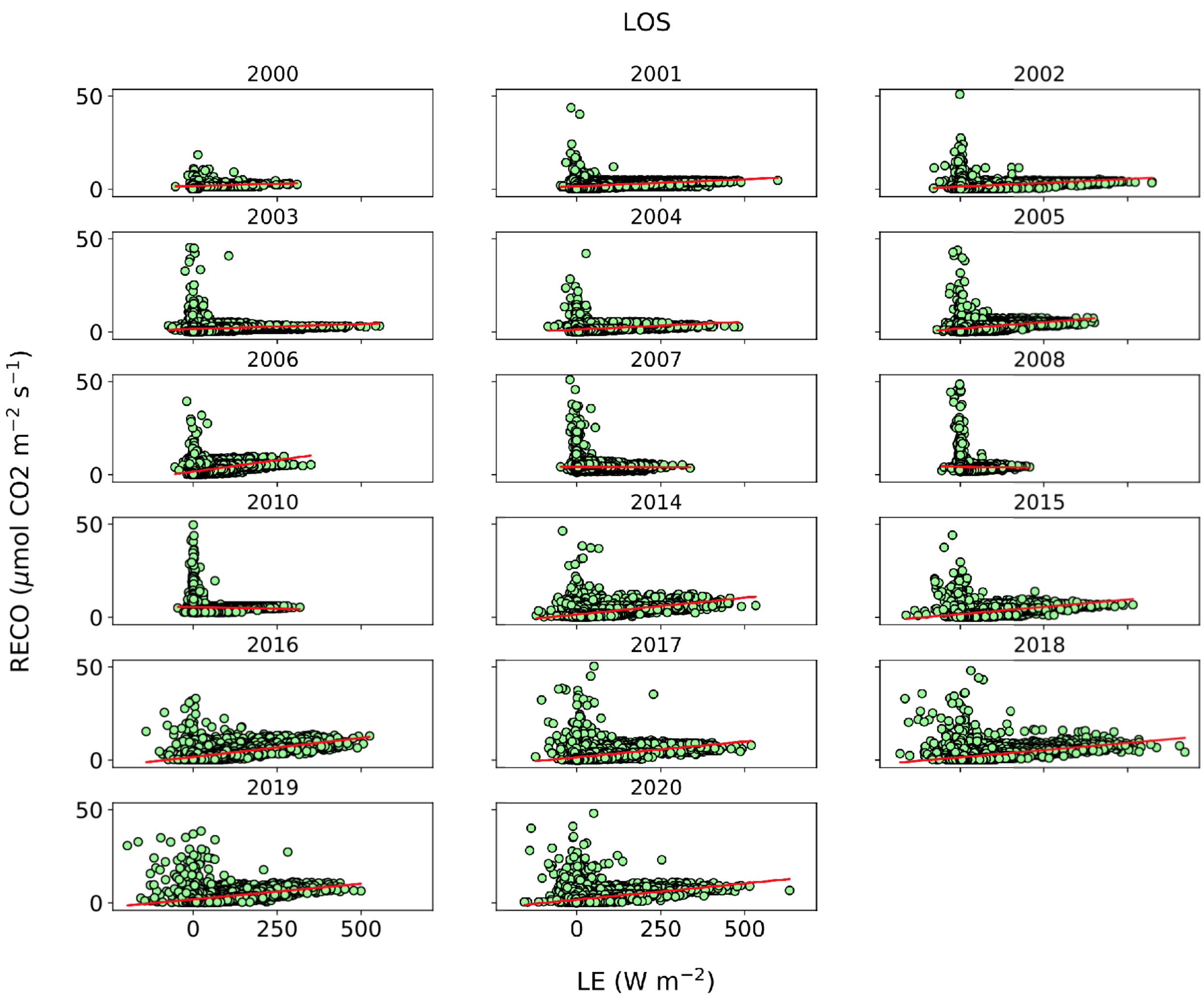
LOS
2000
2001
2002
2003
2004
2005
2006
2007
2008
2010
2014
2015
2016
2017
2018
2019
2020
RECO (μmol CO2 m^{-2} s^{-1})
LE (W m^{-2})
50
0
250
500

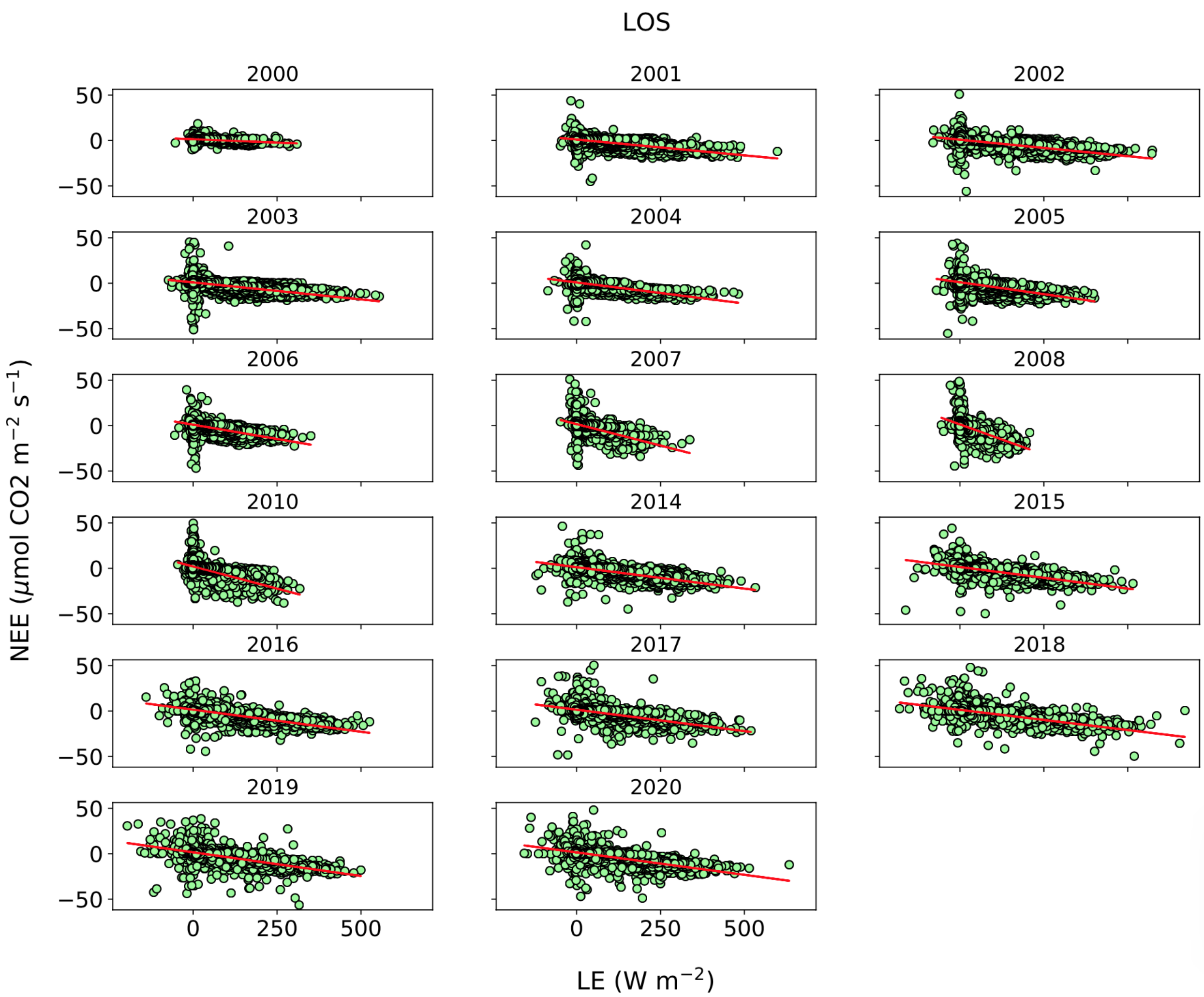

LOS
2000
2001
2002
2003
2004
2005
2006
2007
2008
2010
2014
2015
2016
2017
2018
2019
2020
50
0
−50
0
250
500
NEE (μmol CO2 m^{-2} s^{-1})
LE (W m^{-2})

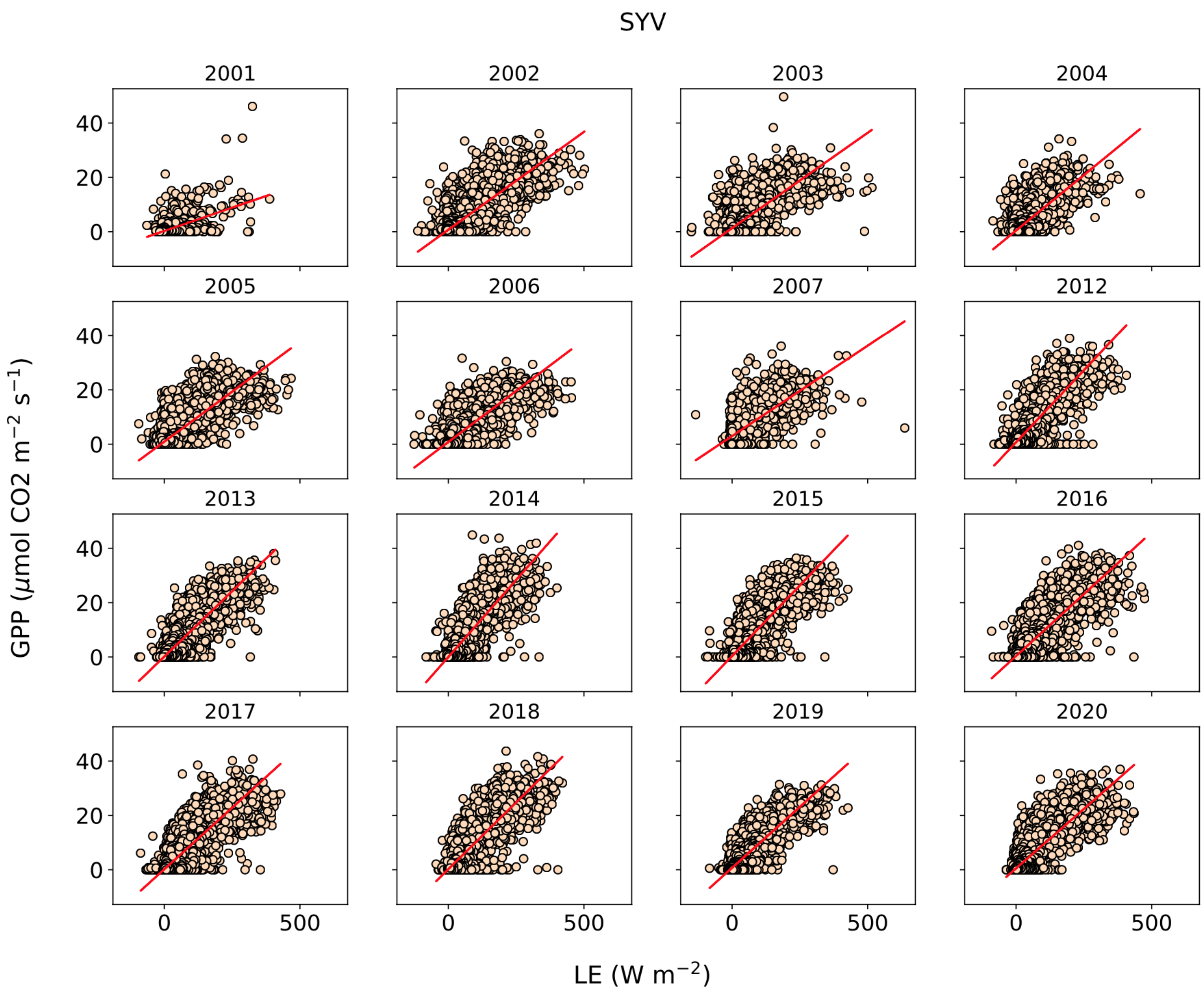
SYV
2001
2002
2003
2004
2005
2006
2007
2012
2013
2014
2015
2016
2017
2018
2019
2020
GPP (μmol CO2 m^{-2} s^{-1})
LE (W m^{-2})
0
20
40
0
500

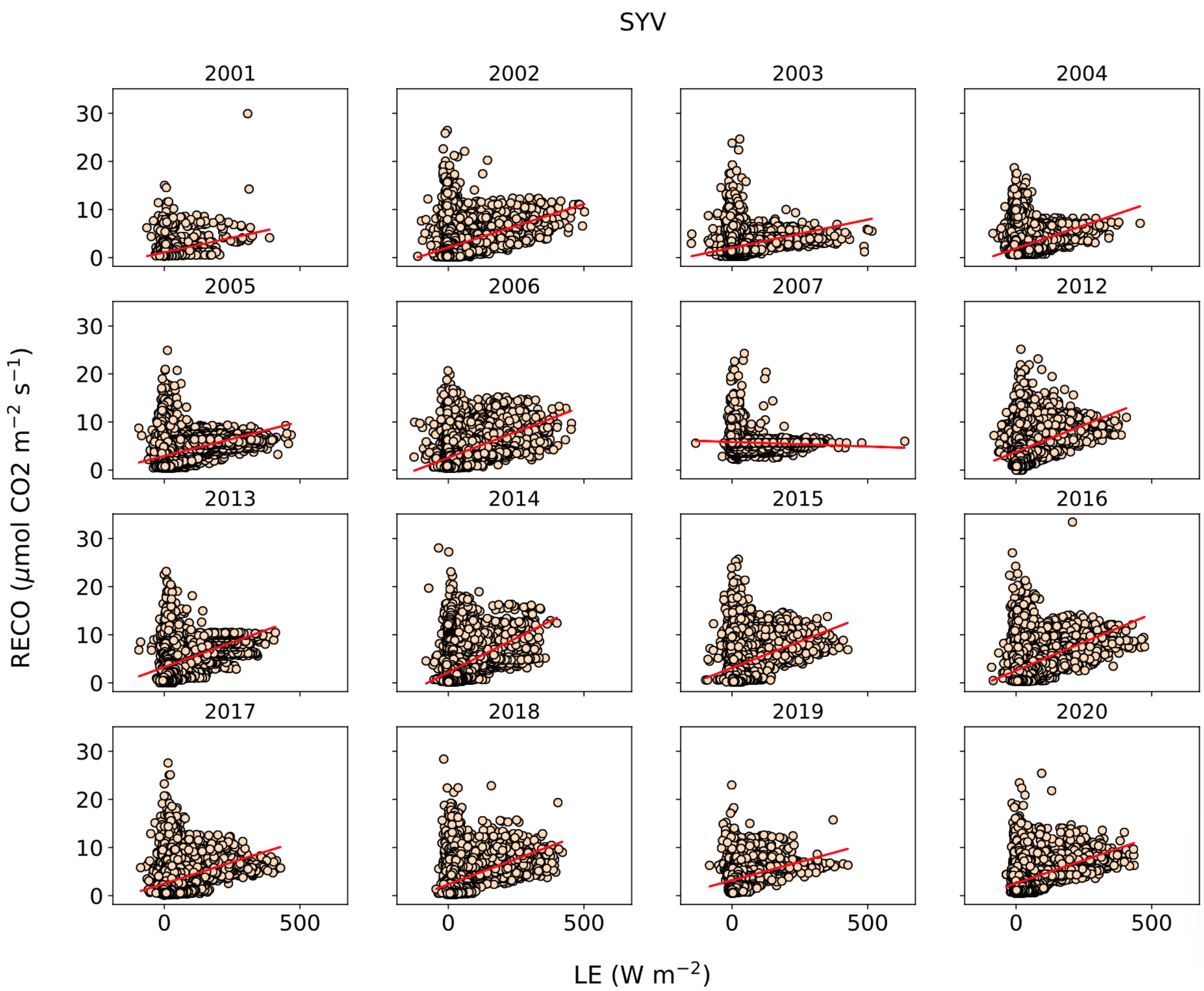

SYV
2001
2002
2003
2004
2005
2006
2007
2012
2013
2014
2015
2016
2017
2018
2019
2020
RECO (μmol CO2 m−2 s−1)
LE (W m−2)
0
10
20
30
0
500

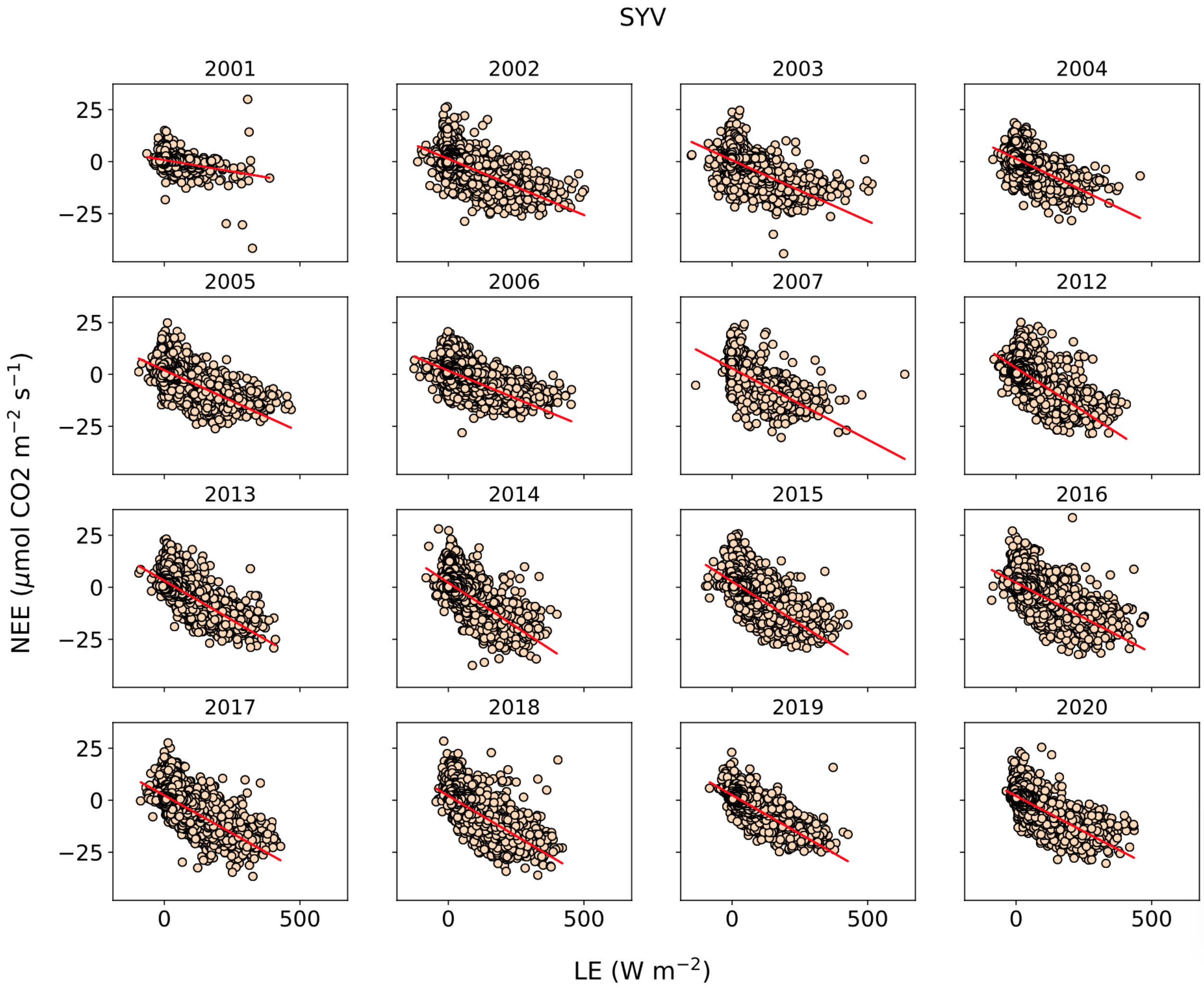
SYV
2001
2002
2003
2004
2005
2006
2007
2012
2013
2014
2015
2016
2017
2018
2019
2020
25
0
−25
500
NEE (μmol CO2 m−2 s−1)
LE (W m−2)

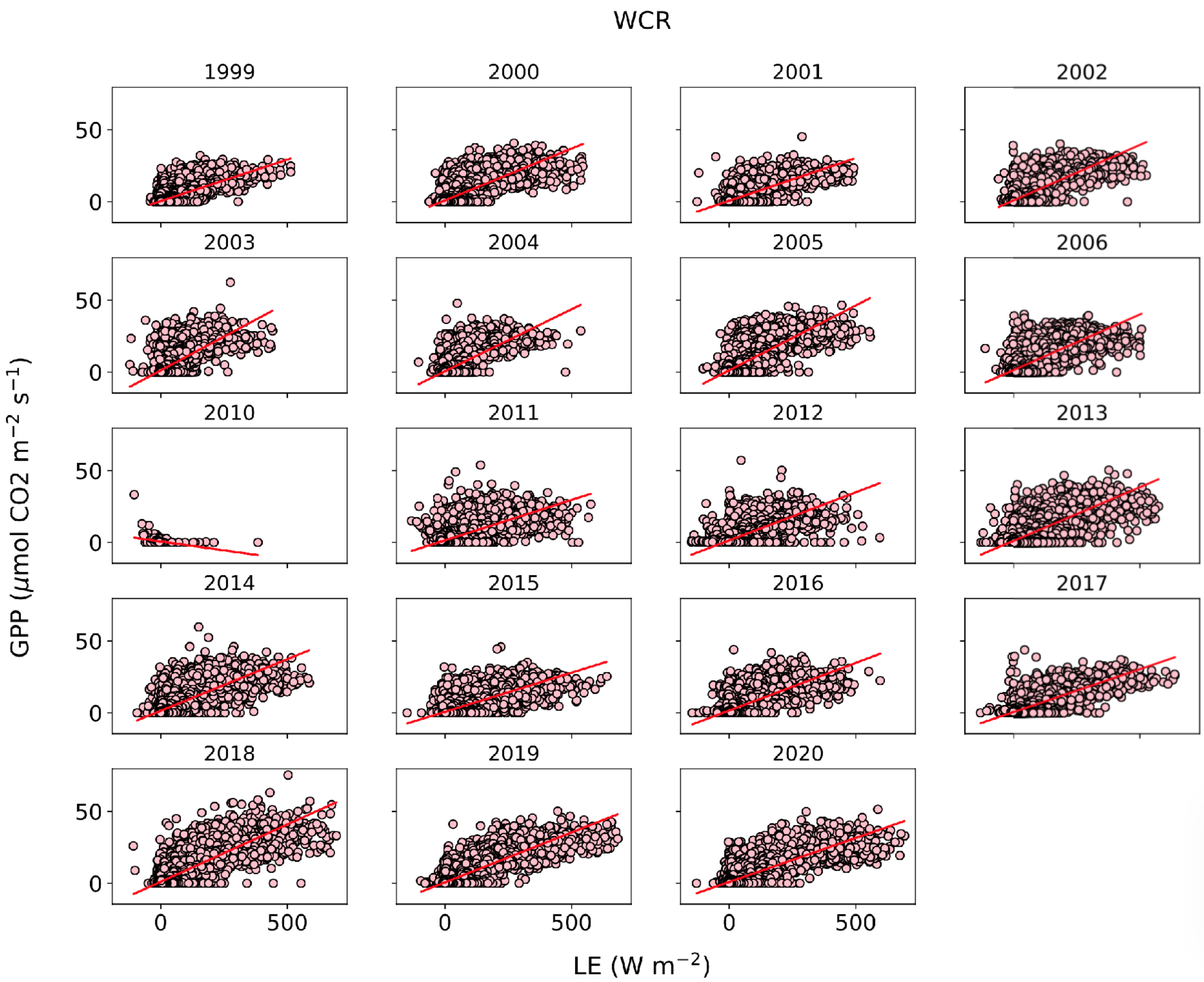

WCR
1999
2000
2001
2002
2003
2004
2005
2006
2010
2011
2012
2013
2014
2015
2016
2017
2018
2019
2020
50
0
500
GPP (μmol CO2 m^{-2} s^{-1})
LE (W m^{-2})

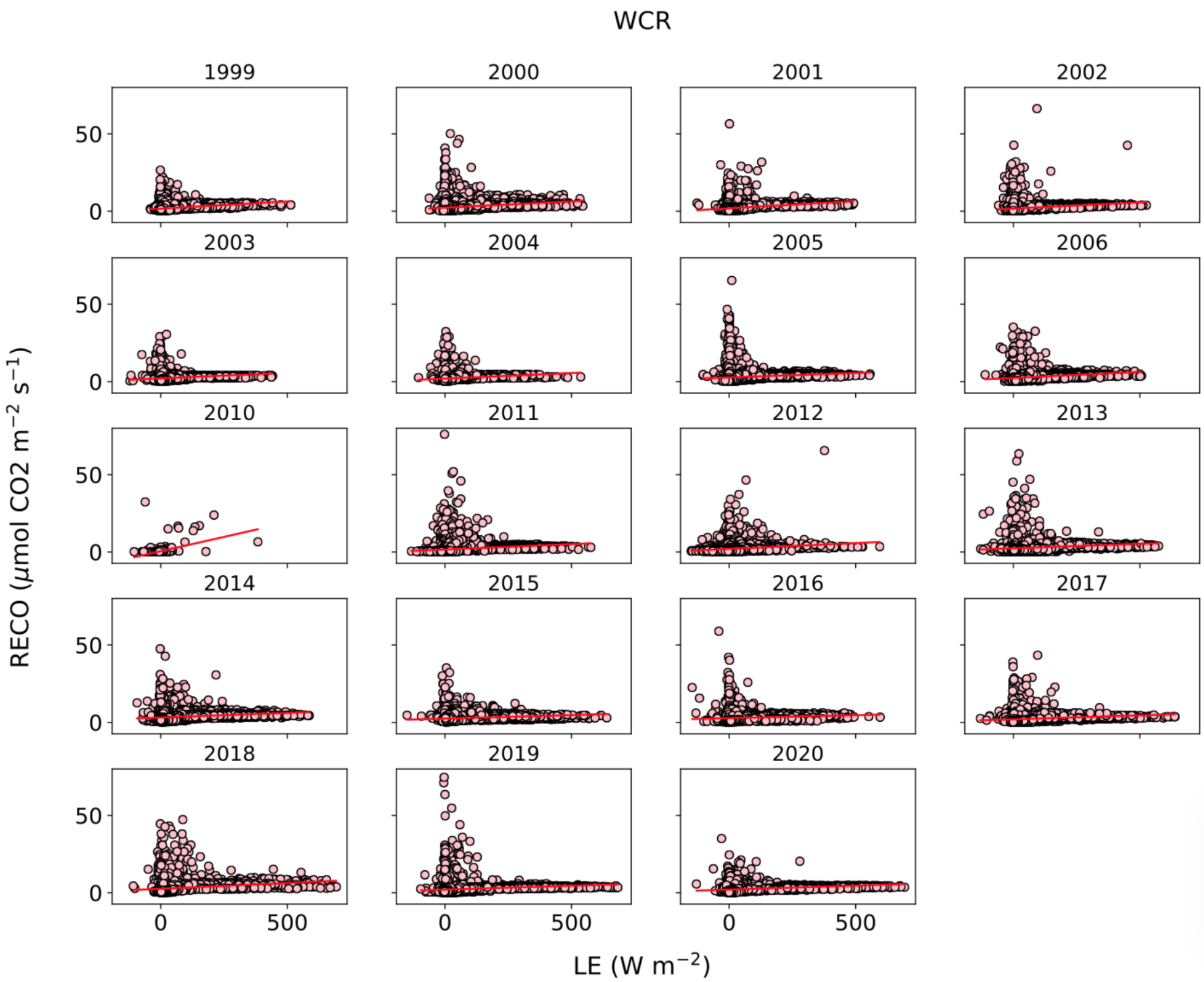

WCR
1999
2000
2001
2002
2003
2004
2005
2006
2010
2011
2012
2013
2014
2015
2016
2017
2018
2019
2020
RECO (μmol CO2 m^{-2} s^{-1})
LE (W m^{-2})
0
50
500

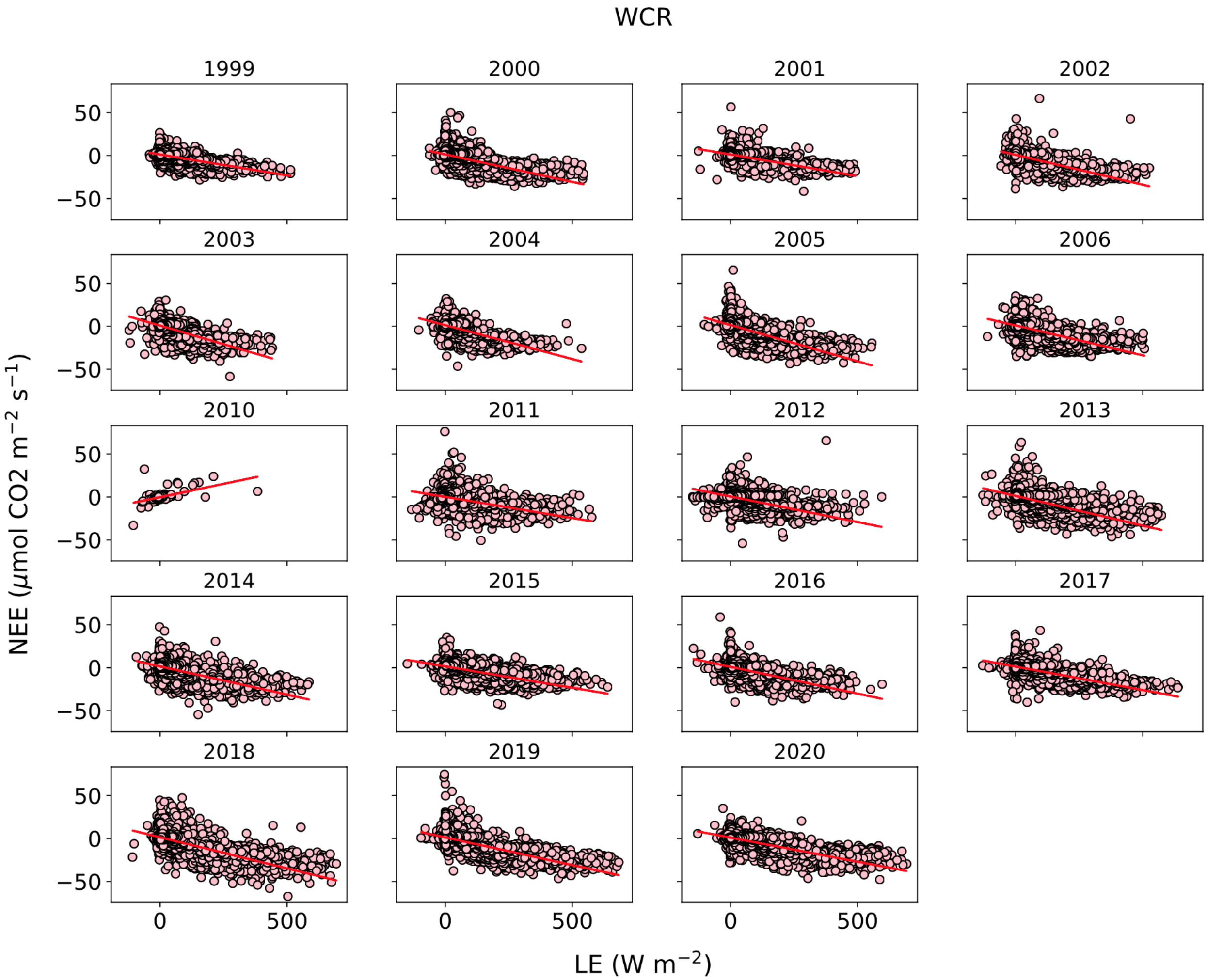

Figures A.5: *C components plotted as a function of latent heat across all sites and years. The red lines indicate the best fit line with corresponding r and p-values listed in* ***Table A.6****.*

GPP and LE											
ALQ			LOS			SYV			WCR		
YEAR	r-value	p-value	YEAR	r-value	p-value	YEAR	r-value	p-value	YEAR	r-value	p-value
1998	-	-	1998	-	-	1998	-	-	1998	-	-
1999	-	-	1999	-	-	1999	-	-	1999	0.74930628	0
2000	-	-	2000	0.47945842	3.03E-147	2000	-	-	2000	0.81692664	0
2001	-	-	2001	0.72087347	0	2001	0.57674509	1.25E-251	2001	0.77300001	0
2002	-	-	2002	0.74493024	0	2002	0.8370781	0	2002	0.81147025	0
2003	-	-	2003	0.66885978	0	2003	0.76245939	0	2003	0.71564177	0
2004	-	-	2004	0.78112315	0	2004	0.76983087	0	2004	0.74826837	0
2005	-	-	2005	0.73218637	0	2005	0.83064366	0	2005	0.81424157	0
2006	-	-	2006	0.76358951	0	2006	0.82480237	0	2006	0.81335017	0
2007	-	-	2007	0.78313572	0	2007	0.7456031	2.90E-310	2007	-	-
2008	-	-	2008	0.75279653	0	2008	-	-	2008	-	-
2009	-	-	2009	-	-	2009	-	-	2009	-	-
2010	-	-	2010	0.73778679	0	2010	-	-	2010	-0.3476407	5.44E-27
2011	-	-	2011	-	-	2011	-	-	2011	0.71746885	0
2012	-	-	2012	-	-	2012	0.85874793	0	2012	0.72649253	0
2013	-	-	2013	-	-	2013	0.8753496	0	2013	0.80634369	0
2014	-	-	2014	0.83160534	0	2014	0.87878678	0	2014	0.76976406	0
2015	0.6722496	0	2015	0.83590819	0	2015	0.86704103	0	2015	0.75006983	0
2016	0.73510185	0	2016	0.86799958	0	2016	0.86353692	0	2016	0.76301985	0
2017	0.37350896	1.06E-107	2017	0.83724361	0	2017	0.8701187	0	2017	0.84943841	0
2018	0.31324263	2.35E-121	2018	0.8419282	0	2018	0.86852889	0	2018	0.85925847	0
2019	0.8701102	0	2019	0.8144782	0	2019	0.86610034	0	2019	0.8803186	0
2020	0.86844214	0	2020	0.83505202	0	2020	0.86666306	0	2020	0.84617679	0

RECO and LE											
ALQ			LOS			SYV			WCR		
YEAR	r-value	p-value	YEAR	r-value	p-value	YEAR	r-value	p-value	YEAR	r-value	p-value
1998	-	-	1998	-	-	1998	-	-	1998	-	-
1999	-	-	1999	-	-	1999	-	-	1999	0.33667322	4.72E-195
2000	-	-	2000	0.17690847	1.95E-19	2000	-	-	2000	0.27057481	3.81E-204
2001	-	-	2001	0.27779293	1.04E-264	2001	0.30210418	4.94E-61	2001	0.3026585	2.49E-206
2002	-	-	2002	0.31758249	0	2002	0.40982851	0	2002	0.25747572	9.73E-171
2003	-	-	2003	0.19566022	1.43E-116	2003	0.33714867	0	2003	0.21778323	7.02E-99
2004	-	-	2004	0.2960323	9.63E-260	2004	0.36492115	0	2004	0.21360251	2.16E-81
2005	-	-	2005	0.35405559	0	2005	0.37687269	1.28E-282	2005	0.16072604	9.01E-76
2006	-	-	2006	0.47820878	0	2006	0.43870525	0	2006	0.27624196	1.24E-193
2007	-	-	2007	-0.0128438	0.31374152	2007	-0.0769185	0.00128511	2007	-	-
2008	-	-	2008	-0.0462039	0.00043517	2008	-	-	2008	-	-
2009	-	-	2009	-	-	2009	-	-	2009	-	-
2010	-	-	2010	-0.0640462	3.07E-06	2010	-	-	2010	0.43515747	6.34E-43
2011	-	-	2011	-	-	2011	-	-	2011	0.21468417	6.71E-126
2012	-	-	2012	-	-	2012	0.45318705	1.06E-289	2012	0.24109744	1.74E-147
2013	-	-	2013	-	-	2013	0.42740485	2.53E-253	2013	0.19161628	5.10E-92
2014	-	-	2014	0.53700361	0	2014	0.49512481	0	2014	0.21703819	1.04E-97
2015	0.16284939	5.69E-31	2015	0.4824288	0	2015	0.41781281	0	2015	0.20639138	1.98E-137
2016	0.3788355	0	2016	0.58401746	0	2016	0.5075771	0	2016	0.12789395	1.39E-36
2017	0.16980878	2.29E-22	2017	0.4894312	0	2017	0.40463372	0	2017	0.2334035	6.05E-169
2018	0.4514053	2.81E-265	2018	0.47895269	0	2018	0.45653133	0	2018	0.27469333	4.72E-208
2019	0.51631657	0	2019	0.43136926	0	2019	0.40494909	1.28E-161	2019	0.21308488	1.64E-137
2020	0.52379741	0	2020	0.47147016		2020	0.50995432	0	2020	0.31274828	2.98E-265

NEE and LE											
ALQ			LOS			SYV			WCR		
YEAR	r-value	p-value	YEAR	r-value	p-value	YEAR	r-value	p-value	YEAR	r-value	p-value
1998	-	-	1998	-	-	1998	-	-	1998	-	-
1999	-	-	1999	-	-	1999	-	-	1999	-0.6706558	0
2000	-	-	2000	-0.3566817	1.23E-77	2000	-	-	2000	-0.7635532	0
2001	-	-	2001	-0.6601022	0	2001	-0.3782897	2.45E-97	2001	-0.6924021	0
2002	-	-	2002	-0.6852991	0	2002	-0.717447	0	2002	-0.7603535	0
2003	-	-	2003	-0.6267372	0	2003	-0.6865631	0	2003	-0.687413	0
2004	-	-	2004	-0.7354311	0	2004	-0.6592964	0	2004	-0.7048459	0
2005	-	-	2005	-0.6669535	0	2005	-0.7501264	0	2005	-0.7641197	0
2006	-	-	2006	-0.6695137	0	2006	-0.6937146	0	2006	-0.7635728	0
2007	-	-	2007	-0.7388747	0	2007	-0.7095986	6.19E-268	2007	-	-
2008	-	-	2008	-0.713269	0	2008	-	-	2008	-	-
2009	-	-	2009	-0.6957857	0	2009	-	-	2009	-	-
2010	-	-	2010	-0.754227	0	2010	-	-	2010	0.53960243	3.24E-69
2011	-	-	2011	-	-	2011	-	-	2011	-0.6149731	0
2012	-	-	2012	-	-	2012	-0.7614097	0	2012	-0.6536565	0
2013	-	-	2013	-	-	2013	-0.7819201	0	2013	-0.7539807	0
2014	-	-	2014	-0.754227	0	2014	-0.7793174	0	2014	-0.726334	0
2015	-0.5262475	0	2015	-0.7596754	0	2015	-0.7701378	0	2015	-0.7015196	0
2016	-0.5507811	0	2016	-0.7897987	0	2016	-0.752052	0	2016	-0.718155	0
2017	-0.1931527	1.41E-28	2017	-0.749387	0	2017	-0.7721812	0	2017	-0.7982281	0
2018	-0.4085796	4.66E-213	2018	-0.7548908	0	2018	-0.7796231	0	2018	-0.8120689	0
2019	-0.6727527	0	2019	-0.7289326	0	2019	-0.8156078	0	2019	-0.8342012	0
2020	-0.6599982	0	2020	-0.7380043	0	2020	-0.7968752	0	2020	-0.8176194	0

Table A.6: *Pearson correlation coefficients and p-values for C components (GPP, RECO, NEE) as a function of latent heat (used here as a proxy for evapotranspiration) across all sites and sites and years.*

References

1. Anderson, Christa M. et al. "Natural Climate Solutions Are Not Enough". *Science*, vol 363, no. 6430, 2019, pp. 933-934. *American Association For The Advancement Of Science (AAAS)*, https://doi.org/10.1126/science.aaw2741. Accessed 26 Dec 2021.

2. Anderson, M., and Lowry, C. (2007). Transient Functioning of a Groundwater Wetland Complex, Allequash Basin, Wisconsin. Available online at: https://www.wri.wisc.edu/wp-content/uploads/FinalWR05R007.pdf

3. Ankur Desai (2021), AmeriFlux US-Los Lost Creek, Ver. 17-5, AmeriFlux AMP, (Dataset). https://doi.org/10.17190/AMF/1246071

4. Ankur Desai (2021), AmeriFlux US-Syv Sylvania Wilderness Area, Ver. 16-5, AmeriFlux AMP, (Dataset). https://doi.org/10.17190/AMF/1246106

5. Ankur Desai (2021), AmeriFlux US-WCr Willow Creek, Ver. 20-5, AmeriFlux AMP, (Dataset). https://doi.org/10.17190/AMF/1246111

6. Aubinet, M. et al. "Estimates Of The Annual Net Carbon And Water Exchange Of Forests: The EUROFLUX Methodology". *Advances In Ecological Research*, 1999, pp. 113-175. *Elsevier*, doi:10.1016/s0065-2504(08)60018-5.

7. Aubinet M. et al. (2012) Nighttime Flux Correction. In: Aubinet M., Vesala T., Papale D. (eds) Eddy Covariance. Springer Atmospheric Sciences. Springer, Dordrecht. https://doi.org/10.1007/978-94-007-2351-1_5

8. Augustin, J. et al. "Factors Influencing Nitrous Oxide And Methane Emissions From Minerotrophic Fens In Northeast Germany". *Biology And Fertility Of Soils*, vol 28, no. 1, 1998, pp. 1-4. *Springer Science And Business Media LLC*, doi:10.1007/s003740050455.

9. BALDOCCHI, DENNIS D. "Assessing The Eddy Covariance Technique For Evaluating Carbon Dioxide Exchange Rates Of Ecosystems: Past, Present And Future". *Global Change Biology*, vol 9, no. 4, 2003, pp. 479-492. *Wiley*, doi:10.1046/j.1365-2486.2003.00629.x.

10. Baldocchi, Dennis et al. *Inter-Annual Variability Of Net And Gross Ecosystem Carbon Fluxes: A Review*. 2017, http://dx.doi.org/10.1016/j.agrformet.2017.05.015.

11. Barr, Alan G. et al. "Inter-Annual Variability In The Leaf Area Index Of A Boreal Aspen-Hazelnut Forest In Relation To Net Ecosystem Production". *Agricultural And Forest Meteorology*, vol 126, no. 3-4, 2004, pp. 237-255. *Elsevier BV*, https://doi.org/10.1016/j.agrformet.2004.06.011. Accessed 22 Dec 2021.

12. Barr, A., Richardson, A., Hollinger, D., Papale, D., Arain, M., Black, T., Bohrer, G., Dragoni, D., Fischer, M., Gu, L., Law, B., Margolis, H., McCaughey, J., Munger, J., Oechel, W. and Schaeffer, K., 2013. Use of change-point detection for friction–velocity threshold evaluation in eddy-covariance studies. *Agricultural and Forest Meteorology*, 171-172, pp.31-45.

13. Beamesderfer, Eric R. et al. "Response Of Carbon And Water Fluxes To Meteorological And Phenological Variability In Two Eastern North American Forests Of Similar Age But Contrasting Species Composition – A Multiyear Comparison". Biogeosciences, vol 17, no. 13, 2020, pp. 3563-3587. Copernicus Gmbh, doi:10.5194/bg-17-3563-2020. Accessed 24 June 2021.

14. Blanken, P.D. et al. "The Seasonal Water And Energy Exchange Above And Within A Boreal Aspen Forest". *Journal Of Hydrology*, vol 245, no. 1-4, 2001, pp. 118-136. *Elsevier BV*, https://doi.org/10.1016/s0022-1694(01)00343-2.

15. Bogard, Matthew J. et al. "Hydrologic Export Is A Major Component Of Coastal Wetland Carbon Budgets". Global Biogeochemical Cycles, vol 34, no. 8, 2020. American Geophysical Union (AGU), doi:10.1029/2019gb006430. Accessed 24 June 2021.

16. BOISVENUE, CÉLINE, and STEVEN W. RUNNING. "Impacts Of Climate Change On Natural Forest Productivity - Evidence Since The Middle Of The 20th Century". Global Change Biology, vol 12, no. 5, 2006, pp. 862-882. Wiley, doi:10.1111/j.1365-2486.2006.01134.x. Accessed 24 June 2021.

17. Bonan, G. B. "Forests And Climate Change: Forcings, Feedbacks, And The Climate Benefits Of Forests". Science, vol 320, no. 5882, 2008, pp. 1444-1449. American Association For The Advancement Of Science (AAAS), doi:10.1126/science.1155121. Accessed 20 May 2021.

18. Bracho, Rosvel et al. "Environmental And Biological Controls On Water And Energy Exchange In Florida Scrub Oak And Pine Flatwoods Ecosystems". Journal Of Geophysical Research: Biogeosciences, vol 113, no. G2, 2008, p. n/a-n/a. American Geophysical Union (AGU), doi:10.1029/2007jg000469. Accessed 24 May 2021.

19. Brent Olson (2021), AmeriFlux US-ALQ Allequash Creek Site, Ver. 5-5, AmeriFlux AMP, (Dataset). https://doi.org/10.17190/AMF/1480323

20. Bruhwiler, L., A. M. Michalak, R. Birdsey, J. B. Fisher, R. A. Houghton, D. N. Huntzinger, and J. B. Miller, 2018: Chapter 1: Overview of the global Carbon cycle. In *Second State of the Carbon Cycle Report (SOCCR2): A Sustained Assessment Report* [Cavallaro, N., G. Shrestha, R. Birdsey, M. A. Mayes, R. G. Najjar, S. C. Reed, P. Romero-Lankao, and Z. Zhu (eds.)]. U.S. Global Change Research Program, Washington, DC, USA,pp. 42-70, https://doi.org/10.7930/SOCCR2.2018.Ch1.

21. Cellucci, C. J. et al. "Statistical Validation Of Mutual Information Calculations: Comparison Of Alternative Numerical Algorithms". *Physical Review E*, vol 71, no. 6, 2005. *American Physical Society (APS)*, https://doi.org/10.1103/physreve.71.066208. Accessed 3 Jan 2022.

22. Chimner, R. and Welker, J., 2005. Ecosystem respiration responses to experimental manipulations of winter and summer precipitation in a Mixedgrass Prairie, WY, USA. *Biogeochemistry*, 73(1), pp.257-270. Doi: 10.1007/s10533-004-1989-6

23. Christensen, T. R. et al. "Environmental Controls On Soil Respiration In The Eurasian And Greenlandic Arctic". *Journal Of Geophysical Research: Atmospheres*, vol 103, no. D22, 1998, pp. 29015-29021. *American Geophysical Union (AGU)*, doi:10.1029/98jd00084. Accessed 8 July 2021.

24. Chu, Housen et al. "Climatic Variability, Hydrologic Anomaly, And Methane Emission Can Turn Productive Freshwater Marshes Into Net Carbon Sources". Global Change Biology, vol 21, no. 3, 2014, pp. 1165-1181. Wiley, doi:10.1111/gcb.12760. Accessed 18 May 2021.

25. COLE, CHRISTOPHER T. et al. "Rising Concentrations Of Atmospheric CO_2 Have Increased Growth In Natural Stands Of Quaking Aspen (Populus Tremuloides)". Global Change Biology, vol 16, no. 8, 2009, pp. 2186-2197. Wiley, doi:10.1111/j.1365-2486.2009.02103.x. Accessed 24 June 2021.

26. Cook, B. D., Davis, K. J., Wang, W., Desai, A., Berger, B. W., Teclaw, R. M., Martin, J. G., Bolstad, P. V., Bakwin, P. S., Yi, C., Heilman, W. (2004) Carbon Exchange And Venting Anomalies In An Upland Deciduous Forest In Northern Wisconsin, USA, Agricultural And Forest Meteorology, 126(3-4), 271-295. Available online at: https://www.fs.fed.us/nrs/pubs/jrnl/2004/nc_2004_cook_001.pdf

27. Cornish, C. R., Percival, D. B., & Bretherton, C. S. (2003). The WMTSA Wavelet Toolkit for data analysis in the geosciences. Eos Trans. AGU, 84(46), Fall Meet. Suppl., Abstract NG11A-0173.

28. Desai, Ankur R. et al. "Comparing Net Ecosystem Exchange Of Carbon Dioxide Between An Old-Growth And Mature Forest In The Upper Midwest, USA". Agricultural And Forest Meteorology, vol 128, no. 1-2, 2005, pp. 33-55. Elsevier BV, doi:10.1016/j.agrformet.2004.09.005. Accessed 3 May 2021.

29. Desai, Ankur R. et al. "Cross-Site Evaluation Of Eddy Covariance GPP And RE Decomposition Techniques". *Agricultural And Forest Meteorology*, vol 148, no. 6-7, 2008, pp. 821-838. *Elsevier BV*, doi:10.1016/j.agrformet.2007.11.012. Accessed 12 July 2021.

30. Drake, Travis W. et al. "Terrestrial Carbon Inputs To Inland Waters: A Current Synthesis Of Estimates And Uncertainty". Limnology And Oceanography Letters, vol 3, no. 3, 2017, pp. 132-142. Wiley, doi:10.1002/lol2.10055. Accessed 19 May 2021.

31. EPA. (2020). Forest sections of land use, land-use change, and forestry (Chapter 6 and Annex 3b). In: Inventory of U.S. greenhouse gas emissions and sinks: 1990–2018. EPA 430-R-19-001. U.S. Environmental Protec-tion Agency.

32. Erwin, Kevin L. "Wetlands And Global Climate Change: The Role Of Wetland Restoration In A Changing World". Wetlands Ecology And Management, vol 17, no. 1, 2008, pp. 71-84. Springer Science And Business Media LLC, doi:10.1007/s11273-008-9119-1. Accessed 23 June 2021.

33. Evans, C. D. et al. "Overriding Water Table Control On Managed Peatland Greenhouse Gas Emissions". Nature, 2021. Springer Science And Business Media LLC, doi:10.1038/s41586-021-03523-1. Accessed 24 June 2021.

34. Falge, Eva et al. "Gap Filling Strategies For Defensible Annual Sums Of Net Ecosystem Exchange". *Agricultural And Forest Meteorology*, vol 107, no. 1, 2001, pp. 43-69. *Elsevier BV*, doi:10.1016/s0168-1923(00)00225-2.

35. Fargione, Joseph E. et al. "Natural Climate Solutions For The United States". *Science Advances*, vol 4, no. 11, 2018, p. eaat1869. *American Association For The Advancement Of Science (AAAS)*, doi:10.1126/sciadv.aat1869. Accessed 19 Aug 2021.

36. Fei, Xuehai et al. "Carbon Exchanges And Their Responses To Temperature And Precipitation In Forest Ecosystems In Yunnan, Southwest China". Science Of The Total Environment, 616-617, 2017, pp. 824-840. Elsevier BV, doi:10.1016/j.scitotenv.2017.10.239. Accessed 1 July 2021.

37. Data Reference: Flanagan, Lawrence B., and Kamran H. Syed. "Stimulation Of Both Photosynthesis And Respiration In Response To Warmer And Drier Conditions In A Boreal Peatland Ecosystem". *Global Change Biology*, vol 17, no. 7, 2011, pp. 2271-2287. *Wiley*, https://doi.org/10.1111/j.1365-2486.2010.02378.x. Accessed 3 Jan 2022.

38. Foken T., Aubinet M., Leuning R. (2012) The Eddy Covariance Method. In: Aubinet M., Vesala T., Papale D. (eds) Eddy Covariance. Springer Atmospheric Sciences. Springer, Dordrecht. https://doi.org/10.1007/978-94-007-2351-1_1

39. Fraser, A. M., & Swinney, H. L. (1986). Independent coordinates for strange attractors from mutual information. *Physical Review A: General Physics*, *33*(2), 1134–1140. https://doi.org/10.1103/physr eva.33.1134

40. Froelich, Norma et al. "Trends Of Carbon Fluxes And Climate Over A Mixed Temperate–Boreal Transition Forest In Southern Ontario, Canada". *Agricultural And Forest Meteorology*, 211-212, 2015, pp. 72-84. *Elsevier BV*, doi:10.1016/j.agrformet.2015.05.009. Accessed 7 July 2021.

41. Frolking, S. E. et al. "Relationship Between Ecosystem Productivity And Photosynthetically Active Radiation For Northern Peatlands". Global Biogeochemical Cycles, vol 12, no. 1, 1998, pp. 115-126. American Geophysical Union (AGU), doi:10.1029/97gb03367. Accessed 24 May 2021.

42. Gao, Yu et al. "Field Observation Of Lateral Detritus Carbon Flux In A Coastal Wetland". Wetlands, vol 38, no. 3, 2018, pp. 613-625. Springer Science And Business Media LLC, doi:10.1007/s13157-018-1005-x. Accessed 24 June 2021.

43. Gedney, N. et al. "Detection Of A Direct Carbon Dioxide Effect In Continental River Runoff Records". Nature, vol 439, no. 7078, 2006, pp. 835-838. Springer Science And Business Media LLC, doi:10.1038/nature04504. Accessed 18 May 2021.

44. Google Earth V 7.3.3.7786. Maxar Technologies, USDA Farm Service Agency 2019. Available online at: https://www.google.com/earth/ (accessed May 4, 2020).

45. GOULDEN, MICHAEL L. et al. "Measurements Of Carbon Sequestration By Long-Term Eddy Covariance: Methods And A Critical Evaluation Of Accuracy". *Global Change Biology*, vol 2, no. 3, 1996, pp. 169-182. *Wiley*, doi:10.1111/j.1365-2486.1996.tb00070.x.

46. Griscom, Bronson W. et al. "Natural Climate Solutions". *Proceedings Of The National Academy Of Sciences*, vol 114, no. 44, 2017, pp. 11645-11650. *Proceedings Of The National Academy Of Sciences*, doi:10.1073/pnas.1710465114. Accessed 19 Aug 2021.

47. Guan, D., Wu, J., Zhao, X., Han, S., Yu, G., Sun, X. and Jin, C., 2006. CO_2 fluxes over an old, temperate mixed forest in northeastern China. *Agricultural and Forest Meteorology*, 137(3-4), pp.138-149.

48. Harriss, Robert C. et al. "Methane Flux In The Great Dismal Swamp". Nature, vol 297, no. 5868, 1982, pp. 673-674. Springer Science And Business Media LLC, doi:10.1038/297673a0. Accessed 20 May 2021.

49. Helfter, C. et al. "Drivers Of Long-Term Variability In CO_2 Net Ecosystem Exchange In A Temperate Peatland". *Biogeosciences*, vol 12, no. 6, 2015, pp. 1799-1811. *Copernicus Gmbh*, doi:10.5194/bg-12-1799-2015. Accessed 8 July 2021.

50. Helbig, M., Chasmer, L., Desai, A., Kljun, N., Quinton, W. and Sonnentag, O., 2017. Direct and indirect climate change effects on Carbon dioxide fluxes in a thawing boreal forest-wetland landscape. *Global Change Biology*, 23(8), pp.3231-3248. Doi: 10.1111/gcb.13638

51. Hollinger DY, Richardson AD. Uncertainty in eddy covariance measurements and its application to physiological models. Tree Physiol. 2005 Jul;25(7):873-85. doi: 10.1093/treephys/25.7.873. PMID: 15870055.

52. Kaarakka, Lilli et al. "Improved Forest Management As A Natural Climate Solution: A Review". *Ecological Solutions And Evidence*, vol 2, no. 3, 2021. *Wiley*, doi:10.1002/2688-8319.12090. Accessed 19 Aug 2021.

53. Kato, T. and Tang, Y., 2008. Spatial variability and major controlling factors of CO_2 sink strength in Asian terrestrial ecosystems: evidence from eddy covariance data. *Global Change Biology*, 14(10), pp.2333-2348. Doi: 10.1111/j.1365-2486.2008.01646.x

54. Kayranli, Birol et al. "Carbon Storage And Fluxes Within Freshwater Wetlands: A Critical Review". Wetlands, vol 30, no. 1, 2009, pp. 111-124. Springer Science And Business Media LLC, doi:10.1007/s13157-009-0003-4. Accessed 20 May 2021.

55. Keenan, T., Baker, I., Barr, A., Ciais, P., Davis, K., Dietze, M., Dragoni, D., Gough, C., Grant, R., Hollinger, D., Hufkens, K., Poulter, B., McCaughey, H., Raczka, B., Ryu, Y., Schaefer, K., Tian, H., Verbeeck, H., Zhao, M. and Richardson, A., 2012. Terrestrial biosphere model performance for inter-annual variability of land-atmosphere CO_2 exchange. *Global Change Biology*, 18(6), pp.1971-1987.
doi: 10.1111/j.1365-2486.2012.02678

56. Kelly, R. D., Hunt, E. R., Reiners, W. A., Smith, W. K., and Welker, J. M., Relationships between daytime Carbon dioxide uptake and absorbed photosynthetically active radiation for three different mountain/plains ecosystems, J. Geophys. Res., 107(D14), doi:10.1029/2001JD001181, 2002.

57. Knapp, A., Ciais, P. and Smith, M., 2016. Reconciling inconsistencies in precipitation–productivity relationships: implications for climate change. *New Phytologist*, 214(1), pp.41-47. Doi: 10.1111/nph.14381

58. Knox, S., Bansal, S., McNicol, G., Schafer, K., Sturtevant, C., Ueyama, M., Valach, A., Baldocchi, D., Delwiche, K., Desai, A., Euskirchen, E., Liu, J., Lohila, A., Malhotra, A., Melling, L., Riley, W., Runkle, B., Turner, J., Vargas, R., Zhu, Q., Alto, T., Fluet‐Chouinard, E., Goeckede, M., Melton, J., Sonnentag, O., Vesala, T., Ward, E., Zhang, Z., Feron, S., Ouyang, Z., Alekseychik, P., Aurela, M., Bohrer, G., Campbell, D., Chen, J., Chu, H., Dalmagro, H., Goodrich, J., Gottschalk, P., Hirano, T., Iwata, H., Jurasinski, G., Kang, M., Koebsch, F., Mammarella, I., Nilsson, M., Ono, K., Peichl, M., Peltola, O., Ryu, Y., Sachs, T., Sakabe, A., Sparks, J., Tuittila, E., Vourlitis, G., Wong, G., Windham‐Myers, L., Poulter, B. and Jackson, R., 2021. Identifying dominant environmental predictors of freshwater wetland methane fluxes across diurnal to seasonal time scales. *Global Change Biology*, 27(15), pp.3582-3604.

59. Law, B., Falge, E., Gu, L., Baldocchi, D., Bakwin, P., Berbigier, P., Davis, K., Dolman, A., Falk, M., Fuentes, J., Goldstein, A., Granier, A., Grelle, A., Hollinger, D., Janssens, I., Jarvis, P., Jensen, N., Katul, G., Mahli, Y., Matteucci, G., Meyers, T., Monson, R., Munger, W., Oechel, W., Olson, R., Pilegaard, K., Paw U, K., Thorgeirsson, H., Valentini, R., Verma, S., Vesala, T., Wilson, K. and Wofsy, S., 2002. Environmental controls over Carbon dioxide and water vapor exchange of terrestrial vegetation. *Agricultural and Forest Meteorology*, 113(1-4), pp.97-120. Doi: 10.1016/S0168-1923(02)00104-1

60. LEUZINGER, SEBASTIAN, and CHRISTIAN KÖRNER. "Rainfall Distribution Is The Main Driver Of Runoff Under Future CO_2-Concentration In A Temperate Deciduous Forest". Global Change Biology, vol 16, no. 1, 2010, pp. 246-254. Wiley, doi:10.1111/j.1365-2486.2009.01937.x. Accessed 20 May 2021.

61. Liang, Shunlin, and Jindi Wang. *Advanced Remote Sensing*. 2nd ed., Academic Press, 2020, pp. 581-620. Doi: 10.1016/C2017-0-03489-4

62. "List Of Cities In Wisconsin - Wikipedia". *En.Wikipedia.Org*, 2021, https://en.wikipedia.org/wiki/List_of_cities_in_Wisconsin.

63. Liu, P. C., 1994: Wavelet spectrum analysis and ocean wind waves. *Wavelets in Geophysics,* E. Foufoula-Georgiou and P. Kumar, Eds., Academic Press, 151–166.

64. Liu, Yibo et al. "Recent Trends In Vegetation Greenness In China Significantly Altered Annual Evapotranspiration And Water Yield". Environmental Research Letters, vol 11, no. 9, 2016, p. 094010. IOP Publishing, doi:10.1088/1748-9326/11/9/094010.

65. Lloyd, J., and J. A. Taylor. "On The Temperature Dependence Of Soil Respiration". *Functional Ecology*, vol 8, no. 3, 1994, p. 315. *JSTOR*, doi:10.2307/2389824.

66. Ma, Jun et al. "Ecosystem Carbon Storage Distribution Between Plant And Soil In Different Forest Types In Northeastern China". Ecological Engineering, vol 81, 2015, pp. 353-362. Elsevier BV, doi:10.1016/j.ecoleng.2015.04.080.

67. Mahecha, M., Reichstein, M., Carvalhais, N., Lasslop, G., Lange, H., Seneviratne, S., Vargas, R., Ammann, C., Arain, M., Cescatti, A., Janssens, I., Migliavacca, M., Montagnani, L. and Richardson, A., 2010. Global Convergence in the Temperature Sensitivity of Respiration at Ecosystem Level. *Science*, 329(5993), pp.838-840. Doi: 10.1126/science.1189587

68. McVeigh, Philip et al. "Meteorological And Functional Response Partitioning To Explain Interannual Variability Of CO_2 Exchange At An Irish Atlantic Blanket Bog". *Agricultural And Forest Meteorology*, vol 194, 2014, pp. 8-19. *Elsevier BV*, doi:10.1016/j.agrformet.2014.01.017. Accessed 8 July 2021.

69. Mitsch, William J. et al. "Wetlands, Carbon, And Climate Change". Landscape Ecology, vol 28, no. 4, 2012, pp. 583-597. Springer Science And Business Media LLC, doi:10.1007/s10980-012-9758-8. Accessed 23 June 2021.

70. Moffat, Antje M. et al. "Comprehensive Comparison Of Gap-Filling Techniques For Eddy Covariance Net Carbon Fluxes". *Agricultural And Forest Meteorology*, vol 147, no. 3-4, 2007, pp. 209-232. *Elsevier BV*, doi:10.1016/j.agrformet.2007.08.011. Accessed 12 July 2021.

71. Munger J.W., Loescher H.W., Luo H. (2012) Measurement, Tower, and Site Design Considerations. In: Aubinet M., Vesala T., Papale D. (eds) Eddy Covariance. Springer Atmospheric Sciences. Springer, Dordrecht. https://doi.org/10.1007/978-94-007-2351-1_2

72. Murty, Danuse et al. "Does Conversion Of Forest To Agricultural Land Change Soil C And Nitrogen? A Review Of The Literature". Global Change Biology, vol 8, no. 2, 2002, pp. 105-123. Wiley, doi:10.1046/j.1354-1013.2001.00459.x.

73. Olsson, L. et al. "Factors Influencing CO_2 And CH_4 Emissions From Coastal Wetlands In The Liaohe Delta, Northeast China". Biogeosciences, vol 12, no. 16, 2015, pp. 4965-4977. Copernicus Gmbh, doi:10.5194/bg-12-4965-2015. Accessed 23 June 2021.

74. Pan, Y. et al. "A Large And Persistent Carbon Sink In The World's Forests". Science, vol 333, no. 6045, 2011, pp. 988-993. American Association For The Advancement Of Science (AAAS), doi:10.1126/science.1201609. Accessed 24 June 2021.

75. Papale D. (2012) Data Gap Filling. In: Aubinet M., Vesala T., Papale D. (eds) Eddy Covariance. Springer Atmospheric Sciences. Springer, Dordrecht. https://doi.org/10.1007/978-94-007-2351-1_6

76. Papale, D., Reichstein, M., Aubinet, M., Canfora, E., Bernhofer, C., Kutsch, W., Longdoz, B., Rambal, S., Valentini, R., Vesala, T. and Yakir, D., 2006. Towards a standardized processing of Net Ecosystem Exchange measured with eddy covariance technique: algorithms and uncertainty estimation. *Biogeosciences*, 3(4), pp.571-583.

77. Parton, W., Morgan, J., Smith, D., Del Grosso, S., Prihodko, L., LeCain, D., Kelly, R. and Lutz, S., 2012. Impact of precipitation dynamics on net ecosystem productivity. *Global Change Biology*, 18(3), pp.915-927.

78. Pastorello et al., 2020. The FLUXNET2015 dataset and the ONEFlux processing pipeline for eddy covariance data. *Scientific Data*, 7(1).

79. Pugh, C.A., Reed, D.E., Desai, A.R. et al. Wetland flux controls: how does interacting water table levels and temperature influence Carbon dioxide and methane fluxes in northern Wisconsin?. Biogeochemistry 137, 15–25 (2018). https://doi.org/10.1007/s10533-017-0414-x

80. Reed, David E. et al. "Time Dependency Of Eddy Covariance Site Energy Balance". *Agricultural And Forest Meteorology*, vol 249, 2018, pp. 467-478. *Elsevier BV*, doi:10.1016/j.agrformet.2017.08.008. Accessed 8 July 2021.

81. Reichstein, Markus et al. "On The Separation Of Net Ecosystem Exchange Into Assimilation And Ecosystem Respiration: Review And Improved Algorithm". *Global Change Biology*, vol 11, no. 9, 2005, pp. 1424-1439. *Wiley*, doi:10.1111/j.1365-2486.2005.001002.x.

82. Reichstein M., Stoy P.C., Desai A.R., Lasslop G., Richardson A.D. (2012) Partitioning of Net Fluxes. In: Aubinet M., Vesala T., Papale D. (eds) Eddy Covariance. Springer Atmospheric Sciences. Springer, Dordrecht. https://doi.org/10.1007/978-94-007-2351-1_9

83. Saigusa, Nobuko et al. "Inter-Annual Variability Of Carbon Budget Components In An Asiaflux Forest Site Estimated By Long-Term Flux Measurements". *Agricultural And Forest Meteorology*, vol 134, no. 1-4, 2005, pp. 4-16. *Elsevier BV*, doi:10.1016/j.agrformet.2005.08.016. Accessed 7 July 2021.

84. Schrope, Mark. "When Money Grows On Trees". Nature Climate Change, vol 1, no. 909, 2009, pp. 101-103. Springer Science And Business Media LLC, doi:10.1038/climate.2009.78.

85. Seddon, Nathalie et al. "Understanding The Value And Limits Of Nature-Based Solutions To Climate Change And Other Global Challenges". *Philosophical Transactions Of The Royal Society B: Biological Sciences*, vol 375, no. 1794, 2019, p. 20190120. *The Royal Society*, doi:10.1098/rstb.2019.0120. Accessed 19 Aug 2021.

86. Serrano‐Ortiz, P. et al. "Transition Period Between Vegetation Growth And Senescence Controlling Interannual Variability Of Carbon Fluxes In A Mediterranean Reed Wetland". *Journal Of Geophysical Research: Biogeosciences*, vol 125, no. 1, 2020. *American Geophysical Union (AGU)*, doi:10.1029/2019jg005169. Accessed 8 July 2021.

87. Shannon, Claude Elwood. "A mathematical theory of communication." *The Bell system technical journal* 27.3 (1948): 379-423.

88. Sjögersten, Sofie et al. "Tropical Wetlands: A Missing Link In The Global Carbon Cycle?". Global Biogeochemical Cycles, vol 28, no. 12, 2014, pp. 1371-1386. American Geophysical Union (AGU), doi:10.1002/2014gb004844. Accessed 23 June 2021.

89. "Streamgaging Basics". usgs.gov, 2021, https://www.usgs.gov/mission-areas/water-resources/science/streamgaging-basics?qt-science_center_objects=0#qt-science_center_objects.

90. Sturtevant, C., Ruddell, B., Knox, S., Verfaillie, J., Matthes, J., Oikawa, P. and Baldocchi, D., 2016. Identifying scale‐emergent, nonlinear, asynchronous processes of wetland methane exchange. *Journal of Geophysical Research: Biogeosciences*, 121(1), pp.188-204.

91. Sulman, B. N. et al. "Contrasting Carbon Dioxide Fluxes Between A Drying Shrub Wetland In Northern Wisconsin, USA, And Nearby Forests". Biogeosciences, vol 6, no. 6, 2009, pp. 1115-1126. Copernicus Gmbh, doi:10.5194/bg-6-1115-2009.

92. Sundquist, Eric et al. "Carbon Sequestration To Mitigate Climate Change". Fact Sheet, 2008. US Geological Survey, doi:10.3133/fs20083097. Accessed 23 June 2021.

93. Syed, Kamran H. et al. "Environmental Control Of Net Ecosystem CO_2 Exchange In A Treed, Moderately Rich Fen In Northern Alberta". *Agricultural And Forest Meteorology*, vol 140, no. 1-4, 2006, pp. 97-114. *Elsevier BV*, https://doi.org/10.1016/j.agrformet.2006.03.022. Accessed 22 Dec 2021.

94. Taillardat, Pierre et al. *Climate Change Mitigation Potential Of Wetlands And The Cost-Effectiveness Of Their Restoration*. 2020. doi:10.1098/rsfs.2019.0129.

95. Trenberth, Kevin. "The Impact Of Climate Change And Variability On Heavy Precipitation, Floods, And Droughts". *Encyclopedia Of Hydrological Sciences*, 2005, https://citeseerx.ist.psu.edu/viewdoc/download?doi=10.1.1.725.372&rep=rep1&type=pdf. Accessed 26 Dec 2021.

96. Turner J, Desai AR, Thom J, Wickland KP and Olson B (2019) Wind Sheltering Impacts on Land-Atmosphere Fluxes Over Fens. Front. Environ. Sci. 7:179. doi: 10.3389/fenvs.2019.00179

97. Valentini, R., Matteucci, G., Dolman, A., Schulze, E., Rebmann, C., Moors, E., Granier, A., Gross, P., Jensen, N., Pilegaard, K., Lindroth, A., Grelle, A., Bernhofer, C., Grünwald, T., Aubinet, M., Ceulemans, R., Kowalski, A., Vesala, T., Rannik, Ü., Berbigier, P., Loustau, D., Guðmundsson, J., Thorgeirsson, H., Ibrom, A., Morgenstern, K., Clement, R., Moncrieff, J., Montagnani, L., Minerbi, S. and Jarvis, P., 2000. Respiration as the main determinant of Carbon balance in European forests. *Nature*, 404(6780), pp.861-865. Doi: 10.1038/35009084

98. Villa, Jorge A., and Blanca Bernal. "Carbon Sequestration In Wetlands, From Science To Practice: An Overview Of The Biogeochemical Process, Measurement Methods, And Policy Framework". Ecological Engineering, vol 114, 2018, pp. 115-128. Elsevier BV, doi:10.1016/j.ecoleng.2017.06.037. Accessed 23 June 2021.

99. Wei, Yawei et al. "Forest Carbon Storage And Tree Carbon Pool Dynamics Under Natural Forest Protection Program In Northeastern China". Chinese Geographical Science, vol 24, no. 4, 2014, pp. 397-405. Springer Science And Business Media LLC, doi:10.1007/s11769-014-0703-4. Accessed 24 June 2021.

100. Were, David et al. "Carbon Sequestration By Wetlands: A Critical Review Of Enhancement Measures For Climate Change Mitigation". Earth Systems And Environment, vol 3, no. 2, 2019, pp. 327-340. Springer Science And Business Media LLC, doi:10.1007/s41748-019-00094-0. Accessed 23 June 2021.

101. Xiao, J., Sun, G., Chen, J., Chen, H., Chen, S., Dong, G., Gao, S., Guo, H., Guo, J., Han, S., Kato, T., Li, Y., Lin, G., Lu, W., Ma, M., McNulty, S., Shao, C., Wang, X., Xie, X., Zhang, X., Zhang, Z., Zhao, B., Zhou, G. and Zhou, J., 2013. C fluxes, evapotranspiration, and water use

efficiency of terrestrial ecosystems in China. *Agricultural and Forest Meteorology*, 182-183, pp.76-90. Doi: 10.1016/j.agrformet.2013.08.007

102. Xiao, J., Zhuang, Q., Law, B., Baldocchi, D., Chen, J., Richardson, A., Melillo, J., Davis, K., Hollinger, D., Wharton, S., Oren, R., Noormets, A., Fischer, M., Verma, S., Cook, D., Sun, G., McNulty, S., Wofsy, S., Bolstad, P., Burns, S., Curtis, P., Drake, B., Falk, M., Foster, D., Gu, L., Hadley, J., Katul, G., Litvak, M., Ma, S., Martin, T., Matamala, R., Meyers, T., Monson, R., Munger, J., Oechel, W., Paw, U., Schmid, H., Scott, R., Starr, G., Suyker, A. and Torn, M., 2011. Assessing net ecosystem Carbon exchange of U.S. terrestrial ecosystems by integrating eddy covariance flux measurements and satellite observations. *Agricultural and Forest Meteorology*, 151(1), pp.60-69. Doi: 10.1016/j.agrformet.2010.09.002

103. Xie, J., Chen, J., Sun, G., Chu, H., Noormets, A., Ouyang, Z., John, R., Wan, S. and Guan, W., 2014. Long-term variability and environmental control of the Carbon cycle in an oak-dominated temperate forest. *Forest Ecology and Management*, 313, pp.319-328. Doi: 10.1016/j.foreco.2013.10.032

104. Xu, Liukang et al. "How Soil Moisture, Rain Pulses, And Growth Alter The Response Of Ecosystem Respiration To Temperature". *Global Biogeochemical Cycles*, vol 18, no. 4, 2004, p. n/a-n/a. *American Geophysical Union (AGU)*, doi:10.1029/2004gb002281.

105. Yi et al 2010 Environ. Res. Lett. 5 034007. doi:10.1088/1748-9326/5/3/034007

106. Yu, G., Zhu, X., Fu, Y., He, H., Wang, Q., Wen, X., Li, X., Zhang, L., Zhang, L., Su, W., Li, S., Sun, X., Zhang, Y., Zhang, J., Yan, J., Wang, H., Zhou, G., Jia, B., Xiang, W., Li, Y., Zhao, L., Wang, Y., Shi, P., Chen, S., Xin, X., Zhao, F., Wang, Y. and Tong, C., 2012. Spatial patterns and climate drivers of Carbon fluxes in terrestrial ecosystems of China. *Global Change Biology*, 19(3), pp.798-810. Doi: 10.1111/gcb.12079

107. Zhou, Li, and Guangsheng Zhou. "Measurement And Modelling Of Evapotranspiration Over A Reed (Phragmites Australis) Marsh In Northeast China". Journal Of Hydrology, vol 372, no. 1-4, 2009, pp. 41-47. Elsevier BV, doi:10.1016/j.jhydrol.2009.03.033. Accessed 24 May 2021.

108. Zscheischler, J., Fatichi, S., Wolf, S., Blanken, P., Bohrer, G., Clark, K., Desai, A., Hollinger, D., Keenan, T., Novick, K. and Seneviratne, S., 2016. Short-term favorable weather conditions are an important control of interannual variability in Carbon and water fluxes. *Journal of Geophysical Research: Biogeosciences*, 121(8), pp.2186-2198. doi:10.1002/2016JG003503